THE EFFECT OF FIBER CORROSION ON SHEAR CAPACITY OF STEEL FIBER

REINFORCED CONCRETE BEAMS AND AN INITIAL INVESTIGATION ON

ALKALI-SILICA REACTION IN STEEL FIBER REINFORCED CONCRETE


by


REGINA NYAMBURA WAWERU


Presented to the Faculty of the Graduate School of

The University of Texas at Arlington in Partial Fulfillment

of the Requirements

for the Degree of


MASTER OF SCIENCE IN CIVIL ENGINEERING


THE UNIVERSITY OF TEXAS AT ARLINGTON

August 2011

ACKNOWLEDGEMENTS

ABSTRACT

THE EFFECT OF FIBER CORROSION ON SHEAR CAPACITY OF STEEL FIBER

REINFORCED CONCRETE BEAMS AND AN INITIAL INVESTIGATION ON

ALKALI-SILICA REACTION IN STEEL FIBER REINFORCED CONCRETE

Regina Nyambura Waweru, M.S

The University of Texas at Arlington, 2011

Supervising Professor:  Shih-Ho Chao

The first part of this research aims to investigate the effect of fiber corrosion on the shear

capacity of Steel Fiber Reinforced Concrete beams. It will also strive to determine at

what reduction in minimum diameter of the fiber does the effect of corrosion become

most severe on the shear capacity of the beam. Four simply-supported beams with a shear

span to depth ratio of 3.3 were subjected to a monotonically increasing load. The targeted

concrete compressive strength for all beams was 6000 psi. This however differed from

the measured strength due to a number of factors as will be discussed in the paper. The

fixed parameters for the experiment were the beam size, shear span-to-effective depth

ratio, and concrete compressive strength, while the varied parameters were the fiber

content and the extent of corrosion of the steel fibers. Pre-corroded fibers were used in

this research to give the worst case scenario because in real life situations, only the fibers

closest to the surface of the concrete (0.10 in. from surface) or those close to a crack will

be corroded. Hooked steel fibers were used at a volume fraction of 0.75% with an aspect

ratio of 125 and a length of 1 in.. Small specimen tests were also conducted to determine the change in the mechanical properties of SFRC at different levels of corrosion. The tests conducted were: the three point loading test, the compression test and the fiber pullout tests.

Test results revealed that a 12.5% reduction in the minimum fiber diameter, has almost no effect on the shear capacity of beams. Results from the fiber pullout tests showed a slight increase in the pullout load which seems to indicate an increase in the bond between the fiber and cementitious matrix. However, for beams with a 50% reduction in the minimum fiber diameter a 24% reduction in the shear strength of the beam was witnessed. These observations indicated that the type of failure for these beams was through fiber breakage before pullout. The results from the fiber pullout specimens also seemed to support this failure mode as 80% of the fibers broke before pullout. Finally recommendations are made for more future research on the topic.

The second part of the thesis covers the initial investigation on alkali-silica reaction (ASR) in SFRC. Most importantly, it tries to determine whether the addition of fibers to concrete can actually arrest cracks due to ASR in concrete and thus counteract its effect on the durability of the structure. Four beams with dimensions of 20 x 6 x 6 in. were cast using reactive aggregates, in accordance to ASTM C1260 and C1293 and subjected to an accelerated ASR test. Two beams were reinforced with 1% fibers while the control specimens had no fibers. From the preliminary observations on the beams by measuring their elongation, the SFRC beams showed less expansion compared to the plain concrete

beams. Based on these these initial findings, a more intense research was recommended on the effect of steel fibers on ASR. This is an ongoing research that will take a couple of years as the specimens with reactive aggregates will be cast and put in the natural environment for cracking to occur due to ASR. The specimens will then be compared with their counterparts with no fibers to reach a conclusion.

TABLE OF CONTENTS

LIST OF FIGURES

LIST OF TABLES

CHAPTER 1

INTRODUCTION

## 1.1 Introduction on Effect of Fiber Corrosion on Shear Capacity of SFRC Beams

1.1.1 SFRC Background and Motivation of the Research

*1.1.1.1 History and Application of SFRC*

According to ACI committee 544 (1998), Steel Fiber Reinforced Concrete (SFRC) is concrete made of hydraulic cements, fine and/or coarse aggregate and evenly distributed steel fibers. SFRC fails in tension after the steel fiber pullout or break from the concrete matrix. Although the concept of using fibers to reinforce concrete is not new, its application to the concrete industry did not advance until early 1960s. Compared to other types of fibers in the market (glass, carbon or synthetic material), steel fibers are the most preferred and widely used by the construction industry. Steel fibers when added to concrete will greatly improve the concrete's post-cracking tensile resistance and toughness (Hannant, 1978). Steel Fiber Reinforced Concrete (SFRC) has been widely used in construction of bridge deck overlays, tunnel lining, dams, spillways, industrial floors, highway pavements, in precast products and for slope stabilization. In 1971, the first commercial SFRC pavement in the United States was placed at a truck weighing station near Ashland, Ohio. Although steel fibers have been shown to enhance the flexural and shear behavior of concrete members, its use in buildings has been very limited.

## 1.1.1.2 Effect of Steel Fibers on the Shear Resistance of SFRC Beams

An alternative to stirrup reinforcement is the use of randomly oriented steel fibers. Experimental research on the shear behavior of SFRC beams have been conducted over the past three decades. A number of the researches have shown that steel fibers increase the shear resistance of the beam (Kwak et al., 2002). The increase in shear resistance is attributed to the fact that steel fibers bridge cracks thus delay the widening of cracks and redistribute tensile stresses. It has been shown that in sufficient quantities, and depending on the geometric shape, steel fibers can increase the shear strength of the concrete beams to a level where a flexural failure occurs and hence avoid a catastrophic diagonal tension failure. In fact, the use of deformed steel fibers in place of minimum stirrup reinforcement is currently allowed in the ACI-318 Code Section 11.4.6 (ACI Committee 318, 2008).

## 1.1.1.3 Durability of SFRC

The durability of SFRC is a material property as important as its mechanical properties. A number of experimental studies have been conducted in the area of fiber corrosion. Since the concrete cover to the fibers near the surface is essentially zero, it is apparent that fibers would be susceptible to severe corrosion. According to Naaman and Kosa (1990), since the diameter of the fiber is adversely reduced by corrosion, any substantial corrosion of the fiber would lead to a considerable decrease in both the strength and toughness of SFRC. This was due to the change in the failure mode from fiber pullout to fiber fracture.

Nevertheless according to Bentur (1998), the much smaller sensitivity of steel fibers to corrosion in SFRC compared to reinforcing bars in Reinforced Concrete (RC) can be attributed to several mechanisms:

- The lower tendency to cracking in SFRC

- The small diameter of the fibers does not lead to spalling due to the low pressure of the corrosion products.

- Due to the discrete nature of the steel fibers, there is lack of electrical conductivity for electrochemical corrosion to occur.

- There is an improved matrix microstructure and a dense interfacial transition zone.

It should be mentioned that most of the research has been conducted in a saturated chloride environment, either in real life situation (marine tidal zone) or experimentally in a laboratory.

### 1.1.1.4 Motivation of the Research

Tests on corrosion of steel fibers have centered on flexural strength, toughness, direct tension, bending or compression of the SFRC specimen. However no research on large scale beams has yet been carried out to test the effect of fiber corrosion on the shear strength of SFRC beams. As mentioned earlier, the use of deformed steel fibers in place of minimum stirrup reinforcement is currently allowed in ACI-318 Code Section 11.4.6 (ACI Committee 318, 2008). In Section R11.4.6.1 (f), it states that there is no data for use of steel fiber as shear reinforcement in concrete members exposed to chlorides from deicing chemicals, salt, salt water, brackish water, seawater or sprays from these sources.

Thus there is a need to find out the consequences of corrosion of the steel fibers on the shear strength of beams.

## 1.2 Introduction on Alkali-Silica Reaction in SFRC

1.2.1 Background

Alkali Silica Reaction (ASR) was first observed in the 1920's. Although acceptable standards of construction and quality control were applied, a number of structures were observed to develop severe cracking within a few years of their construction. Thomas E. Stanton was the first researcher to explain ASR in a comprehensive way in 1940's.

Alkali-silica reaction is the reaction between the alkali hydroxide in Portland cement and certain siliceous rocks and minerals present in aggregates. High alkali content in the pore water provides the hydroxyl ions that react with the silica to form a gel at the cementitious matrix and aggregate interface.

ASR is a time dependent phenomenon as it occurs throughout the life of a structure and gives external warning of internal damage. Although ASR appears to be harmless to the useful life of a structure, experience has shown that the effect of ASR can be profound when considered in the context of construction globally. ASR can affect strength, stiffness, serviceability, safety and stability. It provides a means through which other deterioration mechanisms can develop and operate.

ASR is a major cause of the deterioration of highway structures and pavements in United States. The Figure 1.1 shows the regions of the US that were identified to be affected by ASR.
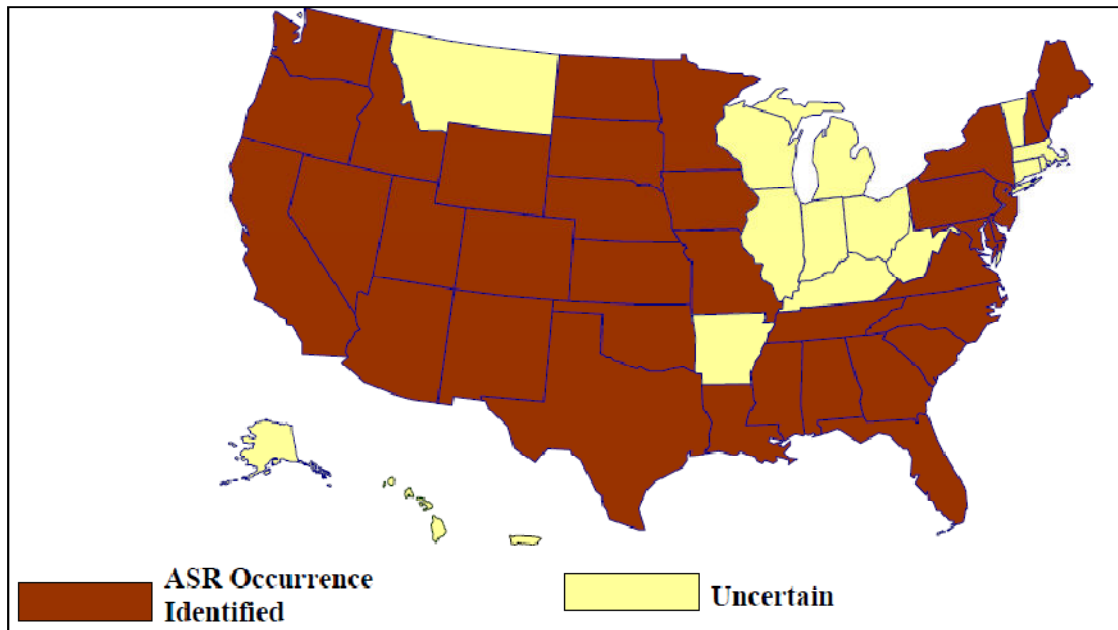
Figure 1.1 Occurrence of ASR in the USA (Adapted from FHWA Showcase Workshop
on ASR, 1994)

The figure shows that almost 90% of the country is affected by ASR. There is therefore a
need to come up with strategies to mitigate its effect on the structures.

### 1.3 Objectives of the Research

1.3.1 Objectives of the Research on the Effect Fiber Corrosion on the Shear Capacity of
SFRC Beams

According to Dinh (2009), shear failure in SFRC beams subjected to a monotonic
increasing concentrated load goes through four phases of cracking:

1. Flexural cracks in the maximum moment region.

2. Web shear cracks occur in mid-depth of the beam and change of direction of
   existing flexural cracks and their propagation toward the compression region. At
   the same time new flexural cracks develop and spread toward the supports.

3. Shear and flexural cracks widen.

4. Beam fails with opening of the critical diagonal shear crack.

Since an SFRC beam resists shear through a number of mechanism; shear force across the compression region, aggregate interlock, dowel action and tension in fibers, it is imperative that the mechanical properties of the fibers are preserved.

Higgins and Farrow (2006) in their research observed that the damage of stirrup reinforcement due to corrosion resulted in significant reduction in the shear capacity and a reduction in the overall deformation at failure.

### *1.3.1.1 Objectives*

Based on the preceding discussion, the objectives of this research are as follows:

1. To study the shear failure mechanism, ultimate shear strength and ductility of SFRC.

2. Investigate the effect of steel fiber corrosion at different extents on the above mentioned properties of the affected SFRC specimen.

3. Determine at what reduction in the minimum fiber diameter does the mode of failure change from fiber pullout to fiber fracture.

4. As mentioned in section 1.1.1.4, ACI committee 318-08 in Section R11.4.6.1 (f) states that there is no data for the use of steel fibers as shear reinforcement in concrete members exposed to chlorides. Therefore this research also aims at providing data on the use of steel fibers as shear reinforcement in concrete members exposed to chlorides and especially when the fibers have been corroded due to exposure to chlorides.

1.3.2 Objectives of the Research on ASR in SFRC

The primary objectives of this research are to:

1   Investigate the effect of adding steel fibers to the expansion and crack formation in concrete due to ASR.

2   Evaluate the effectiveness of varying the steel fiber content toward the expansion and crack formation of concrete due to ASR.

**1.4 Organization of Research**

The thesis is organized in five chapters. Chapter 1 includes the introduction on the effect of fiber corrosion on shear capacity of SFRC beams and investigations of Alkali-Silica Reaction on SFRC. Chapter 2 deals with the literature review. In this chapter, some theories on the shear strength of beams (both RC and SFRC) are covered. Also theories on corrosion and alkali-silica reaction are explained in detail. Finally, past research and findings by researchers on related work will are presented.

Chapter three covers the experimental work conducted in this research. The design, construction, testing of the beam specimens and test on mechanical properties of the specimens are discussed. Also the casting of the ASR specimens is explained along with the standard testing methods used to determine expansion of the specimens. The proposed research plan on the alkali-silica reaction in steel fiber reinforced concrete will also be discussed in this chapter.

Chapter four analyses the test results of the beam specimens and small specimens tests.

Finally, major findings, conclusions and recommendations will be found in chapter five of this paper.

CHAPTER 2

LITERATURE REVIEW

**2.1 Theories on Steel Fiber Reinforced Concrete (SFRC)**

2.1.1 Mechanical Properties of SFRC
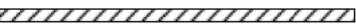
The mechanical properties of SFRC are influenced by a number of factors:

- Fibers: type, geometry, aspect ratio, volume, orientation, distribution

- Matrix: strength (water-cement ratio), maximum aggregate size

- Specimen: size, geometry, method of preparation, loading rate

Stress is transferred from the matrix to the fibers by a combination of interfacial shear and mechanical interlock between the deformed fibers and the matrix. The load is carried by both the matrix and the fibers to the point where the matrix cracks; once cracking occurs, the fibers then carry the entire stress by bridging across the cracked portions of the matrix until they are pulled out completely. Therefore, fibers are particularly effective in resisting direct tensile stress due to flexure, or shear, under static, impact or fatigue loading. They are, however, less effective under compressive loading (Bentur and Mindess, 2007). Theoretically, the resistance of fibers to pullout increases with increased aspect ratio. Bond strength between steel fibers and the matrix can be greatly improved by introducing deformations in fibers. Fibers fabricated with a crimped profile, surface deformations or improved end anchorage by hooking, teeing or end enlargement in form of a spade or dog bone shape have enhanced resistance to pullout. These types are more

effective than equivalent uniform straight fibers of the same length and diameter (ACI Committee 544, 1998). The common types of deformed steel fibers are hooked fibers, crimped fibers, stranded fibers with enlarged ends, and twisted fibers (Table 2.1).

Table 2.1 Types of Steel Fibers

| Types of Steel Fibers | Geometric Configuration |
|---|---|
| Hooked fibers | |
| Crimped fibers | |
| Stranded fibers | |
| Twisted fibers | |
| Straight fibers | |

When pullout occurs, the ends of a hooked steel fiber must deform significantly and yield before the fiber can be pulled out of the concrete. This will normally result in the straightening of the ends of the fiber that were previously deformed before pullout as show in Figure 2.1. Thus SFRC with hooked steel fibers absorbs a great amount of energy prior to a complete failure. Therefore, the use of hooked fibers with higher yield strength will result in a stronger composite (Dinh, 2009).
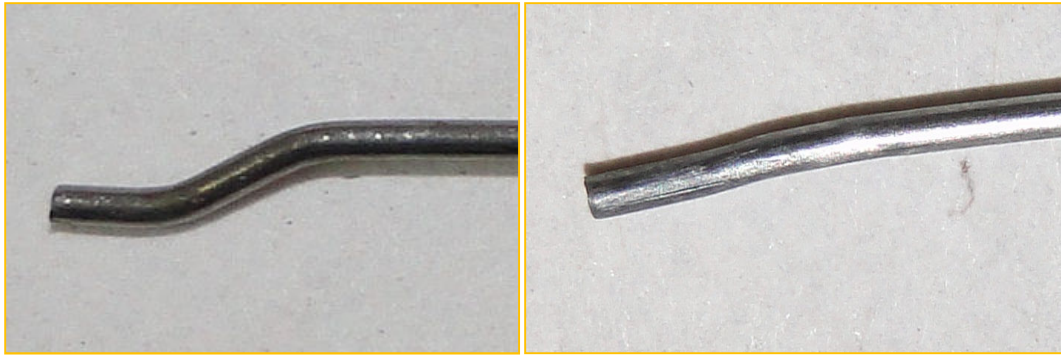
<center>(a)                                              (b)</center>

<center>Figure 2.1 Hooked end of a fiber (a) before and (b) after pullout</center>

2.1.2 Fiber Orientation and Distribution

One should keep in mind that changing fiber cross section, increasing fiber aspect ratio, or introducing mechanical anchorage will not always lead to improved fiber matrix bond strength. This is because these changes may lead to an SFRC mix with inadequate workability and fiber distribution (ACI Committee 544, 1998).

When examining or describing the effects of fiber additions, changes in SFRC properties are always expressed in terms of average fiber content. It is implicitly assumed that the fibers are uniformly distributed and randomly oriented throughout the matrix. These assumptions are least likely to be correct after the placement and compaction of the SFRC and this may lead to a considerable amount of scatter in the test data. In addition there may be considerable variability in measured values due to the direction of loading (in relation to the direction of casting).

Edgington and Hannant (1972), observed that fibers tend to be aligned in horizontal planes when compacted using table vibration (Figure 2.2).
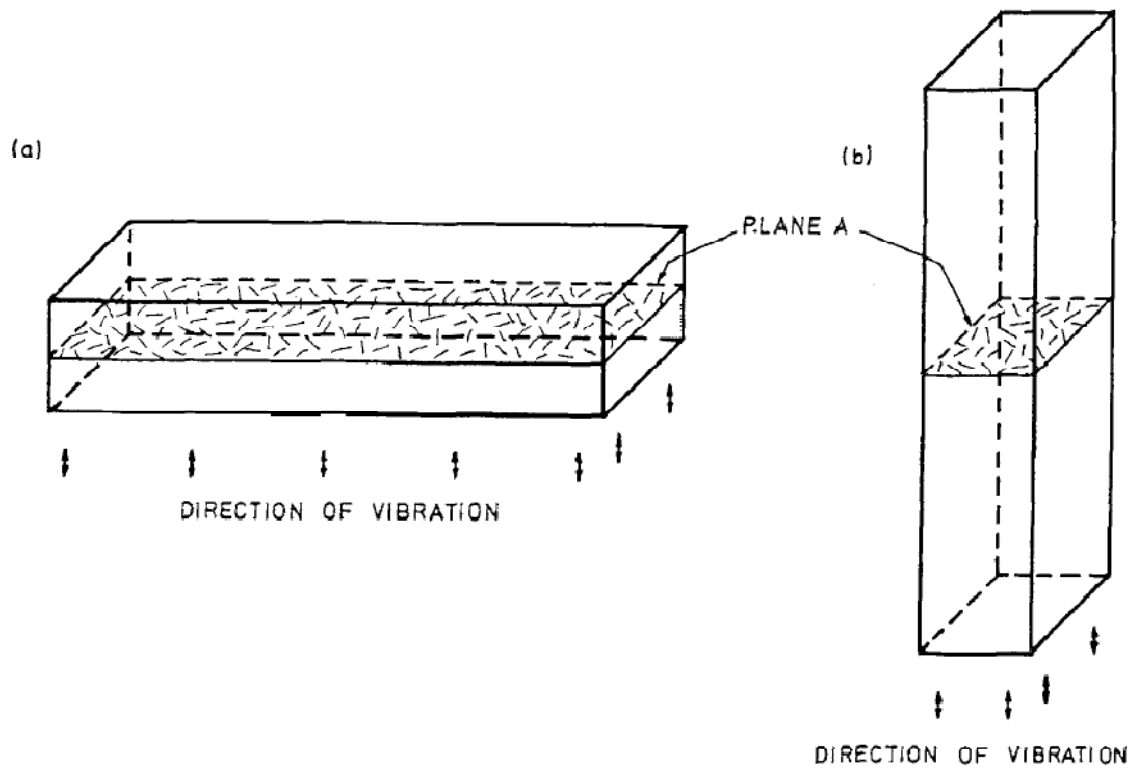
Figure 2.2 Effect of casting flexural specimens horizontally and vertically on fiber orientation (adapted from Edgington and Hannant, 1972)

Internal vibration exerts a smaller influence on fiber alignment compared to excessive vibration that can lead to preferred horizontal orientation of the fibers and also segregation. Fibers close to the bottom and sides of the forms usually align themselves parallel to the forms. Also there is a tendency of a higher fiber concentration near the faces of the specimen ("wall effect") (Bentur and Mindess, 2007).

2.1.3 Static Mechanical Properties

Extensive studies have been made on the effect of fiber reinforcement in concrete in terms of fiber efficiency (i.e. resistance to pullout) resulting in the breakdown of the interfacial bond between the fiber and the matrix.

Several researches have attempted to relate the mechanical properties of SFRC to the bond strength. Due to the gradual nature of fiber pullout, fibers improve the post-crack ductility of the concrete which would have otherwise failed in a brittle manner. This improvement in ductility depends on the type and volume percentage of fibers present as earlier mentioned.

Although steel fibers improve the ductility of concrete under all modes of loading, their effectiveness in improving strength varies among tension, shear, compression, torsion, and flexure (ACI Committee 544, 1998).

*2.1.3.1 Compression Strength*

Fibers have little effect in increasing the compressive strength of the concrete. The increase in compressive strength ranges from 0% to 15% for a fiber volume fraction of ≤ 1.5%. However, the fibers do substantially increase the post-cracking ductility or energy absorption of the material (Bentur and Mindess, 2007).

*2.1.3.2 Tensile Strength*

For an addition of 1.5 % by volume of fibers in concrete, an increase in the direct tensile strength of 30% to 40%t has been reported.

Thus there is a significant increase in the direct tensile strength of concrete due to the addition of concrete. However one should keep in mind that the orientation of the fibers with respect to the tensile stress will also affect the tensile strength of the SFRC. Fibers that are aligned in the direction of the tensile stress may cause very large increase in the direct tensile strength. An increase of 133% in the tensile strength has been reported for a fiber volume fraction on 5%. On the other hand, for fibers that are randomly distributed

in the concrete, the increase in the tensile strength was not as much as it ranged between 0 to 60 percent. However, unlike in compression, very high fiber volume fractions appear to be effective in tension.

*2.1.3.3 Flexural Strength*

Steel fibers have been found to have a greater effect on the increase in flexural strength as compared to tensile and compressive strength. This is due the ductile behavior of the SFRC which will change the elastic distribution of stress and strain over the member depth. Tensile strength increase of more than 100 percent has been reported in some cases. The increase in flexural strength is related to the fiber volume fraction as well as the aspect ratio of the fiber. Earlier studies have shown that an increase of about 4 percent in fiber volume fraction can more than double the flexural strength (ACI Committee 544, 1998). As concerns the aspect ratio, deformed fibers are more effective than straight, smooth fibers (Bentur and Mindess, 2007). The maximum practical fiber volume fraction has been limited to 2 percent because higher volume fractions will affect the workability of the concrete mix as it pertains to mixing and placing.

*2.1.3.4 Shear and Torsional Strength*

Steel fibers increase the shear and torsional strength of SFRC having conventional reinforcing bars. However little is known on the shear and torsional strength of strictly SFRC with no reinforcing bars. Fibers bridge across the cracks that form in the concrete matrix preventing further crack opening and hence maintaining the integrity of the material. Fibers lead to an improvement in the residual strength of the concrete which in turn lead to an increase in the shear capacity of the concrete. It has been shown that the

increase in pure shear strength SFRC depends on both the shear testing technique employed and the resulting orientation or alignment of the fibers in the shear failure zone. There are a number of advantages for substituting vertical stirrups or otherwise supplementing them with steel fiber. These are:

- Fibers can be randomly distributed throughout the volume of the concrete at much closer spacing as compared to the smallest reinforcing bar thus leading to distributed cracking with reduced crack size.

- Fibers lead to an increase in the tensile strength at first crack and at ultimate or failure.

- The resistance of the fiber to pullout and its ability to bridge cracks results in an increase in the shear-friction strength

Steel fiber in sufficient amount and shape can increase the shear strength of a concrete beam enough to prevent a catastrophic diagonal tension failure and force a flexural failure of the beam.

From the above discussion on the physical and mechanical properties of fibers, we can conclude that the advantages of adding fibers to reinforced concrete are as follows:

1. Significantly improve post-cracking tensile resistance and toughness

2. In an SFRC beam, steel fibers play a role similar to that of stirrup reinforcement in an RC beam.

3. steel fibers carry redistributed tensile stress and delay the propagation and opening of diagonal cracks.

4. Prevent premature concrete splitting along the tensile reinforcement, same way as stirrups (Figure 2.3).



(a)

(b)
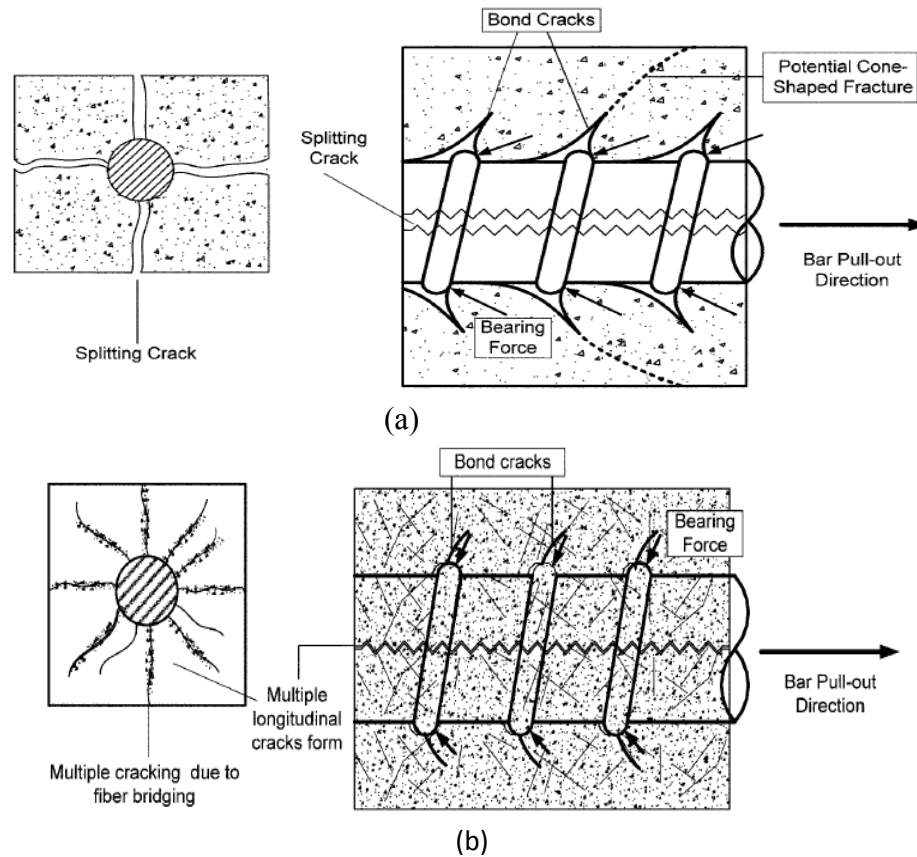
Figure 2.3 Bond mechanisms in (a) reinforced concrete and (b) SFRC (adapted from Chao et al., 2009)

5. Effective in controlling crack width and fostering the formation of multiple diagonal cracks.

## 2.2 Shear Beam Theory

Shear forces and shear stresses exist in those parts of a beam where the moment changes from section to section. The change in bending moment gives rise to diagonal tension in the concrete and bond stresses between the reinforcement and the concrete.

15

In a homogeneous elastic beam a vertical shear force will cause complimentary shear stresses and diagonal tensile and compressive stresses of the same magnitude. Figure 2.4 below shows the stresses on a small element near the neutral axis.
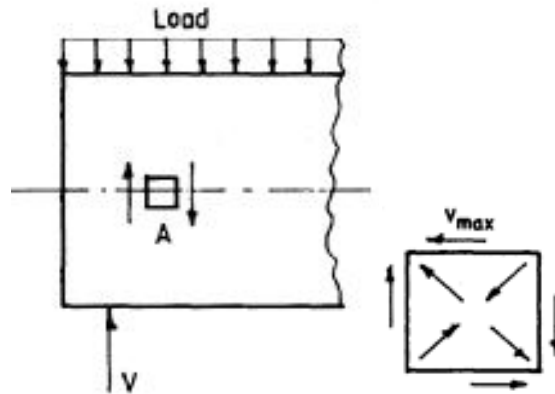


Figure 2.4 Shear stresses on a small element (adapted from Park and Paulay, 1975)

The maximum shear stress at the neutral axis of the section is given by

$$v_{max}=1.5V/bd$$

2.2.1 Failure of RC Beams without Stirrup Reinforcement

Beam flexural strength increases significantly when longitudinal reinforcement is added to the beam. Due to the ability of the longitudinal reinforcement to bridge cracks and transfer stresses to the concrete, more flexural cracks will be seen on the beam. In a region of large bending moments, these stresses are greatest at the extreme fiber of the member and are responsible for the initiation of cracks in flexure perpendicular to the axis of the member. Significant principal tensile stresses (diagonal tension) may be generated in regions of high shear force. This stresses are generated at approximately 45° to the axis of the member and may result in inclined cracks. In most cases these inclined cracks are extensions of flexural cracks. In special cases for example webs of flanged

beams, diagonal tension cracks may be initiated in the vicinity of the neutral axis (Park and Paulay, 1975). A reinforced concrete flexural member can either collapse immediately after diagonal cracks form or an entirely new shear carrying mechanism is developed that can carry more load on the cracked beam.

The diagonal cracking load originating from flexure and shear is usually much smaller than would be expected from principal stress analysis and the tensile strength of concrete. This is largely due to the presence of shrinkage stresses, the redistribution of shear stresses between flexural cracks and the local weakening of a cross section by transverse reinforcement which causes a regular pattern of discontinuities along a beam. Diagonal cracking under service loads is acceptable provided crack widths remain within the same limits accepted for flexure.

2.2.1 Equilibrium in the Shear Span of a Beam

A simply supported beam over which the shear force is constant is shown in Figure 2.5 below.
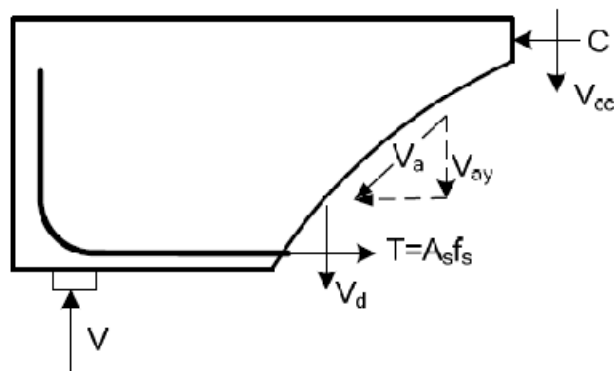


Figure 2.5 Shear resisting components after formation of diagonal crack (adapted from Dinh, 2009)

17

The total external transverse force V is resisted by a combination of:

- Shear force across the compression zone $V_{cc}$

- Dowel force transmitted across the crack by flexural reinforcement $V_d$

- The vertical component of inclined shearing stresses $V_{ay}$ transmitted across the inclined crack by means of interlocking of aggregate particles.

When shear displacement along an inclined crack occurs, shear will be transferred by means of dowel action of the longitudinal reinforcement. The effectiveness of the dowel action is greatly reduced once a splitting crack occurs. The splitting also significantly affects the bond performance of the bars. The splitting strength of the concrete depends on the effective concrete area between bars of a layer across which the tension is to be resisted but most importantly it depends on the relative position of the bar at the time of casting.

In beams without shear reinforcement, the contribution of dowel action is not more than 25 percent of the total cantilever resistance. Dowel action is more significant in the presence of stirrup reinforcement as these will aid in confining the longitudinal bars. Cracks will develop parallel to the longitudinal bar before the stirrups can come in and contribute to carrying dowel forces. The Figure 2.6 below shows the qualitative load-displacement relationships for dowel action.
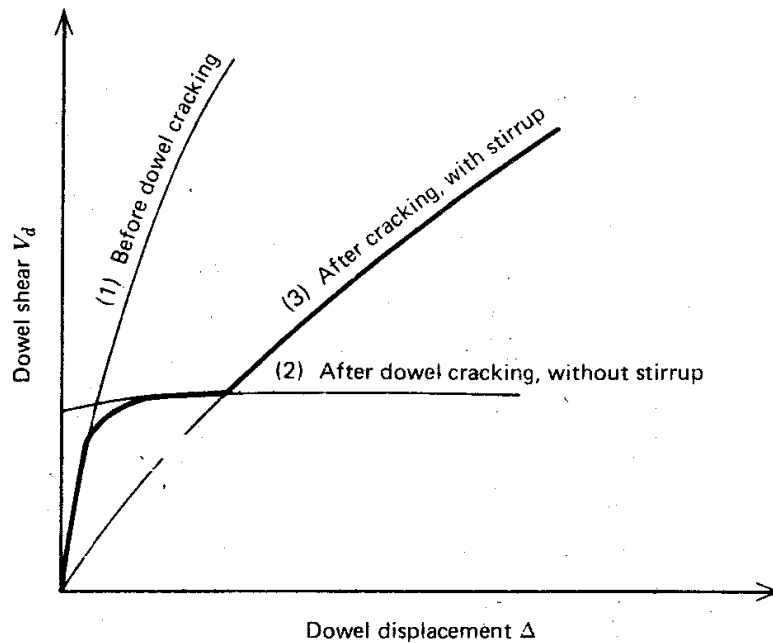
Figure 2.6 Shear-dowel displacement relationships (adapted from Park and Paulay, 1975)

The shear strength of beams without web reinforcement decreases with increase in the effective depth. I large beams, aggregate interlock and dowel action can be reduced significantly if the aggregate and reinforcing bars are not correctly scaled.

The shear failure mechanisms of simply supported beams under monotonically increasing point load fall into three categories as defined by ASCE-ACI Committee 426 (1973).

1. **Diagonal tension failure:** An inclined crack propagates rapidly due to inadequate shear reinforcement.
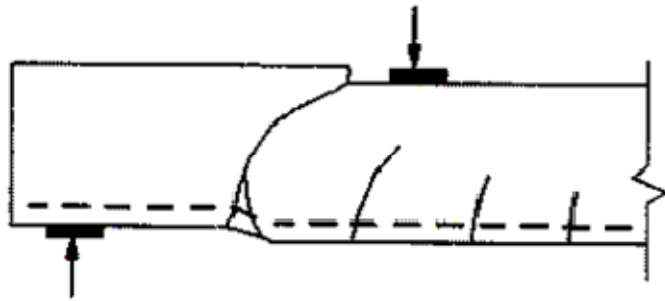
Figure 2.7 Diagonal tension failure

2. **Shear compression failure:** Crushing of the concrete occurs near the compression flange above the tip of the inclined crack.
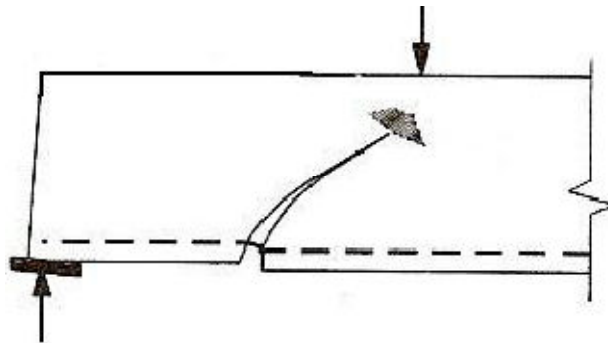


Figure 2.8 Shear compression failure

3. **Shear tension failure:** The diagonal cracks propagate horizontally along the longitudinal bars due to lack of enough anchorage.
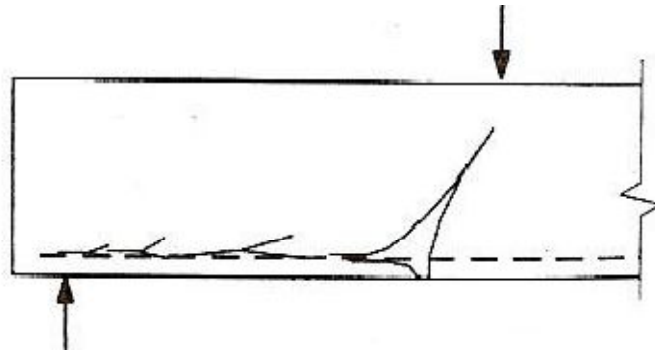
Figure 2.9 Shear tension failure

2.2.2 Failure of SFRC Beams without Stirrup Reinforcement

Steel fibers in a longitudinal-reinforced SFRC beam, play a similar role to that of stirrups in a reinforced concrete beam.

1. Steel fibers delay the propagation and widening of diagonal cracks by redistributing the tensile stresses.

2. They prevent premature concrete splitting along the tensile reinforcement in the same way stirrup reinforcement does and hence prevent bond failure.

3. Steel fibers are effective in controlling crack widths and the formation of multiple diagonal cracks which leads to the beam being able to carry more load.

The shear behavior of a simply supported SFRC beam subjected to a monotonically increasing concentrated load is controlled by a number of parameters namely:

- Beam size especially depth
- Cross section shape
- Tensile reinforcement ratio
- Aggregate size
- Beam slenderness

- Tensile strength and ductility of SFRC

As mentioned earlier the ductility of SFRC is affected by the fiber's property to pullout and bridging of cracks. However the distribution of the fibers in the concrete is not certain, which is a big issue as this is the key to develop uniform mechanical properties in SFRC. Also in SFRC beams without shear reinforcement, the widening of diagonal cracks is due to fiber pullout as opposed to shear reinforcement yielding in RC beams. The bond between fibers and concrete and the pullout of fibers is a somewhat complicated problem (Dinh, 2009).

Realizing what an important role steel fibers play in SFRC beams without shear reinforcement in enhancing the shear strength, there is need to investigate the durability of the same beam when the fibers have been subjected to corrosion.

.

## 2.3 Corrosion Theory

2.3.1 Corrosion Process

Corrosion comes from the latin word 'corrodere' which means gnaw apart. It is an electrochemical process that involves the exchange of electrons. Oxygen and humidity are the two parameters needed for corrosion to take place. The oxidation-reduction process in iron is as shown below where Equation 2.1 shows the oxidation process and Equation 2.2 the reduction reaction whereas Equation 2.3 is the resultant from the two processes.

$$Fe \rightarrow Fe^{2+} + 2e^{-} \tag{2.1}$$

$$\frac{1}{2}O_2 + H_2O + 2e^- \rightarrow 2OH \qquad (2.2)$$

$$Fe + \frac{1}{2}O_2 + H_2O + 2e^- \rightarrow Fe^{2+} + 2e^- + 2OH^- \qquad (2.3)$$
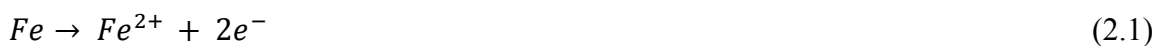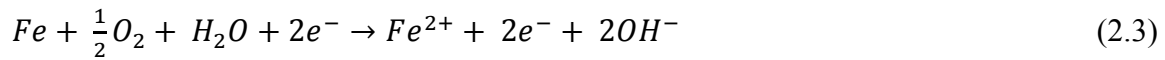
Types of corrosion commonly occurring in metals are as follows;

| | |
|---|---|
| Uniform | Corrosion fatigue |
| Electrochemical | Intergranular |
| Galvanic | Fretting |
| Concentration cell | Impingement |
| Erosion corrosion | Dezincification |
| Embrittlement | Graphitization |
| Stress corrosion | Chemical recation |
| Filiform | |

Atmospheric corrosion differs from the action that occurs in water or underground in that a plentiful supply of oxygen is always present. The formation of insoluble films and the presence of moisture and deposits from the atmosphere become the controlling factor. Presence of contaminants such as sulphur and salt particles are additional compounds that accelerate the corrosion process.

Atmospheric corrosion is mainly an electrochemical process rather than a chemical process. Since the cathodic and anodic areas are usually small and close together, the corrosion is apparently uniform rather than in form of severe pitting that occurrs in water or in soil.

Pitting is often caused when there is a difference in dissolved oxygen concentration. A part of metal which is in contact with water relatively low in dissolved oxygen is anodic to adjoining parts that are high in dissolved oxygen.

Due to the different spatial locations of anode and cathode, corrosion of steel in concrete can occur in different forms.



$$Fe^{2+} + 2OH^- \rightarrow Fe(OH)_2 \quad \text{Ferrous Hydroxide}$$

$$4Fe(OH)_2 + O_2 + 2H_2O \rightarrow 4Fe(OH)_2 \quad \text{Ferric Hydroxide}$$

$$2Fe(OH)_2 \rightarrow Fe_2O_3.H_2O + 2H_2O \quad \text{Hydrated Ferric Oxide (rust)}$$
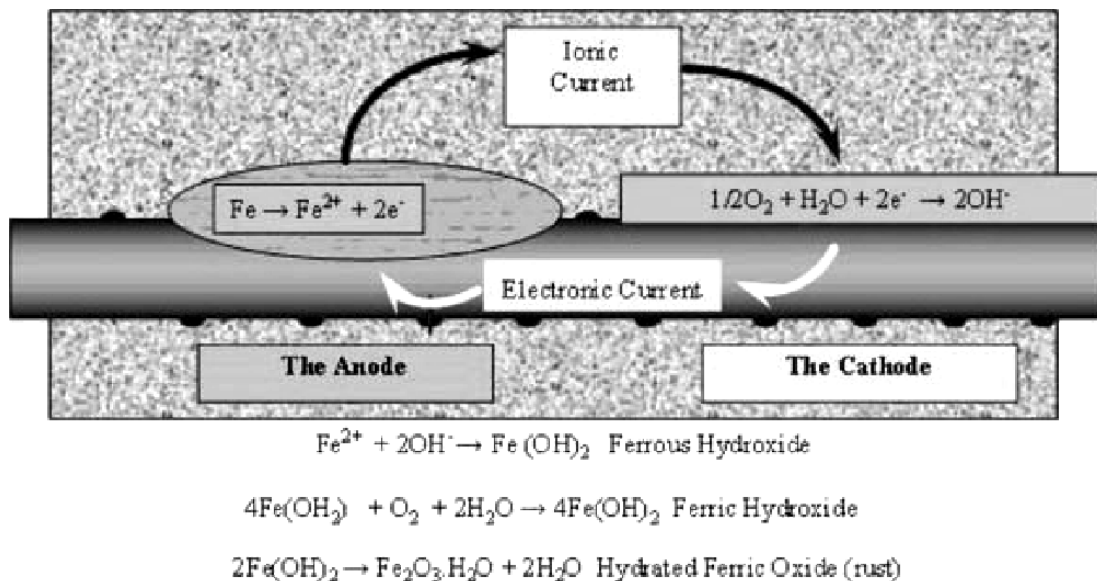
Figure 2.10 Corrosion process (adapted from BS EN 1504)

- Microcells: the anode and cathode are immediately adjacent to each other leading to uniform iron dissolution over the whole surface. Uniform corrosion can usually

24

be caused by high chloride content at the reinforcement bars or carbonation of the concrete.

- Macrocells: There is a clear distinction between the corroding part of the bar (anode) and the passive part of the bar (cathode).This normally happens in chloride induced environment because the anode is smaller in respect to the total rebar area (Jaggi et al., 2001).

All structural metals corrode to some extent in natural environments. Bronzes, brasses, stainless steels, aluminium and Zinc corrode slowly under the service conditions which they are placed and are expected to survive for long periods without protection. However, corrosion of structural grades of iron and steel proceed rapidly unless the metal is adequately protected.

The presence of an electrolyte is a key condition for corrosion process to occur. Therefore water and especially salt water is an excellent electrolyte.

### 2.3.1.1 Initiation by Chloride

Chloride-induced reinforcement corrosion is one of the most common durability problems associated with reinforced concrete structures exposed to marine environments. The time needed for corrosion initiation depends on how fast chloride ions penetrate the concrete cover and the critical chloride concentration needed to deteriorate the steel reinforcement (Kuhail et al., 2010). Seawater contains a great number of elements in different proportions. These elements in solution combine and precipitate as salts with the evaporation of seawater.

The critical chloride content in the concrete from which steel corrosion develops depends on many factors, namely:

- type of binder (particularly its C3A content);

- proportion between free and bond chlorides;

- ratio between the chloride ion and the hydroxyl ion contents;

- water/binder ratio;

- temperature and relative moisture;

- electrochemical potential of steel.

Sandberg (1995) suggested that the mechanism of corrosion initiation by chloride ions occurs as follows:

The dissolution of iron oxide occurs in the presence of chloride ions as shown:

$$2Fe_2O_3 \rightarrow 4Fe^{2+} + 3O_2 + 8e^- \quad\quad (2.4)$$
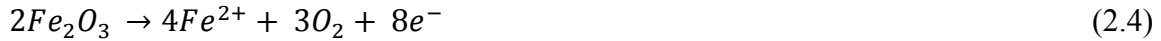
Soluble iron chloride at the interface steel/concrete is formed by the equation below:

$$Fe^{2+} + 2Cl^- \rightarrow FeCl_2(aq) \quad\quad (2.5)$$
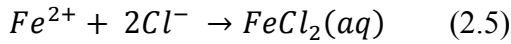
Should oxygen be easily accessible close to reinforcement, oxidation of iron ions $Fe^{2+}$ to $Fe^{3+}$ will take place and the medium at the pitting zone will be acidified according to the equation:

$$4FeCl_2(aq) + O_2 + 6H_2O \rightarrow 4FeO.OH + 8HCl(aq) \quad\quad (2.6)$$
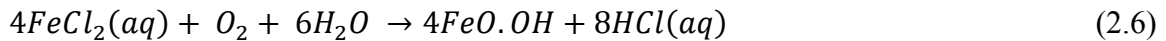
In cases whereby access of oxygen is limited, there can be either two types of situations as seen.

$$Fe^{2+} + 2Cl^- + xH_2O \rightarrow FeCl_2xH_2O(s) \quad\quad (2.7)$$

$$FeCl_2(aq) + 2OH^- \rightarrow Fe(OH)_2(s) + 2Cl^- \quad\quad (2.8)$$
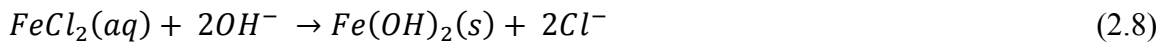
In Equation 2.7, the dissolution of iron oxide results in stable hydrated iron chloride while Equation 2.8 shows the dissolution of the resulting iron chloride.

Wetting and drying cycles can increase the rate of corrosion in reinforced concrete structures as a result of the chloride ion concentration. Increase in rate of corrosion occurs during the drying phase by the evaporation of water. Concrete structures, subjected to cyclic wetting and drying of seawater, are more liable to deterioration compared to those permanently immersed in seawater. The zone where the water splashes on the concrete is claimed to be the area most vulnerable to corrosion due to these wetting and drying cycles. Surface levels of chloride have been found to be the highest in this area though the depth of penetration is little different from immersed concrete. Underwater concrete has generally been found to be less permeable than concrete above water. This is probably as a result of the pores in the concrete being blocked by materials formed from chemical reactions with seawater like brucite and aragonite (Kuhail et al., 2010).

### 2.3.1.2 Initiation by Carbonation.

The carbon dioxide reacts with both hydrated and non-hydrated cement components. The most significant reaction is the one involving calcium hydroxide. Concrete carbonation is usually represented by the reaction:

$$Ca(OH)_2 + CO_2 \xrightarrow{H_2O} CaCO_3 + H_2O \qquad (2.9)$$

Other additional reactions are nonetheless possible, this include the CaO group of some components combining with carbon hydroxide to form calcium carbonate and hydrated silica as shown by the reaction:

$$3CaO.SiO_2 + 3CO_2 + yH_2O \rightarrow SiO_2.yH_2O + 3CaCO_3 \hspace{2cm} (2.10)$$

$$2Cao.SiO_2 + 2CO_2 + yH_2O \rightarrow SiO_2.yH_2O + 2CaCO_3 \hspace{2cm} (2.11)$$
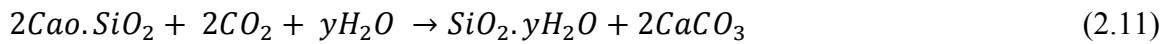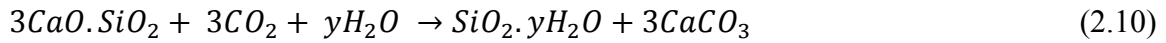
Calcium carbonate comes in the form of minerals like calcite, aragonite and vaterite, with calcite being the most stable form. The proportion of the different forms depends on the hydration level. Concrete forms a thin carbonated surface layer with no regard to the quality of the concrete. Due to the difference in concentration between the atmosphere and the porous structure of the concrete, the carbon dioxide disseminates through the porous structure of the concrete and is likely to progress until reaching the reinforcement. Carbonation causes a decrease in the pH of the concrete to about 8.5, value for which the passivation film is no longer thermodynamically stable.

The rate of carbonation is significantly influenced by several interacting factors. The main factors are:

- the permeability of the concrete

- the calcium dioxide content and the CaO available for the reaction

- the concentration in carbon dioxide

- the exposure conditions.

2.3.2 Factors Affecting Corrosion of Steel in Concrete

A large amount of calcium and other alkaline hydroxides form in concrete made with Portland cement during the liquid phase and the initial hardened state. The high alkalinity (pH between 12 and 13) results in an insoluble oxide film which forms on the surface of the steel which is protected from further corrosion while the film is unbroken. However, a weak carbonic acid is formed by the atmospheric carbon dioxide which reacts with the

alkalis in the pore water to form carbonates. This reduces the pH and thus the film is lost and with presence of water and oxygen, corrosion can occur.

A number of factors accelerate the corrosion of steel especially those that increases conductivity, acidity or provide oxidizing agents. Some of these factors are discussed below.

*Quality of Concrete*

Since the pH of cement paste in neutral water is about 2.5 and steel is essentially passive in alkaline solution, just a thin coat of cement paste on steel is sufficient to prevent corrosion of steel. This coat may sometimes not be uniform along the entire length of the steel and due to this; the quality of the concrete matrix plays an important role in preventing corrosion (Shroff, 1966).

The permeability of concrete is perhaps the single most important factor affecting the corrosion of reinforcement provided that there are no cracks or honeycombing. Concrete of high permeability will allow the penetration of deleterious substances to the reinforcements and due to presence of ions it will also have a low electrical resistivity. Permeability depends on a number of factors such as: quality of mix, water-cement ratio, aggregate size, aggregate grading, curing, method of compaction etc. Use of sea water as mixing water is one of the sources of contaminants introduced into the concrete. Seawater especially introduces chloride ions which makes the pore water a good electrolyte and disrupt the protective coating on the surface of embedded steel. It has been proved the consistency of mortar and concrete has a more pronounced effect on the rate of rusting.

Concrete or mortar mixes that had a plastic consistency were shown to offer the best protection compared to mixes that were either too dry or too wet.

*Heterogeneities of the Concrete Surrounding Embedded Steel*

The heterogeneous nature of the concrete matrix surrounding steel may exist as: differential-aeration cells, metal ion cells or salt concentration cells. Heterogeneities are sometimes due to differences in velocity, temperature and impingement.

*Factors Associated with Steel*

The heterogeneous nature of the steel may cause the steel to display differences in effective potential thus establishing probable corrosion cells. The heterogeneity of the steel may be caused by differences of chemical composition over the surface, discontinuity of the steel surface or differences in texture. Surface conditions are taken to be more important than the bulk metal characteristics when it comes to total corrosion.

*Environment or Location of the Reinforced Concrete Structure*

Reinforced concrete structures may be built in a number of environments that may affect the rate of corrosion. These environments include soil, water and atmosphere. It should be noted that irrespective of the environment, moisture in the air greatly affects the rate and extent of corrosion of embedded steel in concrete. In the absence of moisture, all corrosive factors such as oxygen, carbon dioxide, sodium chloride etc. cannot penetrate into the concrete. It has been observed that if the relative humidity of the region surrounding the concrete is less than 50%, the corrosive action may be reduced to zero.

However of more importance is the presence of chloride ions which destroy the inherent property of concrete to inhibit corrosion. The threshold level of chloride concentration, above which corrosion may develop in the presence of moisture and oxygen, may be as low as about 0.20% total chloride by weight of cement (Banthia et al., 1989). Therefore in marine environment where sea water and windblown salt can increase the chloride ion content and also in highways where deicing salts is used to get rid of ice on the road, corrosion may occur.

*Depth of Concrete Cover*

This is an important factor to be considered with permeability of the concrete mix and location of structure. The concrete cover should be thick enough to protect the embedded steel and should be of even thickness throughout. The evenness of the cover is more decisive in protecting the steel that its density.

2.3.3 Stages of Steel Corrosion

There are two stages of corrosion in steel (Tuutti, 1982). The first stage involves the transfers of aggressive elements, such as chloride and carbon dioxide due to presence of water and oxygen, inducing the corrosion initiation. This is also called the initiation stage. The second stage known as the propagation stage involves the growth of corrosion leading to concrete damage, spalling and cracks in concrete. It starts when these aggressive elements are in high concentrations at the reinforcement level.

Stages of corrosion with rusting

(1) Initiation

(2) Propagation

(3) Concrete cracking
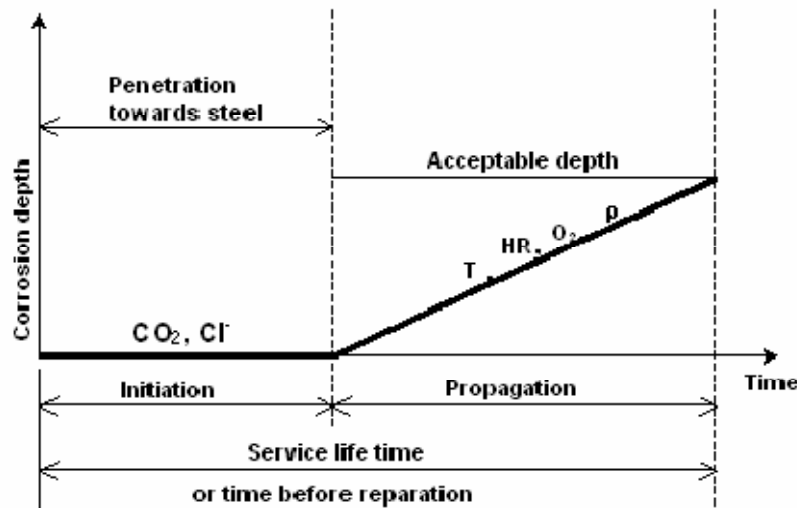


Figure 2.11 Stages of Corrosion (adapted from Tuutti, 1982)

## 2.4 Previous Research on Corrosion of Fibers in SFRC

A number of papers have been written relating to the topic of durability of steel in concrete and specifically on Fiber reinforced concrete. Below is a brief description of the researches done and their findings.

Naaman and Kosa (Naaman et al., 1990) investigated the deterioration of steel fiber reinforced concrete due to fiber corrosion. They conducted two parallel test programs, one dealt with the effect of corrosion on steel fiber reinforced mortar specimens and the other using precorroded steel fibers in mortar specimen. They used different exposure periods with typically three days intermittent drying and wetting in 3.4 percent standard sodium chloride solution and in laboratory air. The Figure 2.12 and Figure 2.13 below

shows the flow chart of the experimental program adapted for the accelerated corrosion

test and precorroded fibers test respectively.

| Composite type | Mortar mix | Exposure condition | Type of loading | Exposure time [*] prior to testing |
|---|---|---|---|---|
| SFRM | High permeability | 50 C (A) | FLEXURE / TENSION | 2 months / 6 months / 9 months |
| | | | COMPRESSION | 2 months / 6 months |
| | Carbonated | 50 C (B) | FLEXURE / TENSION | 2 months / 6 months / 9 months |
| | Crack (large size) / Crack | 50 C (C) / 50 C (D) | FLEXURE | 2 months / 6 months / 9 months |
| | Crack | 20 C (E) / 50 C (E) / 80 C (E) | FLEXURE | 2 months / 6 months / 10 months |

[*] Exposure condition

Each cycle consists of three days of saturation in sodium-chloride water
at the indicated temperature and three days of drying at room temperature

Specimen (A) : High permeability specimens
Specimen (B) : Carbonated specimens
Specimen (C) : Precracked specimens loaded to a 0.12 in. deflection point
Specimen (D) : Precracked specimens loaded to peak strength
Specimen (E) : Standard specimens

Figure 2.12 Flowchart for accelerated corrosion tests of steel fiber reinforced mortar
(SFRM) specimens (Naaman and Kosa, 1990)

| Composite Type | Exposure Condition | Period of Exposure |
|---|---|---|

```
                    ┌──────────┐
                 ┌──┤  20 C    ├──┐
┌────────┐       │  └──────────┘  │    ┌──────────┐
│ SFRM   ├───────┤  ┌──────────┐  ├────┤ 1 month  │
└────────┘       ├──┤  50 C    ├──┤    │          │
                 │  └──────────┘  │    │ 2 months │
                 │  ┌──────────┐  │    │          │
                 └──┤  80 C    ├──┘    │ 3 months │
                    └──────────┘       └──────────┘
```
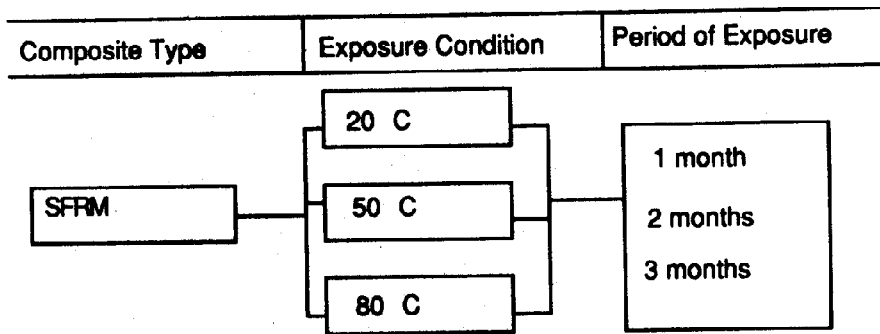
* Exposure condition for typical cycles
  Steel fibers were saturated in sodium-chloride water at indicated temperature
  for 3 days, and dried at room temperature for 3 days.
* After exposure, the fibers were used in mortar to build flexural specimens with a 0.42
  W/C ratio
* Each series of tests comprises 6 to 12 specimens.

Figure 2.13 Flowchart for test using pre-corroded fibers (Naaman and Kosa, 1990)

The effects of corrosion were evaluated through the mechanical properties of the composites in direct tension, compression and bending. Also toughness, evaluation of corroded surface of fibers and measure of the minimum diameter of fibers after exposure was evaluated.

Experimental results seemed to indicate that after a certain degree of exposure, strength and toughness decrease with increase in degree of corrosion. These were caused by increased reduction in minimum fiber diameter due to corrosion. However no cracking was detected on the surfaces of the steel fiber reinforced concrete specimens subjected to corrosion despite the change of coloring at the surface from orange to dark brown. Upon observation of the fracture surfaces of SFRC specimens tested in tension and bending, he concluded that the effect of corrosion on the minimum fiber diameter gradually changes the type of failure from fiber pullout to fiber breakage before failure. Results from pre-

corroded fibers led to similar conclusions. In certain levels of corrosion, Naaman found out that the reduction in toughness became more dramatic than the reduction of strength. He developed a simple analytic model that accounts for the reduction in minimum diameter of fibers on the tensile properties which led to predictions that supported the experimental observations.

Schiessl and Weydert (Schiessl, et al., 1998) studied corrosion mechanism in cracked SFRC. Also included were a few sprayed concrete samples. Corrosion was initiated by both the ingress of chlorides and carbonation. The beams were sawn out from large slabs. Crack widths were between 0.05-0.4mm and were divide into two test rounds. After exposure the beams were evaluated dismembering into small plate around cracked area and creating chloride profiles both from the exposed surfaces as well as perpendicular to the crack surface.

No significant correlation between crack widths and chloride content could be found. The experiment showed decreasing chloride content with increasing distance from crack opening same goes for the extent of corrosion. They suggested that no critical crack width can be stated under which corrosion does not occur since chlorides can still penetrate very thin cracks.

In the accelerated carbonation, fibers still did not corrode to great extent. Authors suggest this is due to lack of humidity thus suggesting that humidity is the ruling factor. Galvanized fibers were also tested and although they gave a delay in initiation of corrosion, they still corroded after some longer exposure.

Mangat & Gurusamy (1985, 1987) in their first investigation aimed at defining the chloride diffusion in SFRC exposed to a marine environment. The specimens were sprayed with seawater in the laboratory to simulate tidal marine situation. The chloride penetration was measured both from the exposed surface as well as 10mm perpendicular to the crack surface. They could not find any significant difference between SFRC and plain concrete. They also stated that chloride diffusion coefficient decreased with time due to both continued hydration and by deposit of a brucit-like material formed from ions in sea water. Chloride concentration increases with increase in crack width. At crack widths above 0.5mm the effect is significant while below 0.2mm there was no different from un-cracked specimen.

In another article Mangat and Gurusamy (1987) presented results on residual strength. Pre-cracked specimens of SFRC which were exposed to wet and dry cycles of marine spray in the laboratory were tested. They used two types of concrete mixes, one with standard concrete constituents and OPC and the other substituting about 26% of cement with pfa. Low carbon steel fibers and melt extract steel fibers were used at an aspect ratio of 100 and 147 respectively. Prism specimens measuring 100 x 100 x 500 mm were cast and pre-cracked to induce cracks of widths ranging from 0.03 and 1.73mm. Test were carried out on the specimens after 650 marine cycles and 1450 marine cycles to determine the flexural strength, energy absorption capacity, stiffness and state of corrosion of the fibers.

He observed at crack widths below 0.2mm there was increase of residual strength compared to un-cracked. This he explained as autogenous healing and/or increased anchorage of fibers. He also concluded that pitting is initiated in low-carbon steel fibers and melt-extract fibers bridging cracks of widths greater than 0.24mm and 0.94mm respectively. The researchers therefore recommend 0.2mm as the permissible crack width for SFRC using melt-extract fibers and a lower limit than this for low carbon steel fibers.

Mangat (1987) also tested the effect of different steel quality. Three types of steel fiber were used namely; low carbon steel, corrosion resistant and melt extract steel fibers. The aspect ratio of the three fibers was maintained at a constant value in order to facilitate direct comparison of their reinforcing efficiency. 100 x 100 x 500mm prisms and 100 x 100 x 100mm cube specimens were cured under marine exposure both in the laboratory and under normal environmental conditions (Aberdeen beach) for up to 2000 wet-dry cycles. The specimens were tested to determine their long-term compressive strength, flexural strength and ductility. He showed that low carbon fibers did not show any corrosion below crack widths of 0.24mm.Stainless steel fibers showed corrosion above crack widths of 0.94mm due to the stability of the passive oxide layer on the fibers. The authors concluded that low carbon steel and corrosion resistant fibers exposed at the surface of the concrete specimens are prone are prone to corrosion under marine exposure while melt extract fibers displayed no such corrosion. The results indicated that melt extract fibers are the most suitable for marine applications although they are the least effective in mechanical strength.

Hannant & Edgington (1975, 1976) investigated the effect of steel fibers corrosion in cracks on the remaining load carrying capacity. Experiments were not accelerated and cracking on the beams were performed eight days after concreting. Some samples showing most damage at precracking had their cracks sealed before exposure. Evaluation of the load carrying capacity was made before exposure and after different exposure lengths. Due to uneven fiber distribution, a relatively large scatter in ultimate load occurs. The residual strength generally increased after exposure though corrosion was initiated. Carbonation of the crack surfaces occurred and the depth of the area with corroded fibers increased with increased time of exposure. The sealed specimens showed little or no increase in load carrying capacity. Hannant et.al (1975) states that residual strength is not an efficient tool to determine rate of corrosion due to increase in load carrying capacity despite different degree of corrosion.

From another 8 months of exposure Hannant (1976) uses a model to estimate the bond strength the fiber and concrete with results from flexural loading as base. He suggests that increased bond possibility can be derived from shrinkage around fibers. From the model he suggests that fiber diameter has to be reduced with 52% before turning from bond failure to tensile fiber failure.

Teruzzi and Cadoni (Teruzzi et al., 2004) investigated the durability aspects of steel fiber reinforced concrete. The research aimed to answer the following questions:

- Can presence of fibers introduce preferential ways for ingress of aggressive agents?

- How does the durability of the mix change in terms of freeze-thaw resistance, carbonation resistance, and chloride and oxygen permeability?

Three mixtures were chosen, two for the construction of industrial floors: one for an internal environment and one for an external environment. The third mixture was selected for construction of precast elements for industrial halls. Three mixtures not having fibers were also prepared for comparison purposes.

The researchers conducted tests on the specimens which were aimed at evaluating the following properties of the concrete.

Fracture properties: Four point bending tests were performed on beams having a size of 150x150x600 mm with a 45mm depth notch.

Mechanical properties:  Tests were performed after 28 days curing to determine the compressive strength, flexural strength, splitting tensile strength, the elastic modulus and shrinkage coefficient after 90 days.

Durability affecting properties: Some tests were performed to determine concrete properties that affect durability like chloride diffusion, oxygen permeability, and total air-void porosity.

They concluded that fibers slightly reduce compressive strength of normal concrete while they increase the compressive strength of high strength concrete. Also the splitting tensile strength and the elastic modulus as well as the shrinkage coefficient are not influenced by the presence of 40-60Kg/m$^3$ of steel fibers.  Fracture tests on notched beams specimens

evidenced the enhanced toughness of SFRC.As of concerning durability; the researchers concluded that addition of steel fibers does not induce any significant change in the concrete performance. Their research demonstrated the fact that fibers or more precisely, the concrete boundary zone around the fibers does not act as a preferential path for the penetration of degradation agents.

Schupack (Schupack, 1985) conducted an experimental program in three different aggressive environments. In 1975 he installed 39 SFRC and 11 reference plain concrete beams at half tide elevation on the exposure rack at treat Island, Maine to determine the effects of sea water and freezing and thawing action on the flexural strength and other properties of various fiber concrete.

The field evaluation methods used were:

-Frequency reading: Where the transverse frequency at regular intervals during exposure.

-Pulse velocity readings at regular intervals during exposure.

-Visual inspection.

The beams were made from 9 different mixtures. The number and types of beams exposed were: 12 152 x 152 x 762 mm, 21 152 x 152 x 914 mm, 17 229 x 229 x 1143 mm. The 229 x 229 x 1143 mm beams were yoked and stressed by 3-point loadings of 35% of the ultimate.

The results led to these conclusions:

- Beams with low air behaved the poorest.

- Beams with high air and low percentage of fibers behaved the best.

- At the time of publishing the paper, the beam had not been evaluated for the depth of corrosion so it was still unknown.

- There seems to be a trend showing that air entrained SFRC with lower percentage of steel fibers performs better than a high percentage in this environment and for these concrete mixtures.

Shroff (1966) investigated the effect of a corrosive environment on the properties of steel fiber reinforced portland cement mortar. He studied the corrosion of steel fibers using two types of mortar- one plain cement mortar and the other with calcium chloride and air-entraining admixtures. These were exposed to intermittent immersions in salt water while the control specimens were submerged in tap water.

He cast small beam samples measuring 17 x 2 x 1 inch and these were tested in triplicate for load-deflection characteristics under third point loading. The test was carried out after periods of submersion in salt water for 90 days. He conducted a subsidiary study on 8 x 2 x 1 inch prismatic specimens in triplicate for the fundamental frequency in transverse and torsional vibrations in order to evaluate the bulk properties of the matrix. Microscopic examination of polished cross-section of the fiber-reinforced mortar was used to determine the extent of corrosion after a period of 30, 60 and 90 days of alternate immersion in 3.5% salt water.

He observed that the flexure tests indicated no change in mechanical behavior of the beam specimens during the 90 days period of exposure. Sonic test also seemed to support this observation. From his microscopic tests he also observed no general corrosion of the steel fibers in the beams. He concluded that the mortar used was apparently rich enough to protect the fibers from corrosion.

Granju and Balouch (2004) investigated the effect of corrosion of fibers on the spalling of concrete as well as its influence on the durability of the structure. The tests were performed on cracked SFRC specimens with 0.5mm crack widths exposed to marine-like environment for one year. Concrete prisms of 10 x 10 x 50cm in dimension were cast and cured for one week before being cracked in three positions as shown in the Figure 2.14 below.
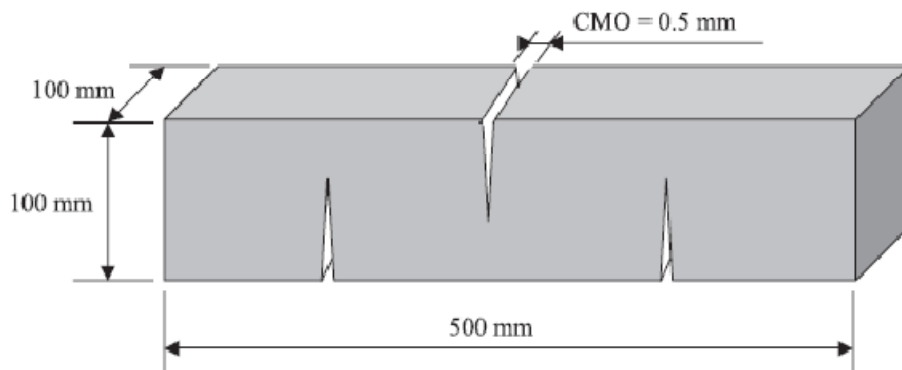


Figure 2.14 Crack positions (Granju and Balouch, 2004)

The prisms were then loaded in three-point bending on a span of 20 cm. The results showed that the crack-bridging strength of the fiber reinforcement was not weakened by corrosion. Due to an increase in the flexural strength in the specimens with open cracks,

the researchers came to the conclusion that the light corrosion that had developed at the surface of the fibers enhanced their bond through increased friction with the cement matrix. The visual examination carried out on the specimens after the flexural test showed that no concrete bursting or spalling had occurred due to corrosion of fibers. They also observed that fibers within a rim of 2 to 3mm wide from the surface of the specimen were severely corroded (Figure 2.15).
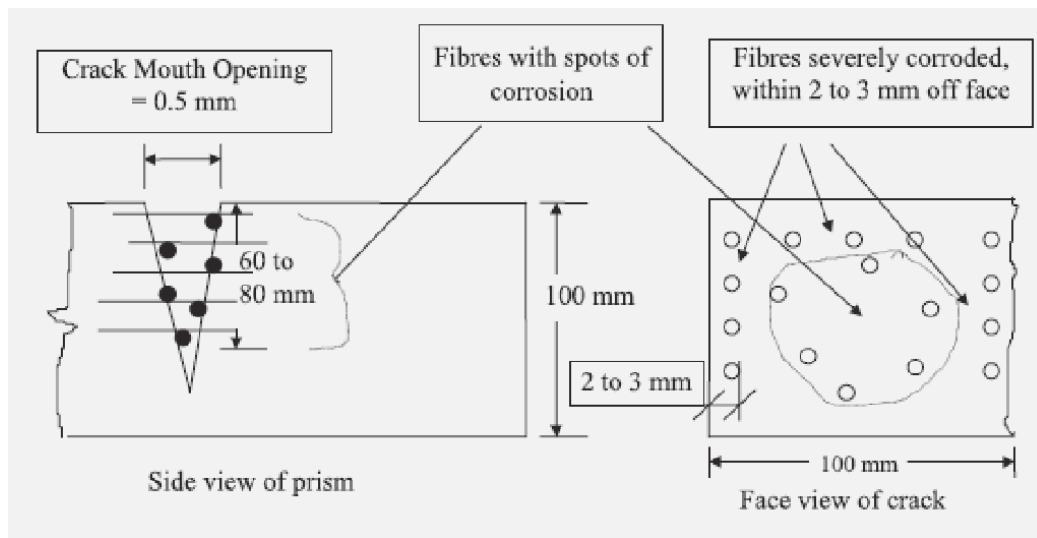


Figure 2.15 Visual examination of corrosion in the crack

They concluded that there will be no corrosion in specimens with crack widths less than 0.1mm and that the gain in strength results from the light corrosion on the surface of the fibers which makes the fiber less smooth and hence slippage of the fiber is more difficult. They also concluded that the pressure from corrosion products is not strong enough to cause spalling of the concrete.

Higgins and Farrow (2006) investigated the corrosion of stirrups and its effect on the shear capacity of conventionally reinforced concrete beams. Large size beam specimens were cast and the embedded stirrups subjected to accelerated corrosion. Three different cross sectional shapes were investigated as shown on Figure 2.16 below. The flexural reinforcement was epoxy coated to isolate corrosion to the stirrups.
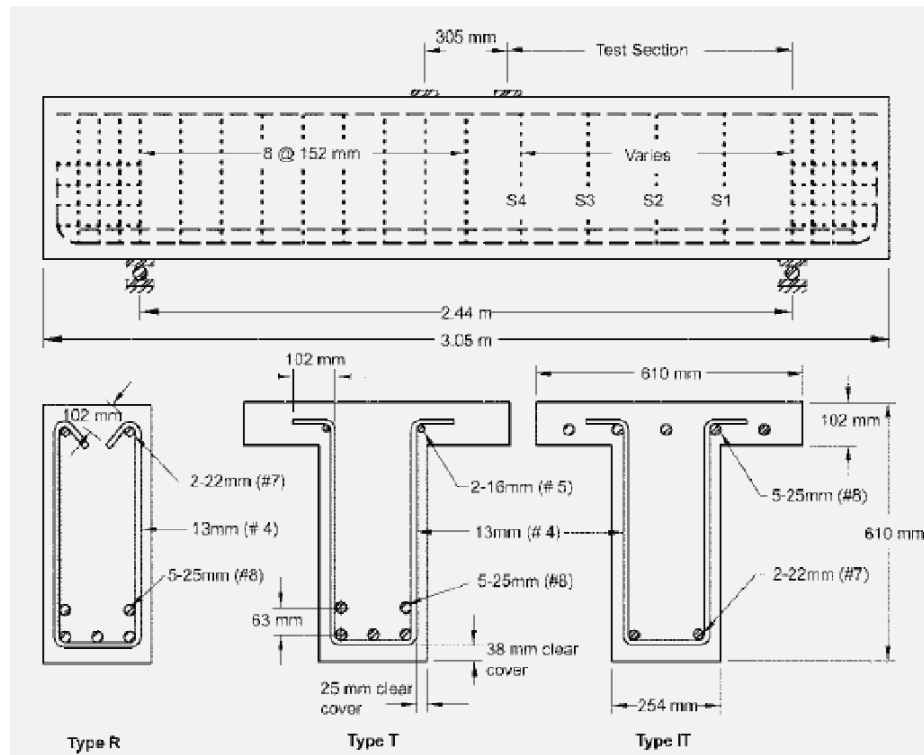


Figure 2.16 Specimen cross sections (Higgins and Farrow 2006)

The accelerated corrosion process was conducted using a corrosion cell to pass current through the stirrups within the test span. Beams were tested in four-point bending once the beams had reached the targeted corrosion damage. The beams were later visually inspected by specialists to access the damage to structural elements. The observed that

although significant areas of delamination were noted, sufficient areas of contact remained to keep the concrete cover attached. The authors concluded that the locally reduced areas on stirrups led to localized yielding and reduced ductility. Also that stirrup fracture occurred at severally corroded locations thus limiting strength and deformation capacity. The authors also concluded that diagonal cracking occurred at lower loads for uncorroded specimens and that corrosion damage reduced the ability of the stirrup to constrain diagonal cracks upon initiation.

## 2.5 Theories on Alkali-Silica Reaction

2.5.1 What is ASR?

Alkali-Silica Reaction (ASR) is the reaction between the alkali hydroxide in Portland cement and certain siliceous rocks and minerals present in the aggregates, such as opal, chert, chalcedony, tridymite, cristobalite, and strained quartz. A high alkali concentration in the pore water provides the hydroxyl ions that react with the silica to form a gel at the cementitious matrix and aggregate interface. This gel grows as it absorbs water from the environment, consequently generating expansive forces that can produce map cracking, surface pop-outs or even ultimate failure of the concrete structure as shown in Figure 2.17 and 2.18 below. The presence of gel does not necessarily indicate destructive ASR because some gel expand very little or not at all (ACPA, 2007).The amount of gel and the swelling pressure exerted are very variable depending on reaction temperature, type and proportion of reacting materials, gel composition, and other factors. Like other deterioration processes, ASR is a time-dependent phenomenon. It occurs during the service life of a structure (often after several years of satisfactory performance) and gives

external warnings of internal damage. ASR generally appears to be harmless to the useful life of a structure. Although there are few number of structures actually affected by ASR, experience has shown that, when considered in the context of construction globally, the effects of ASR can be very profound to concrete structures, affecting strength, stiffness, serviceability, safety and stability. ASR is more complex and unusual because it is much more difficult to recognize, identify and monitor. Furthermore it provides a means through which other deterioration mechanisms can develop and operate, and indeed structures affected by environmental or other structural deterioration may provide favorable conditions for the reappearance of a dormant ASR problem (Swamy, 1992).

```
┌─────────────────────────┐      ┌─────────────────────────┐
│ Alkali Ions and Hydroxyl │─────│    Siliceous Material    │
└─────────────────────────┘      └─────────────────────────┘
                     │
            ┌─────────────────┐
            │  Alkali-silica gel │
            └─────────────────┘
                     │
                     │            ┌──────────┐
                     │◄───────────│  Water   │
                     │            └──────────┘
            ┌─────────────────┐
            │  Gel Expansion  │
            └─────────────────┘
                     │
            ┌─────────────────┐
            │    Cracking     │
            └─────────────────┘
               │            │
    ┌──────────────┐  ┌───────────────────┐
    │ Strength loss │  │ Serviceability issues │
    └──────────────┘  └───────────────────┘
```
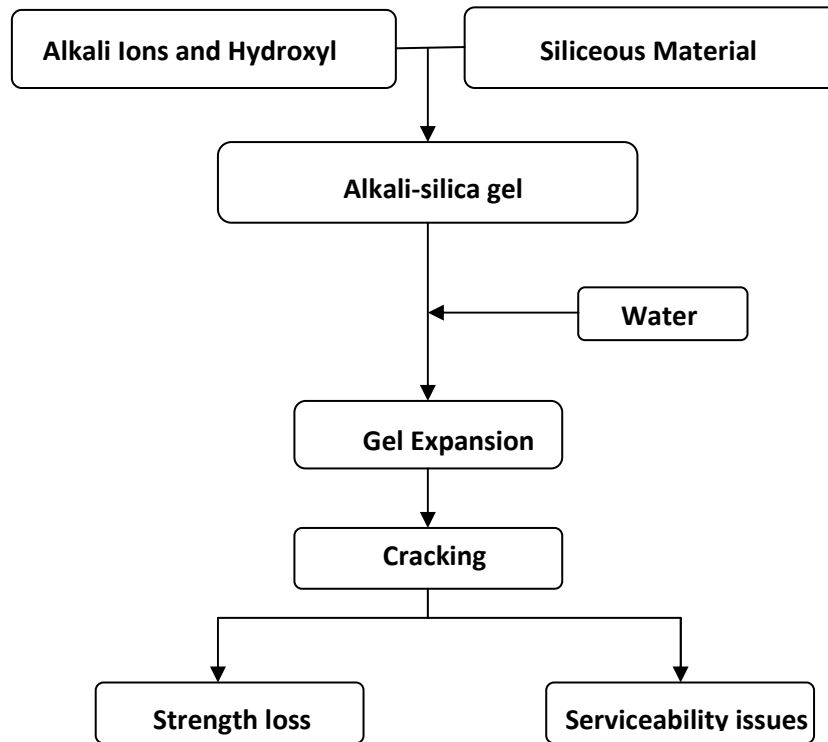
Figure 2.17 Schematic illustrating the effects of ASR

46

Figure 2.18 Noticeable cracking, joint closing and spalling of concrete surface on parapet wall due to ASR (adapted from ACPA, 2007).

2.5.2 History of ASR

As early as nineteenth century it was realized that, although concrete was a very durable material, it could deteriorate with frost and seawater as the principal agents. Although quite acceptable standards of construction and quality control of materials were employed, a number of concrete structures were observed to develop severe cracking within a few years of their construction during the 1920s and 1930s (Swamy, 1992).

ASR was first explained in a comprehensive way by Thomas E. Stanton in 1940 in his publication from his investigation of cracked concrete structures in California. He proposed that the deterioration was caused by expansion of a gel generated by the reactive silica from the aggregate and the alkalies from the cement. Stanton with his research team investigated several cases of damaged concrete by alkali-silica reaction and concluded the following:

- In plain concrete, ASR generates cracks in form of maps or alligator skin.

- In reinforced concrete the cracks tend to form parallel to the reinforcing bars.

In 1941, Blanks and Meissner described cracking and deterioration in the concrete of Parker dam. They showed that ASR product was being produced in the concrete by reactive components in the aggregate which represented 2% of the total aggregate. During the following decades research on alkali-aggregate reaction was carried out in many laboratories, first in United States but later in Europe, Canada and other parts of the world. In 1974 the first series of international meetings of scientists interested in alkali-aggregate reactivity in concrete was held in Denmark; the Portland Research and Development Seminar on ASR at Køge (Swamy, 1992).

2.5.3 Conditions for ASR

The conditions required for ASR to occur are:

- Sufficiently high alkali content of the cement or from other sources.

- aggregate with reactive silica

- Water - since alkali-silica gel formation requires water

The parameters strongly affecting the ASR expansion are temperature, humidity and confining stresses.

*2.5.3.1 Alkalies*

The majority of structures that have been reported as showing deterioration due to ASR were constructed using high-alkali cement (Swamy, 1992). Sodium oxide and potassium oxide ($Na_2O$ and $K_2O$) are generally derived from Portland cement but may be derived

from pozzolans, chemical admixtures and in rare cases, aggregates. They may also be available from external sources like deicing salt (alkali-acetate and alkali-formate deicers), sea water, soils and industrial processes. The alkali content of cement is given as the weighted average of potassium and sodium ions according to the following equation:

$$Na_2O_e = Na_2O + (.658)xK_2 \hspace{4cm} (2.12)$$

The alkali-silica reaction cannot proceed in the concrete if the alkali concentration is below a certain threshold value. A report made by Hawkins suggested that to minimize or avoid the risk of damage to concrete, the alkali content of the cement used should be below 0.6% by weight and that from the mass of alkalis from all sources should be kept below 3.0kg/m$^3$ in the concrete. The effects of the reaction are observed in some cases where the alkali levels are well below the minimum of 3.0kg/m$^{3.}$ Several possibilities arise from this observations .The low alkali figures obtained from concrete structures may be the results of alkalis having been leached from the structure with time. From detailed electron probe microanalysis, although the overall alkali levels in the cement paste may be very low, the reacting aggregates in the same concrete may be very high in alkalis. It should not be overlooked that the addition of alkalis to the concrete from other sources can occur although the principal source is the cement. Although mix water will not normally contain significant amount of alkali, there is a possibility that sodium chloride will be incorporated into the mix, for example by the use of seawater (Swamy, 1992). As the pH, or alkalinity, of the pore solution increases, the potential for ASR increases. At higher concentrations of alkali hydroxides, even more stable forms of silica are susceptible to attack (Bauer, et al., 2006).

*2.5.3.2 Silica*

The type and forms of silica that are present in the aggregate dictate the reactivity of silica (silicon oxide) in an aggregate. Completely crystalline silica is usually chemically and mechanically stable whereas completely amorphous silica is more porous and very reactive.

An aggregate that is poorly crystalline, amorphous, glassy, and micro-porous, and that has many lattice defects presents a large surface area for reaction and is susceptible to attack from alkali hydroxides.

The potential reactivity of an aggregate is thus a function of both the degree of crystallization of the silica in the aggregate and the amount of energy stored in the crystal structure. The surface area per unit volume of the reactive silica will affect the rate of reaction. The silica content of an aggregate also influences its reactivity.

An essential requirement for ASR to take place is a certain form of silica even though the volume needed to produce deleterious effects need only be very small. In certain cases where severe distress has been observed in certain structures, the volume of reactive component was as little as 2% (Swamy, 1992). Many varieties of rocks used as aggregates may contain a small proportion of reactive silica as part of their constituents. It is therefore only through some laboratory test results that an aggregate can be declared as reactive or not. It is incorrect to consider rock type as a clear indication of aggregate potential for reactivity. It is much more important to focus on the constituents in the rock (Swamy, 1992).

Aggregates containing the following constituents in the quantities are considered potentially reactive:

• Opal – more than 0.5% by mass

• chert or chalcedony – more than 3.0%

• tridymite or cristobalite – more than 1.0%

• Optically strained or microcrystalline quartz – more than 5.0%

• Natural volcanic glasses – more than 3.0% (Farny, et al., 1997)

*2.5.3.3 Moisture*

Concrete will not suffer from deleterious ASR if it remains dry throughout its service. The presence of sufficient moisture allows the migration of alkali ions to reaction sites, and the reaction product gel absorbs moisture, leading to expansion. Expansive ASR can occur in concrete that has a relative humidity above 80 percent. A reduction in permeability through the use of a low water-cement ratio, supplementary cementing materials, or other means, reduces the movement of moisture and alkalis into and within the concrete. It has been found that lower

water-cement ratio (0.35) concretes expand significantly less than higher water-cement ratio concretes at ages up to 19 months (Farny et al., 1997), but at later ages, ASR has been known to even in low water-cement ratio plain concrete mixtures.

2.5.4 Process of ASR

An alkali-silica gel is produced as a result of the reaction between the alkali pore fluids in the concrete and siliceous components of the aggregate particles. As it absorbs moisture it increases in volume thus generating pressures sufficient to disrupt the fabric of the

concrete (Swamy, 1992). ASR can be described as a two-step reaction between alkalis (sodium and potassium) in concrete and silica reactive aggregates.

The first step is the chemical reaction between the reactive silica in the aggregate with the alkali present in concrete to produce alkali-silica gel.

Reactive silica in aggregate + alkali in concrete →alkali-silica gel

$$4SiO_2 + 2NaOH = Na_2Si_4O_9 + H_2O \qquad (2.13)$$

$$SiO_2 + 2NaOH = Na_2Si_3 + H_2O \qquad (2.14)$$
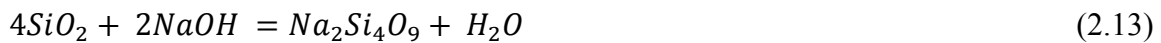
The second step is the expansion of the alkali-silica gel when it comes in contact with moisture

Alkali-silica gel + moisture → expanded alkali-silica gel

The swelling pressures produced by the gel induce the formation of microcracks close to the reaction sites, these progress and combine to form cracking in the concrete and overall expansion of the structural elements affected (Swamy, 1992).It is expected that the development of cracks will lead to the corrosion of reinforcement in the concrete. There has been little evidence of this and has been purported that the gel produced fill the pore spaces and cracks surrounding the reinforcement thus preventing the corrosion of the fibers.

However, ASR can be mitigated in concrete by three complementary approaches:

- Limit the alkali metal content of the cement. Many standards impose limits on the "Equivalent $Na_2O$" content of cement.

- Limit the reactive silica content of the aggregate. Certain volcanic rocks are particularly susceptible to ASR because they contain volcanic glass (obsidian) and

should not be used as aggregate. The use of calcium carbonate aggregates is sometimes envisaged as an ultimate solution to avoid any problem. However, while it may be considered as a necessary condition, it is not a sufficient one. In principle, limestone ($CaCO_3$) is not expected to contain high level of silica, but it actually depends on its purity. Indeed, some siliceous limestones may be cemented by amorphous or poorly crystalline silica and can be very sensitive to the ASR reaction as observed with some siliceous limestones exploited in quarries in the area of Tournai in Belgium. So, the use of limestone as aggregate is not a guarantee against ASR in itself. The silica content of the limestone and its reactivity must remain below a threshold value that has to be carefully experimentally assessed by the aggregate producer.

- Add very fine siliceous materials to neutralize the excessive alkalinity of cement with silicic acid by voluntary provoking a controlled pozzolanic reaction at the early stage of the cement setting. Convenient pozzolanic materials to add to the mix may be, e.g.,pozzolan, silica fume, fly ashs, or metakaolin. These react preferentially with the cement alkalis without formation of an expansive pressure, because siliceous minerals in fine particles convert to alkali silicate and then to calcium silicate without formation of semi permeable reaction rims.

### 2.5.4.1 Gel Product

The reaction between the alkali in the cement and the reactive silica in the aggregates produces an alkali-silica gel that swells on absorption with water. Depending on the

composition of the alkali pore fluid, nature of reactive silica, temperature of reaction and concentration of reactants, the composition of the gel varies considerably.

When a sample of affected concrete is cut open, the gel appears to be transparent, having a resinous appearance with a viscosity between that of thick motor oil and resin (Figure 2.19). Typically gels will carbonate with time and with exposure to air to become white and hard with cracks similar to the ones seen in dried mud. Researchers are advised to look for gel immediately after breaking the suspected concrete because drying of the gel on the surface of the concrete make it less visible. Cores taken from structures suspected to be affected by alkali-silica reaction are usually wrapped in layers of cling film and sealed in polythene while still moist from coring process. This is done to allow the gel to be identified on the surface on concrete when unwrapped the gel appears as shiny or sweaty patches on the surface. This occurs due to the hygroscopic nature of the gel (Swamy, 1992).
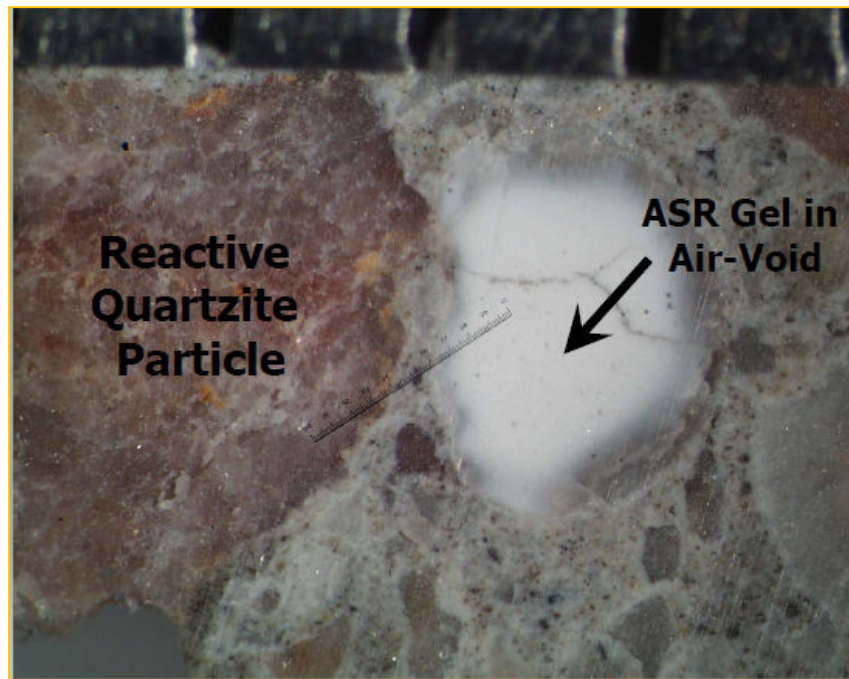
Figure 2.19 The ASR gel (Rangaraju, 2008)

Gel analyses indicate that a wide range of compositions are possible though care is necessary for their correct interpretation. This is usually because the analysis is made using an electron probe microanalyser which requires a completely dessicated specimen. Gel viscosities also exhibit a wide range of values and can produce pressures up to 11MPa. The alkali silica gel first develops at the reaction sites, as it absorbs water, it becomes less viscous until it is fluid enough to move through the cracks, filling voids and permeate the micro pores in the cement paste (Swamy, 1992).

## 2.6 Test Methods for Identification of ASR

**ASTM Standards**

A number of ASTM standards can be used to identify materials having potential ASR. Some of the tests in the Standard are outlined in Table 2.2:

Table 2.2 Current ASTM Tests on ASR

| Name of Test | Purpose | Methodology | Test Duration | Comments |
|---|---|---|---|---|
| **ASTM C 227,** Potential alkali-reactivity of cement-aggregate combinations (mortar-bar method) | Determination of the susceptibility of cement-aggregate combinations to expansive reactions involving hydroxyl ions associated with alkalies | Mortar bars stored over water at 37.8°C (100°F) and high relative humidity. Expansion is calculated as the difference between the initial length of the specimen and the length at each | First measurement at 14 days, then 1, 2, 3, 4, 6, 9, and 12 months; every 6 months after that as necessary | Not recommended as a means to detect the latter reaction. |
| **ASTM C 289,** Potential alkali-silica reactivity of aggregates | Determination of the potential reactivity of siliceous aggregates with alkalies in Portland cement concrete. | Crushed aggregates sieved to pass the 300µm sieve and be retained on a 150µm sieve, are reacted with 1 N sodium hydroxide solution at 80°C (176°F). | 24 hours | Results from this test should not be used as the sole basis for acceptance or rejection of sources with regard to ASR. |

Table 2.2- Continued

| | | | |
|---|---|---|---|
| **ASTM C 294,** Constituents of natural mineral aggregates | To give descriptive nomenclature for the more common or important natural minerals—an aid in determining their performance | Visual identification | As long as it takes to visually examine the sample | Accurate identification of rocks and minerals can in most cases be made only by a qualified geologist, mineralogist or petrographer. |
| **ASTM C 295,** Petrographic examination of aggregates for concrete | Petrographic examination of samples representative of materials proposed for use as aggregates in cementitious mixtures or as raw material | Visual and microscopic examination of prepared samples— sieve analysis, microscopy, scratch or acid tests, optical microscopy, XRD analysis, differential thermal analysis, or infrared spectroscopy | Short duration—visual examination does not involve long test periods | Petrographic examinations as described should be performed by a petrographer with at least 5years of experience. |

58

Table 2.2- Continued

| ASTM C 342, Potential volume change of cement-aggregate combinations | To determine the potential ASR expansion of cement-aggregate combinations | Mortar bars stored in water at 23°C (73.4°F) | 52 weeks | Primarily used for aggregates from Oklahoma, Kansas, Nebraska, and Iowa. |
|---|---|---|---|---|
| ASTM C 441, Effectiveness of Pozzolans or Ground Blast-Furnace in preventing excessive expansion of concrete due to alkali-silica reaction | Determination of the effectiveness of pozzolans or slag in preventing expansion from ASR | Mortar bars—using Pyrex glass as aggregate—stored over water at 37.8°C (100°F) and high relative humidity | Varies: first measurement at 14 days, then 1, 2, 3, 4, 5, 9, and 12 months; every 6 months after that as necessary. | Highly reactive artificial aggregate may not represent real aggregate conditions. Pyrex contains alkalies. |

59

Table 2.2- Continued

| | | | | |
|---|---|---|---|---|
| **ASTM C 856**, Petrographic examination of hardened concrete | To outline petrographic examination procedures for hardened concrete for determining performance | Visual (unmagnified) and microscopic examination of prepared samples | Short duration | Supplementary information provided to the petrographer may be helpful. |
| **ASTM C 856 (AASHTO T 299)**, Annex uranyl- acetate treatment procedure | To identify products of ASR in hardened concrete | Staining of a freshly-exposed concrete surface and viewing under UV light | Immediate results | Identifies small amounts of ASR gel whether they cause expansion or not. Tests must be supplemented by petrographic examination and physical tests for determining concrete expansion |

60

Table 2.2- Continued

| | | | |
|---|---|---|---|
| **ASTM C 1260 (AASHTO T303),** Potential alkali reactivity of aggregates (mortar-bar method) | Detection of the potential for deleterious alkali-silica reaction of aggregate in mortar bars | Immersion of mortar bars in alkaline solution at 80°C (176°F) | 16 days | Does not evaluate combinations of aggregates with cementitious materials |
| **ASTM C 1293,** Determination of length change of concrete due to alkali-silica reaction (concrete prism test) | Determination of the susceptibility of aggregate or combination of an aggregate with pozzolan or slag for participation in ASR expansion. | Concrete prisms stored over water at 38°C (100.4°F) | Varies: first measurement at 7 days, then 28and 56 days, then 3,6,9,and 12 months; every 6 months as after that as necessary | This test does not address the general suitability of pozzolans or slag for use in concrete.. |

Table 2.2- Continued

| ASTM C 1567, Potential alkali-silica reactivity of combinations of cementitious materials and aggregate (accelerated mortar-bar method) | Detection of the potential for deleterious alkali-silica reaction of cementitious materials and aggregate combinations in mortar bars | Immersion of mortar bars in alkaline solution at 80°C (176°F) | 16 days | Very fast alternative to C 1293. May underestimate the expansion of cementitious systems containing pozzolans with alkali content>4.0%. |
|---|---|---|---|---|

Aggregates determined to be potentially reactive with alkalies can be used only in concrete with cementitious materials conforming to the ASTM standards tabulated above. Three options are suggested to control alkali-silica reaction:

1. Use a combination of a pozzolan or slag with a Portland or a blended cement.

2. Use blended hydraulic cement that has been demonstrated to be effective in controlling expansion.

3. Select portland cement and other concrete ingredients to limit concrete alkali content based on proven field performance under similar conditions with the potentially reactive aggregate (ACPA, 2007).

## 2.7 Methods to Evaluate the Effects of ASR

A number of parameters can be monitored so as to evaluate the effect of ASR on a structure or specimen. These parameters are:

1. Environment inside and outside a structure can affect the effect and rate of ASR. The factors considered here are the following:

- Chemical composition

- Temperature

- Relative humidity

- Wind exposure

- Moisture exposure

The chemical composition including that of the pore water and its temperature determine the rate of the reaction. The amount of pore water in the structure affects the expansion of

the gel. This can be determined by measuring the relative humidity, wind exposure and moisture exposure.

2. The exterior and exterior deformations can also help to identify the effect off ASR. These can be measure by a number of ways:

- Internal and exterior  strains

- Internal  and exterior cracks

- Overall deflection of the structure

Figure 2.20 shows the different types of cracks that can help to identify a structure affected by ASR.
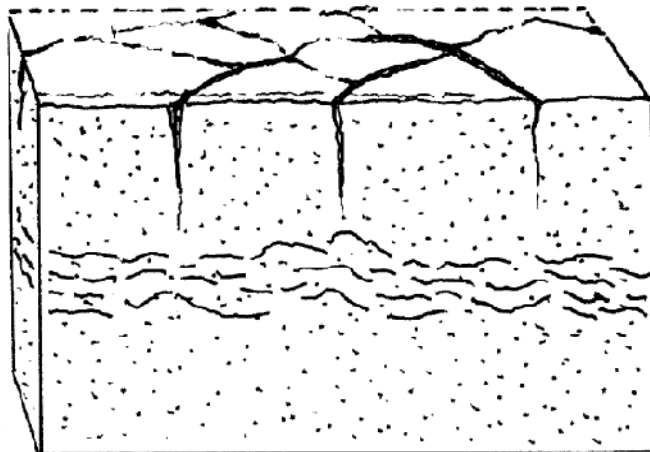


Figure 2.20 The sketch shows some typical features of map cracking and sub-parallel cracks due to ASR (adapted from ACI, 2008).

Measurement of strain helps to identify the expansion or elongation of concrete due to ASR.

The table below (Table 2.3) summarizes the methods employed to measure the different parameters mentioned above.

Table 2.3 Parameter measurement methods

| Parameter | Method |
|---|---|
| Relative humidity | • multiple ring sensors<br><br>• microwave sensors<br><br>• electrical resistance<br><br>• di-electrical constant<br><br>• Radiography<br><br>• Nuclear magnetic resonance<br><br>• Infrared reflection |
| Chemical composition | • Microscopic analysis (scanning electron Microscope) |
| Interior and exterior cracks | • radar/ active acoustic emission<br><br>• radiography<br><br>• Passive acoustic emission<br><br>• Infrared reflection<br><br>• Video records |

Table 2.3-Continued

| Internal and external deformations | <ul><li>mechanical gages</li><li>vibrating wire gages</li><li>strain gages</li><li>glass fiber</li><li>Photogrammetry</li><li>inductive gages</li><li>speckle correlation</li><li>Moiré Method</li></ul> |
|---|---|

## 2.8 The Purpose for Mitigating ASR

The main reason for treating existing ASR-affected structures is to prevent the ingress on water which is a prerequisite for the reaction. While it prevents water from going in, the treatment should also permit the escape of water already in the structure, so that it does not continue to promote the reaction. Accordingly, the treatment, whether a penetrating coating or an encapsulation, must be impermeable to liquid water and permeable to water vapor (Klingner, et al., 2000)

## 2.9 Mitigation Methods for ASR

The mitigation of ASR can be approached in two ways; either to treat the cause or the symptoms of ASR. In case of treating the cause of ASR, one has to keep in mind the conditions necessary for ASR and thus prevent those conditions from occurring. On the

other hand when dealing with treating the symptoms of ASR, one has to prevent the effects of ASR gel expansion to the structure. The table below summarizes the two approaches.

Table 2.4 Approaches in Mitigating ASR

| Treat Cause | Treat Symptoms |
|---|---|
| Reduce Alkali Content (or pH)<br><br>• Low-alkali cement<br>• Lithium compound<br>• Fly ash<br>• Slag<br>• Silica fume | Crack Filling<br><br>• Aesthetics<br>• Protection (sealant) |
| Prevent ingress<br><br>• Sealants<br>• Cladding<br>• Improved drainage | Restraint<br><br>• Prevent expansion (fibers)<br>• Strengthen/ stabilization |
|  | Relieve Stress<br><br>• Slot cutting to accommodate movement |

2.9.1 Low-Alkali Cement/Concrete

The use of low-alkali cement will suppress ASR because alkalis are needed for the reaction to occur. Limiting the cement content of the mix will also lower the total available alkalis in the concrete. Higher alkali contents result in more ASR reaction product, which can lead to more expansion (Leming, et al., 2000). It has been suggested that the total available alkali content of the concrete should be limited to less than about 5 lb per cubic yard (Duchesne, et.al., 1994). However, Leming and Nguyen (Leming, et al., 2000) found that no deleterious ASR expansion occurred when the alkali content of the concrete, expressed as Na2Oeq, was less than 2.5 pcy. When this value was greater than 3.4 pcy, deleterious ASR occurred (Leming, et al., 2000).They suggested that one should base specifications on the total alkalis per volume of concrete rather than placing limits on only the alkali content of the cement. If the conditions permit the use of low cement content and/or low alkali cements, both will help reduce the damaging effects of ASR.

2.9.2 Fly Ash

Fly ash controls alkali-silica reaction by increasing the alkali binding capacity of the hydrates and thus reducing the alkalinity of the pore solution, (Thomas, et al., 1999a). According to Thomas, the increased binding capacity of cement fly ash hydrates has been linked to the lower Ca/Si ratio of the hydrates compared to Portland-cement pastes without fly ash.

2.9.3 Slag

Slag is effective in limiting expansion from ASR, but there is not a consensus on what the minimum amount required should be. This minimum level is a function of the aggregate

and the alkali level in the concrete. The CSA recommends a minimum of 50 percent replacement, which is difficult to achieve in practice because of low early strength concerns and resistance to deicing salts (Thomas, et al., 1998). The beneficent effects of slag are seen in the results of concrete prism tests. "Slag affects a reduction in the rate and ultimate magnitude of expansion; the effect increases with the level of slag" (Thomas, et al., 1998). The reductions of ionic mobility and water permeability are the means by which slag is able to reduce ASR expansion. The level of slag needed depends on the type of aggregate and the amount of alkalis in the concrete mix. Thomas (Thomas, et al., 1998) suggest that concrete specifications should be flexible regarding the minimum amounts of slag needed, basing it on the alkali content of the concrete and reactivity of the aggregate.

2.9.4 Silica Fume

By employing several mechanisms for example, reducing the pore water alkalinity, ionic diffusion and water permeability, silica fume can help reduce expansion caused by ASR. It also helps in consuming Ca $(OH)_2$ or improving its distribution at the interface (Thomas, 1996).

Silica fume also decreases the permeability of concrete, implying a reduction in the mobility of ions in the pore solution that helps control ASR (Durand, et al., 1990).

The limitations of using silica fume are that, if it is not properly mixed, it may cause ASR rather than prevent it because of the reaction of undispersed agglomerates (Shayan, 1997). Also the fact that there is not a consensus on the amount needed to control ASR

makes it unreliable. There is also not enough field data to verify the laboratory results (Thomas ,1996).

2.9.5 Lithium Salts

Lithium salts can eliminate expansion caused by ASR, although lithium hydroxide also increases the concentration of OH ions in the mix (Shayan, 1997). For this reason, lithium hydroxide must be used in the correct amount in order to avoid this pessimum effect. Lithium, combined with fly ash, reduces expansions more than lithium would alone (Barringer, 1999). However, the specific amounts of lithium and lithium-fly ash combinations required must be determined by testing (McKeen, et al., 2000).

**2.10 Case Studies on ASR**

Alkali-aggregate reaction (AAR), which includes alkali-silica reaction (ASR), is the leading cause of deterioration of concrete dams and also affects other concrete structures. This reaction in concrete is causing millions of dollars of damage worldwide.

*Case Study1: Parker Dam, California*

The hydroelectric dam (Figure 2.21) built in 1938 that experienced 180 mm of arch deflection due to alkali silica gel expansion. Also noted was cracking and gel flow in the concrete (www.*people.ce.gatech.edu).*

Figure 2.21 Alkali-Aggregate Reactions in Hydroelectric Plants and Dams (adapted from
http://www.acres.com/aar/)

*Case Study 2: I-85 - Atlanta, Georgia*



Figure 2.22 Possible ASR damage on concrete retaining wall (adapted from
www.people.ce.gatech.edu)

*Case study 3: The Stewart Mountain Dam*

The Stewart Mountain Dam located 41 miles (66 km) east of Phoenix, Ariz., on the Salt

River, was completed in March 1930. It is a 212 ft (64.6 m) high multi-curvature thin

arch dam. The structure contains an arch dam, two thrust blocks for simulating abutments for the arch dam, three gravity dams, and two spillways. The structure has experienced alkali-silica reactions within the concrete thus exhibiting no bond across horizontal construction lift surfaces. The Alkali-silica reactions and expansions have caused visible surface cracking. Numerous investigations, field measurements, laboratory test, inspection, and on-site tests have been performed over the years to assess material properties, deformation, and deterioration. This structure was analyzed for gravity-, reservoir-, temperature-, and earthquake-induced loads. Results indicated an unsafe structure for earthquake conditions. The results from the tests revealed that, lower temperatures deep in the reservoir and deep within the concrete, higher leaching of available reaction gel into capillary space, and different cements have caused less than usual alkali-aggregate reaction in the lower arch among other results. Also they found out that, poor bonding across horizontal lift surfaces is due to the formation of laitance from severe bleeding of high-water-content concrete on the top of each lift. Post-tensioned cables are found to be a viable solution for the dynamic stability of a thin-arch dam. Methodology presented in this paper is applicable to other deteriorated dams. (Singhal, et al., 2000)

*Case study 4: Elgeseter bridge, Norway*

Field inspection were carried out on several concrete bridges in Trondheim, including Elgeseter bridge in 1989 in Trondheim municipality Norway with the aim to find out actual condition and repair needs . From the inspection, some few cracks were observed in beams and road plate. In two columns rust and concrete scaling were observed.

Numerous "shrinkage cracks" were observed on upstream faces of columns. Due to movement of Southern abutment up to 10 mm wide cracks occur in walls and roof". Generally the bridge was in good condition but needed repair work to be carried out within 5years. Because ASR was recently under investigation as a concrete problem in Norway the road authority responsible for maintenance and function of the bridge ordered an assessment of ASR as the possible cause of damage. Therefore, a field investigation was carried out in 1990.    Map cracking significant of ASR occur on Southern faces of several columns and the western girder were reported. The movement of the bridge and reduction of the expansion joint originally 20 cm but now less than 1 cm was suggested to be caused by either:

- ASR had caused expansion of the beams and the road plate. The expansion of the 200 m long beams/plate should then be 0.01% after 40 years.

- Land slide of abutments had reduced the expansion joint (Euro seminar, 2003).

*Sg. Pontian in Kuala Pontian, Malaysia.*

ASR was reported on the pile head of bridge in Sg. Pontian. Random map cracking was observed (Figure 2.23) and a full analysis was conducted by Dr. Hashim of the University of Malaysia who confirmed the presence of ASR.

Figure 2.23 Map cracking on bridge in Sg. Pontian

*Ririe Dam Bridge*

Ririe dam was built in 1977 and is located 6 miles southeast of Riries Idaho. Shortly after construction, early cracking in the bridge parapet wall was observed. A bridge inspection in 2004 indicated extensive cracking of the bridge abutments and the pier as well as expansion and dislocation of the bridge parapet walls. Petrographic examinations indicated weakening of the bond between the paste and the aggregate due to the effects of ASR on the smooth aggregate particles.

## 2.11 Past Research on Mitigation of ASR

A number of strategies have been suggested and used to mitigate the effects of ASR. Some are as stated below;

R. E. Klingner and T. J. Fowler, (Klingner et al., 2000) came up with a method to help the TxDOT decide what to do with in-service structures experiencing premature concrete deterioration (PCD). This premature concrete deterioration was found to be caused by two expansive damage mechanisms: Alkali-Silica Reaction (ASR) and Delayed Ettringite

Formation (DEF).By using cores extracted from damaged specimens, they investigated decrease in strength and stiffness due to PCD and related this to observed and computed decreases in the capacity of structural elements. They also used a simple numerical index of damage, referred to as a Damage Index (DI), which was developed to quantify visual observations of damage. They calculated the DI using crack widths in thousandths of an inch, and crack lengths in inches. They found out that the damage Index can be estimated quickly for a  particular structure in terms of the maximum crack width in that structure. They also used nondestructive evaluation (NDE) techniques, principally acoustic emission, to relate visual observations of damage to observed strengths. They found out that premature concrete deterioration is more severe in concrete that is kept wet. Also they found out that field  structures show more damage at the ends of girders, under joints in bridge decks because those end regions are normally also subjected to the highest shear.

<u>Coating of the structure</u>

Several researches have been conducted on different coating to prevent water from entering but also to allow the escape of pore water. From past research it is shown that specimens that were coated by epoxy thus not allowing the pore water to escape had much more expansion that specimens that were not covered and those that were coated with a coating permeable to water vapor. All specimens had very high expansion under cycles of wetting and drying.  Below are some of the test conducted and their results and conclusions;

Abe (Abe et al. (1992) addresses the comparative effectiveness of two coatings, one impermeable to water and the other permeable to water vapor, in reducing ASR-related expansion. In the vapor permeable coating, silane was used followed by a polymer-modified cement mortar (PCM). The impermeable coating consisted of three layers of epoxy. They used uncoated control specimens.

All specimens were placed outside for two years. The results showed that specimens with the vapor-permeable coating had continuous negative expansion. The specimens with the impermeable coating had much greater expansion than the uncoated specimens in just after six months. The researchers concluded that the high expansion was due to the excess initial pore water that could not escape through the impermeable epoxy coating.

Kamimoto (Kamimoto et al., 1992) measured the performance of several concentrations of a PCM using the criteria of water permeability, water-vapor permeability, elongation, adhesion, and expansion of a concrete specimen in the field. Their findings suggested that:

- With increasing polymer ratio, water permeability and water-vapor permeability decreased. The greatest tested polymer ratio was 0.75 which gave the lowest permeability.

- Elongation of the PCM increased as the polymer ratio increased.

- Adhesion was greatest for a polymer ratio of 0.525.

For the field expansion tests, small, rectangular specimens were coated with either PCM or epoxy, while other specimens were left uncoated. Expansion was measured by change in length, and vapor permeability was measured by change in weight. Their results

showed that PCM-coated specimens had consistently low expansion, while the uncoated and epoxy-coated specimens had much higher overall expansion and greater rates of expansion. As the water-vapor permeability of the PCM increased, the specimen's expansion decreased.

<u>Lithium based solution</u>

Stokes (Stokes, 2000) described the use of a lithium-based solution to treat ASR. Tests were conducted to compare the penetration ability of various lithium solutions, to assess the efficacy of the best solution, and to study how the timing of the treatment influenced this efficacy.

By placing various lithium salt solutions at several concentrations in cavities in cylinders, penetration ability was assessed and the volume of solute entering the cylinder recorded.

A lithium nitrate solution of 30% with a blend of surfactants, gave the greatest penetration, this was higher than for that of lithium hydroxide, acetate and formate.

Reactive mortar bars and concrete prisms were then used to study efficacy and application timing. In reactive mortar bars, one-half the amount of lithium required as an admixture to control ASR reduced expansion to as little as 55% of that of uncoated control specimens. Also, lithium nitrate reduced expansion twice as much as lithium hydroxide. The lithium nitrate was used on concrete prisms, applied in one and five coats. The one-coat specimens exhibited 0.1% expansion and the 5-coat specimens exhibited 0.05% expansion. From the timing tests on both mortar bars and concrete prisms, the investigators concluded that some prior expansion aided penetration, and thus

effectiveness, by inducing cracking. Existing cracks provided a path for the coating to penetrate.

Electrochemical Chloride Extraction

Whitmore (Whitmore et al., 2000) inferred that electrochemical chloride extraction, used to drive chloride ions out of salt-contaminated structures, can easily be adapted to drive lithium ions into a structure. The potential benefits are shortened treatment time and an increase in the effective amount of lithium in the structure.

Use of pozzolan, slag or blended cement in controlling ASR expansion

Different amounts of pozzolan or slag should be tested to determine the minimum effective dosage according to ASTM standards. Too low dosage of pozzolan or slag may result in the ***pessimum effect*** that is a higher ASR expansion than if no pozzolan or slag was used. Pozzolan, slag and cement shall be evaluated by ASTM C 1567.Those that exhibit mortar bar expansion at 14day exposure of less than or equal to 0.10% shall be considered acceptable. Those material-aggregate combinations that do not meet the criteria in ASTM C 1567 can be further evaluated by ASTM C 1293.ASTM C 1293 is a two year duration test which has been correlated to field performance in Canada.

Mechanical mitigation of ASR

Ostertag (Ostertag et al., 2004) investigated a mechanical approach in mitigating alkali-silica reaction. The mechanical approach focuses on reducing the cracking and ASR gel expansion through steel microfiber (SMF) reinforcements. Microfibers are to control the microcracks that form at onset of ASR and also due to their effectiveness in providing

crack control through toughening mechanisms (Ostertag et al., 2004). The effect of SMFs on ASR was investigated using two different types of reactive aggregates:

- Crushed opal aggregates used to determine the cracking, strength and expansion characteristics due to SMFs.

- Rod-shaped reactive Pyrex aggregate of constant diameter were used to investigate the influence of microfibers on reactivity, gel formation and gel composition.

Using the crushed opal aggregates, the following experiments were conducted:

a) Microscopy analysis on cracking due to ASR

b) Crack propagation test that measure the deterioration of the mechanical properties due to ASR

c) Expansion experiments.

Using Pyrex rod as reactive aggregate, the following experiments were conducted:

- Specimens to determine the difference in reactivity of the reactive aggregates in presence of SMF reinforced matrix.

- Microprobe analysis to reveal and determine the chemical composition of the solid ASR.

- Inductive coupled plasma (ICP) spectroscopy to determine the composition of the liquid alkali-silica complex.

From the experiments conducted they came up with the following results:

I. The opal aggregates reacted with the alkalis and a rim formation could easily be removed during polishing. A microcrack has formed in the unreinforced mortar

specimen due to ASR. None of the long cracks was observed in SMF mortar specimens.

II. For the crack propagation measurements, the load decreased with increasing exposure time to NaOH solution for the unreinforced mortar with the largest reduction between 0 to 7 days of exposure to the NaOH solution. For the SMF reinforced mortar specimen, the maximum load remained nearly constant.

III. For the expansion measurements, the highest rate of expansion was seen to occur during the first 2 days of exposure for the control specimen while slow initial expansion was seen for SMF reinforced specimens.

IV. The pyrex rod in the SMF mortar reacted far less compared with the unreinforced mortar at same exposure times to the NaOH solution.
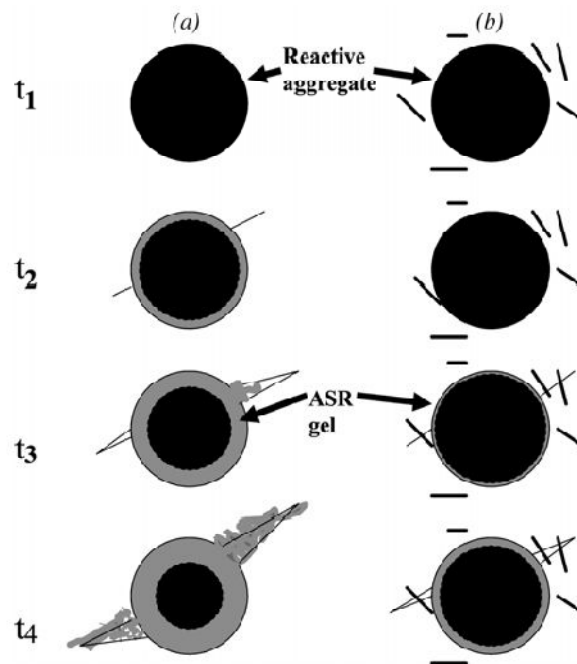


Figure 2.24 ASR gel formation in (a) control specimen and (b) in SMF mortar specimen

They concluded that the SMFs effectively reduce expansion associated with ASR in mortars containing crushed opal as the reactive fine aggregates by over 60%. Also the SMFs virtually eliminate the strength loss observed in unreinforced mortar specimens.

Turanli (Turanli et al., 2001) investigated the reduction in alkali-silica expansion due to steel microfibers. Steel microfibers ranging from 1% to 7% by volume of cement mortar were incorporated to reduce the expansion and cracking due to ASR. Opal aggregates were used at 5% by weight of fine aggregates. Opal aggregates were chosen due to their known high silica content that makes them susceptible to alkali-silica reaction. All specimens were cast and tested according to ASTM C-1260 although for one set the test was slightly modified by allowing a 7-day total water-curing. This allowed the researchers to investigate the influence of fiber/matrix interfacial strength on expansion. Three specimens were cast for each fiber volume fraction for both the longer and shorter curing time. The change in length of the prisms was measured every 24 hours up to 30 days.

The researchers observed that the expansion decreased with increasing steel microfiber volume fractions for both sets of curing times. The highest reduction was observed at 7% in volume fraction of microfibers. They also observed that the decrease in expansion is more pronounced on specimens where curing time was extended. They concluded that microfibers are very effective in reducing the expansion and cracking due to ASR. Also that longer curing time allowed for a stronger bond to form between fibers and the matrix.

Park and Lee (2003) studied the expansion properties of mortars containing glass and fibers. They analyzed ASR expansion and its properties on strength in terms of waste glass, glass color, steel fibers and fiber content in reducing ASR expansion. The researchers used colored soda lime glasses (both green and brown) as the reactive aggregates. The test was conducted in accordance to ASTM C1260. Three mortar specimens were made for each mixing with a w/c ratio of 0.47. Compressive strength test and flexural tests were also performed on specimens.

The researchers observed that green waste glass was more useable than brown because its expansion was less than that of brown glass. They also observed that when fibers were added, there was a reduction in expansion and strength loss due to ASR. The researcher observed that the addition of 1.5% of fibers to concrete containing 20% waste glass can reduce the expansion ratio up to 40% and increase flexural strength up to 110%.

Haddad and Smadi (2003) investigated the role of fibers in controlling unrestrained expansion and arresting cracks in concrete affected by ASR. Polypropylene or brass-coated steel fibers were used. Portland cement concrete and fiber reinforced concrete mixtures were prepared at a w/c ratio of 0.40. Prisms measuring 5 x 5 x 30 cm and plates measuring 13.5 x 13.5 x 3 cm specimens were prepared and cured for 7 or 28 days before exposure to an accelerated ASR treatment. The researchers determined the expansion, the time of cracking and ultrasonic pulse velocity over a treatment period of 65 days for the prism specimens. For the plate specimens, the ultimate cracking pattern and extent were determined after a treatment period of 85 days.

They observed that the fibers played a significant role in delaying crack formation and limiting their extent. The potential of brass coated fibers in arresting ASR cracking was also found to be significantly affected by the age of the concrete when subjected to the treatment.

Carvalho (Carvalho et al., 2009) investigated the influence of steel fibers on the development of alkali-aggregate reaction. Two types of steel fibers were used with a fiber volume fraction of 1% and 2%. Five mortars with Portland cement and diabasic aggregate were produced with the steel fiber content varied from 0%, 1% and 2% for the two types of fibers. The dimensions of the specimens were 75 x 75x 285mm. The experimental procedure followed was similar to ASTM C1260. Compressive test and flexural test were also carried out to determine the main characteristics of the fiber-reinforced mortars subjected to AAR. They also analyzed the microstructure of the specimens by a scanning electron microscopy and energy dispersive X-ray.

They observed that the fibers bridged the cracks reducing the macroscopic mechanical expansion (Figure 2.25). The flexural test showed that that the higher the contents of fibers, the higher the capacity of the specimens to absorb energy.
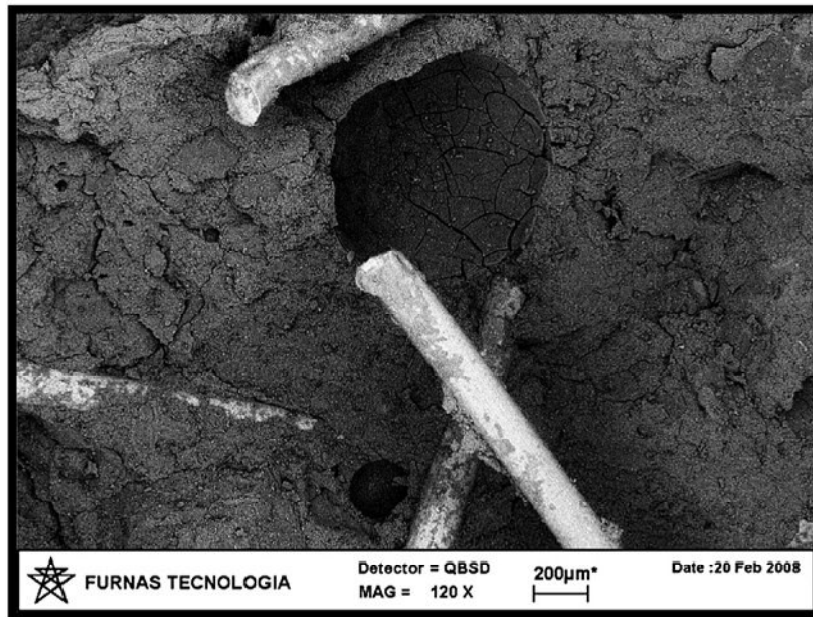
Figure 2.25 Pore filled with cracked gel, and fibers around the pore (Carvalho et al.,

2009)

They concluded that fibers have a beneficial effect on the material, without compromising its main mechanical properties.

CHAPTER 3

EXPERIMENTAL PROGRAM

**3.1 Experimental Program on the Effect of Fiber Corrosion on the Shear Capacity of SFRC Beams**

Although some research has been done on the durability of SFRC, little knowledge is known on the effect of corrosion of fibers on the shear strength of structures. The experimental program of this research aims to enhance the understanding of shear behavior of large-scale SFRC beams affected by corrosion.

The experimental program strived to answer the following questions:

(1) What are the shear failure mechanisms, ultimate shear strength, and ductility of SFRC beams?

(2) How do these results change if fibers are corroded to different extents?

(3) At what extent of corrosion of the steel fibers is the shear strength of the beams most affected?

The experimental program involved the design, construction, and testing of simply-supported beam specimens subjected to a monotonically-increased, concentrated load. Pre-corroded fibers were used for this research. Although in real life fibers will not be corroded equally, this research aims to study the worst-case scenario. It has also been

noticed from research conducted by Naaman (Naaman and Kosa, 1990) that results of tests using precorroded fibers led to conclusions similar to the tests on specimens undergoing accelerated corrosion. The main difference in using precorroded fibers is that the effect of improvement in bond properties due to expansion of corrosive products at the fiber surface is eliminated. A total of 4 beam specimens were tested in addition to tests such as the concrete compression tests, third-point loading tests, and fiber-pull out tests to evaluate the mechanical properties of the concrete.

3.1.1 Materials

This section discusses the materials used throughout this research. All material properties discussed herein are based on mill certificates, manufacturer's data sheets, or analytical testing.

*3.1.1.1 Cementitious Material*

Type II Portland cement was used in this research whereas class C fly ash was used as the supplementary cementing materials provided by Hanson Pipe & Precast Company.

*3.1.1.2 Aggregates*

The aggregates were also provided by Hanson Pipe & Precast Company which originated from Texas quarries. The coarse aggregates size was 3/8 inch. Both the coarse and fine aggregates were graded by the company so no more grading was done in the laboratory.

### 3.1.1.3 Water

The water used in this research was the normal tap water but reference was made to specification D1193 to ensure that it conformed to Type IV water.

### 3.1.1.4 Reinforcement Bars

Grade 60 ($f_y$= 60ksi) reinforcement were used in the beam. The size of the bars to be used was determined according to design calculations as discussed later. #6 bars were used for the tension reinforcement whereas #4 bars were used for the compression reinforcement. Stirrups were designed using #3 bars. The properties of the bars are as shown in table 3.1 below.

Table 3.1 Properties of Reinforcement Bars

| Bar Designation Number | Nominal Diameter (in.) | Metric Designation Number | Weight (lb/ft) |
|---|---|---|---|
| 3 | 0.375 | 10 | 0.376 |
| 4 | 0.500 | 13 | 0.668 |
| 6 | 0.750 | 19 | 1.502 |

### 3.1.1.5 Fibers

Hooked end fibers (Figure 3.1) were used in this research. These fibers were donated and manufactured by Maccaferri Inc.. These fibers are suitable in shear due to their deformed

(hooked) ends that resist pullout and hence lead to an increase in shear strength of SFRC.

Their properties are as presented in the Table 3.2 below.
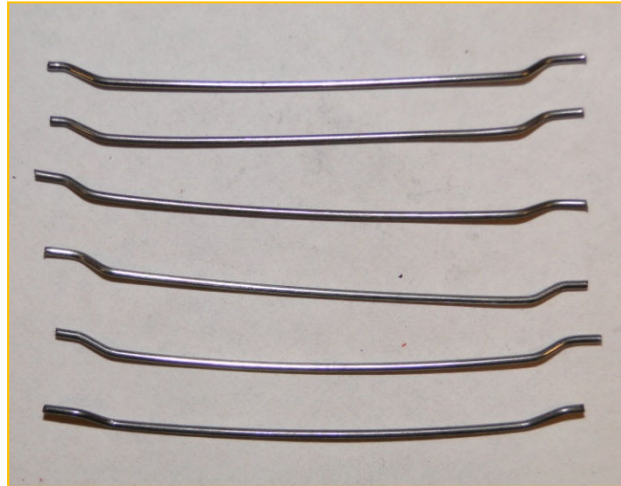


Figure 3.1 Hooked steel fibers

Table 3.2 Properties of Steel Fibers

| Fiber | Geometrical Configuration | Diameter mm (in.) | Length mm (in.) | Aspect Ratio | Tensile Strength Mpa (ksi) |
|---|---|---|---|---|---|
| Hooked Fiber | | 0.76 (0.031) | 47.5 (1.87) | 60 | 159 |

### 3.1.1.6 Sodium Chloride Solution

The sodium chloride solution employed in this research to corrode the fibers was mixed in the lab using normal table salt and water in the right amount to achieve the required concentration.

3.1.2 Design of Beam Specimens

The experimental program consisted of casting two beams for each parameter inorder to reduce the uncertainty of the shear strength of beams. After the testing of the first pair of beams (RC), the decision was made to cast just one for each parameter since the results from the first pair were reasonably similar. The beams were reinforced with sufficient bottom bars to prevent flexural failure of the beam. The parameters that varied were the extent of corrosion whereby two extents were chosen. The three extents of fiber corrosion were 12.5%, 25% and 50% reduction in the fiber diameter. Also for comparison purposes, reinforced concrete beams and SFRC beams without corroded fibers were cast. The fixed parameters for the experiment were the beam size, shear span-to-effective depth ratio, and concrete compressive strength, while the varied parameters were fibers, extent of corrosion of fiber content. Table 3.3 below shows the design properties of the beams.

Table 3.3 Design Properties of the Beams

| Beam Type | d (in) | a/d | ρ % | $V_f$ % | Extent of Corrosion % | Targeted f'$_c$ (psi) | Measured f'$_c$ (psi) |
|---|---|---|---|---|---|---|---|
| RC1 | 16 | 3.3 | 1.83 | 0 | 0 | 6000 | 4800 |
| SFRC1 | 16 | 3.3 | 1.83 | 0.75 | 0 | 6000 | 6207 |
| SFRC2 | 16 | 3.3 | 1.83 | 0.75 | 12.5 | 6000 | 6673 |
| SFRC3 | 16 | 3.3 | 1.83 | 0.75 | 50 | 6000 | - |

**Shear span-to-effective depth ratio**

The beams in this research had a shear span-to-effective depth ratio, *a/d,* of approximately 3.3 to minimize the effect of arch action. A general conclusion from extensive research on the effect of shear span-to-effective depth ratio is that beams with smaller span-to-depth ratio can resist more shear. This is due to the direct transfer of the load through a compressive strut (arch action). The critical value for the shear span-to-depth ratio of 3 was proposed by Batson et.al (1972) for SFRC beams. It is due to these reasons that a *a/d* ratio of 3.3 was selected so as to force a shear failure.

**Beam size**

Each beam in this research was 6 inches in width by 18 inches in depth by 96 inches in length. From past research done on shear of beams by Dinh (2009), it was decided that a minimum beam size of 18 inches depth and 6 inches wide was necessary. A concrete cover of 1 inch from the bottom of the tensile bars to the concrete surface was chosen whereas for the top a concrete cover of 3 inches was chosen.

The length of the bottom reinforcement was designed such that no anchorage failures would occur (Figure 3.2) and the shorter shear span was reinforced with stirrups to ensure a shear failure in the longer shear span. For anchorage, 90$^{\text{o}}$ hooks were used for the bottom bars as shown in Table 3.4. A detailed reinforcement specification is shown in Appendix I.
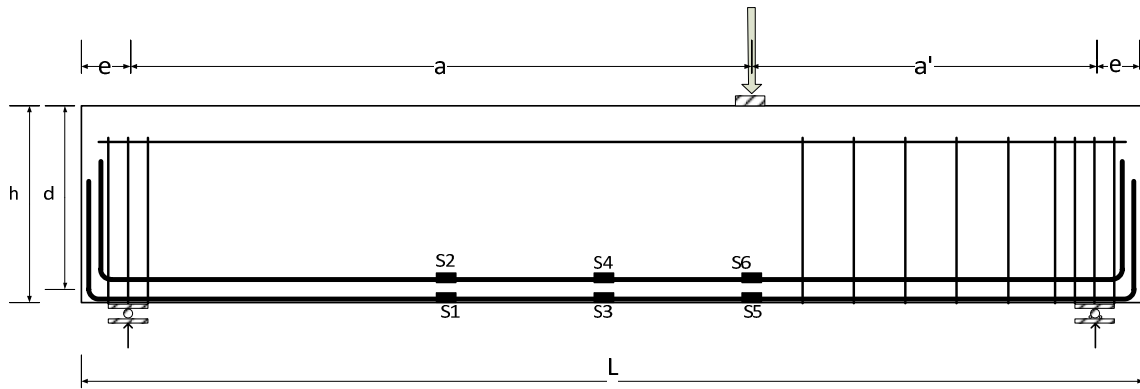
Figure 3.2 Basic beam layout

Table 3.4 End Anchorage of Tensile Reinforcement

| #6 Bar | Bar Diameter (in) | Diameter of Bend (in) | Length of End Anchor (in) |
|---|---|---|---|
| Top Layer | 3/4 | 4.6 | 9 |
| Bottom Layer | 3/4 | 4.6 | 9 |

**Concrete compressive strength.** The design concrete compressive strength was fixed at 6000 psi. However, there was quite a bit of variance in the measured compressive strength. A number of factors have been proposed that may have led to this variability. They are; (1) the fact that while some concrete was delivered by a ready-mix supplier, other mixes were performed in the Civl Engineering Laboratory at the University of Texas at Arlington. This may have led to the variability as better control on the mix was possible in the laboratory as opposed to the ready mix concrete, (2) all beams were not cast at the same time. (4) all beams were not tested at the same age.

**Selection of longitudinal bars.** The longitudinal reinforcement ratio was selected such that the beam would fail in shear. A reinforcement ratio of 1.83% was selected for the beams with a fiber volume fraction of 0.75%.

A shear strength of $3.5\sqrt{f'c}\,bd$ was assumed for beams with a fiber volume fraction of 0.75% as was proposed by Parra-Montesinos (2006).

Traditional methods used for RC beams were employed to calculate the beam flexural strength. Table 3.5 below gives a summary the calculated beam shear and flexural strength. For detailed design calculations refer to Appendix II.

Table 3.5 Calculated Shear and Flexural Strengths of the Beam

| $f'_c$ (psi) | b (in.) | d (in.) | $P_s$ (kip) | $A_s$ (in.$^2$) | $a_c$ (in.) | a (in.) | $M_n$ (k-in) | $P_b$ (kip) | $P_s < P_b$ |
|---|---|---|---|---|---|---|---|---|---|
| 6000 | 6 | 16 | 36.87 | 1.76 | 3.45 | 52.5 | 1507 | 71.17 | OK |

$P_b$: flexural strength
$P_s$: shear strength
$M_n$: nominal moment capacity
$a_c$: compression zone

 It has been noted in the past that the actual shear strength of the beam may be higher than the calculated value despite consideration of actual material properties. Hence the longitudinal reinforcement may yield before shear failure and since increasing the reinforcement ratio may lead to unrealistically high shear strength, this is considered acceptable.
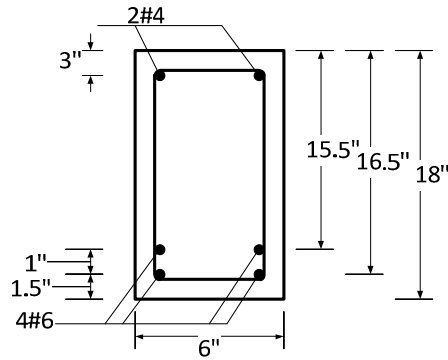
**Selection of stirrups.** The stirrups in the right shear span were selected such that a shear failure would not occur in that span. From reviewed literature #3 stirrups spaced at 5 in were adequate to prevent shear failure. The calculated shear capacity of the beam is shown in appendix II.

**Selection of steel plates.** The size of steel plates under the loading point and at the supports was selected on the basis of permissible bearing stress (0.85f'c). This is chosen to prevent concrete crushing at both the supports and loading point. The steel plates were used at the supports and load point to distribute the loads such that bearing stresses remained below acceptable limits. A layer of non-shrink grout was added between the plates and the beam ensuring the load was uniformly applied over the loading area. A 6 x 6 x 1 in. steel plate was acceptable for this test. Figure 3.3 and 3.4 below shows the reinforcement details and typical cross section for the beams.



Figure 3.3 Reinforcement details

Figure 3.4 Typical beam cross section

*3.1.2.2 Variable Parameters*

**Fiber volume fraction.** The volume fraction of the fibers selected for this research was 0.75%. This volume fraction according to past research is the minimum amount to cause an increase in the shear capacity of SFRC beams. All the SFRC beam specimens had the same volume fraction while the RC beams had zero fibers. As mentioned earlier hooked steel fibers were used and their properties were given in Table 3.2 above.

**Reduction in minimum fiber diameter.** The reduction in the minimum fiber diameter due to corrosion varied from 12.5%, 25% and 50%. According to Naaman (Naaman and Kosa, 1990), at a percentage of less than 12.5%, there was almost no change in strength and toughness of the specimens. Also in 1976, Hannant came up with a theoretical model suggesting that the fiber diameter has to be reduced by 52% before failure turns from bond failure to tensile fiber failure. This was the basis behind the percentages chosen for this research. The range will also give us a clear indication of the change in fiber failure mode.

3.1.3 Fabrication of Reinforcement Cage

**Strain gauges.**

Foil-type strain gauges were installed on the top side of the tensile reinforcing bars. Six strain gauges labeled S1 to S6 were placed at a spacing of 15 inches starting from the loading point. Each strain gauge was glued to a degreased flat area through cyanoacrylate glue and protected by three coating layers, namely polyurethane, nitrile coating, and a rubber pad sealed by electric liquid tape. The Figure 3.5 below shows the mounting of the strain gauge. A voltmeter was then used to check that the strain gauges are working correctly.



Figure 3.5 Attachment of the strain gauge onto the bar

**Caging and Formwork.** Reinforcement cages were constructed at the University of Texas at Arlington Civil Engineering Laboratory. Care was taken during the caging to

avoid damage to the mounted strain gauges. Wooden formwork was fabricated and oiled prior to placement of the reinforcement cage. Stiffeners were attached to the sides of the formwork to avoid bulging in the formwork after concrete is poured. A one inch concrete cover was obtained by placing one inch concrete blocks between the reinforcement cage and the formwork while the cage was fixed into position using wire tied to the formwork. The stirrup locations were then marked by a permanent marker on the top sides of the formwork so that their exact location in the beam could be known. The strain gauge wires were loosened and then taped to the formwork to prevent them from falling in while casting and to give enough sag to prevent them from pulling off. The end of the strain gauge wires was then covered with plastic bags to prevent them from coming into contact with moisture. Clamps were also used during the pouring of concrete to prevent the top part of the formwork bulging due the pressure of the concrete hence maintain the required width. Hooks were installed into the beams at the time of casting to facilitate the lifting and moving of the beam. Figure 3.6 below shows a completed reinforcement cage while the formwork is shown on Figure 3.7



Figure 3.6 Reinforcement cage

Figure 3.7 Fabricated formwork

**Accelerated corrosion of fibers**

Steel fibers were measured according to the mix proportion and subjected to an accelerated corrosion process. Corrosion was achieved by wetting and drying cycles. In the wetting stage, the fibers were immersed in a 3.5% NaCl solution and put in the oven at a temperature of 80°C for three days after which the water was drained and the fibers left at room temperature for another three days. The Figure 3.8 below shows the conditioning of the fibers in NaCl solution. The process was continued with subsequent measuring of the fiber diameter until the required reduction in diameter was reached. The fibers were then washed to remove any salts on the surface and left to dry after which they were ready for use in the casting.
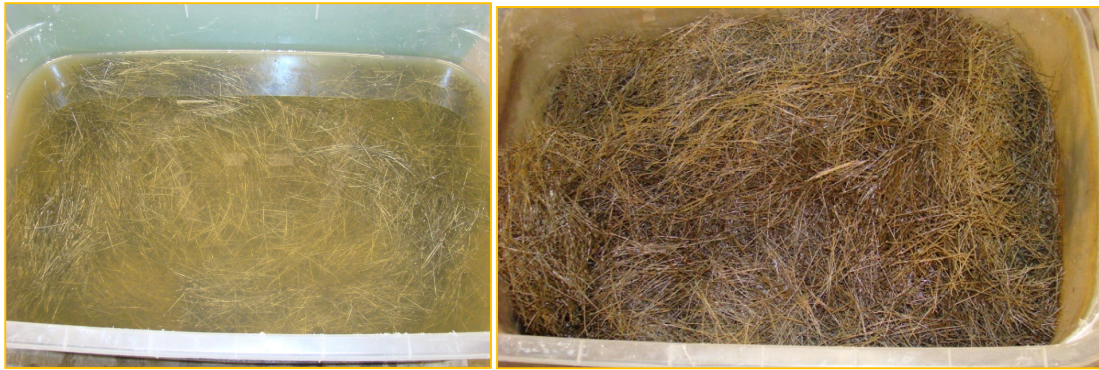
|     |     |
| --- | --- |
| (a) | (b) |

Figure 3.8 Fibers during (a) wet cycle in NaCl solution and (b) dry cycle

To make it possible to measure the loss in fiber diameter, the fibers were cleaned to remove all corrosion products by brushing off. The diameter was measured by a digital caliper. It should be noted that the corrosion of the fibers is not even at most times as was explained earlier in chapter two due to pitting (Figure 3.9).   Thus the fibers were measured along their length and the least diameter recorded. The least diameter was used realizing the fact that this will be the area of least resistance in the fiber and hence will be the controlling one. The loss in minimum diameter is presented as percent of the original diameter.



Localized areas with severe corrosion

Figure 3.9 Fiber pitting

Initially, weighing of fibers to estimate the corrosion extent was an alternative. This idea was however discarded as it is not a realistic approach since there will be at least a 1% variance in original weight. If the fiber diameter reduces by 10% on a 3mm length fiber, it would not be detectable. By measuring say 60 fibers it gives a variance of 0.8% in original diameter which is acceptable. Figure 3.10 below shows the original fibers and fibers with 50% reduction in diameter.



(a)                                                    (b)

Figure 3.10 Fibers with (a) no corrosion and (b) with 50% corrosion

3.1.4 Casting and Curing of Beam Specimens

**Mix proportion**

The Concrete mix design used for this research is as shown in the Table 3.6 below. A water/cementitious ratio of 0.35 was used and the concrete was mixed at the laboratory for the FRC but for the RC a premix truck was used.

Table 3.6 Mix Proportion

| Beam Type | Cement | Fly ash | Sand | Coarse aggregate (3/8″) | Water | Fiber |
|---|---|---|---|---|---|---|
| RC | 262.86 | 131.43 | 446.86 | 262.86 | 157.72 | 0 |
| SFRC | 256.40 | 128.20 | 435.87 | 256.40 | 153.84 | 31.02 |

**Mixing of concrete.** For concrete mixed at The University of Texas at Arlington Civil Engineering Laboratory, cement and sand were mixed until a uniform color was seen throughout the mix. Water was then added in small portions until a consistent mortar was observed after which aggregates were added. Fibers were then added in portions to ensure an even distribution of the fibers in the concrete and mixed until reaching a uniform consistency. The mixture was dumped into carts ready to be poured into the formwork.

For concrete provided by a local concrete supplier, the amount of materials in each batch was assumed to be less accurate than that mixed at the University of Texas at Arlington laboratory.

**Casting of specimens.** Concrete was poured in the beam and compacted by a poker vibrator to ensure even distribution of the concrete between reinforcement and remove air voids. The compaction was done in three layers with care taken to avoid damaging the strain gauges. During casting a measuring tape was used to measure the top of the beam to ensure that bulging of the formwork did not occur. In case of bulging, clamps were used to bring the formwork back to the right dimension. A trowel was then used to smooth out the surface of the beam. Hooks were then inserted at the ends of the beam to aid in the lifting of the beam when demoulding.

*Cylinders*

Twelve mortar cylinders in standard 4x8 in disposable moulds were cast for each beam and gently vibrated by a table-top vibrator to prevent large voids and honeycombing. These were then finished by a trowel and cover for 24 hour to cure. After curing the cylinders were demoulded, labeled and stored for testing after 28 days.

*Flexure beam specimens*

At least four 6 x 6x 20 in. beams were cast for each beam. These beams were vibrated by a table-top vibrator and finished by a trowel. The specimens were then covered by a plastic sheet for curing after which they were demoulded, labeled and stored.

*Fiber pullout specimens*

Fiber pullout tests are generally used as an indirect method to evaluate bond. The test specimens were prepared using Plexiglas molds having 0.98 x 0.90 in. cross section and 2.76 in. length. Fibers were selected from each of the corrosion extents and embedded within the desired embedded length ($l_d/4$). The fibers were kept in place by embedding them in styrofoam blocks measuring 1x 2 in. The Figure 3.11 below shows the specimen preparation. The concrete mix was poured into the moulds and lightly vibrated. The specimens were then finished and covered by plastic sheet for 24 hours; after which they were demoulded, labeled and stored for testing. Figure 3.12 shows the demoulded pullout specimen.
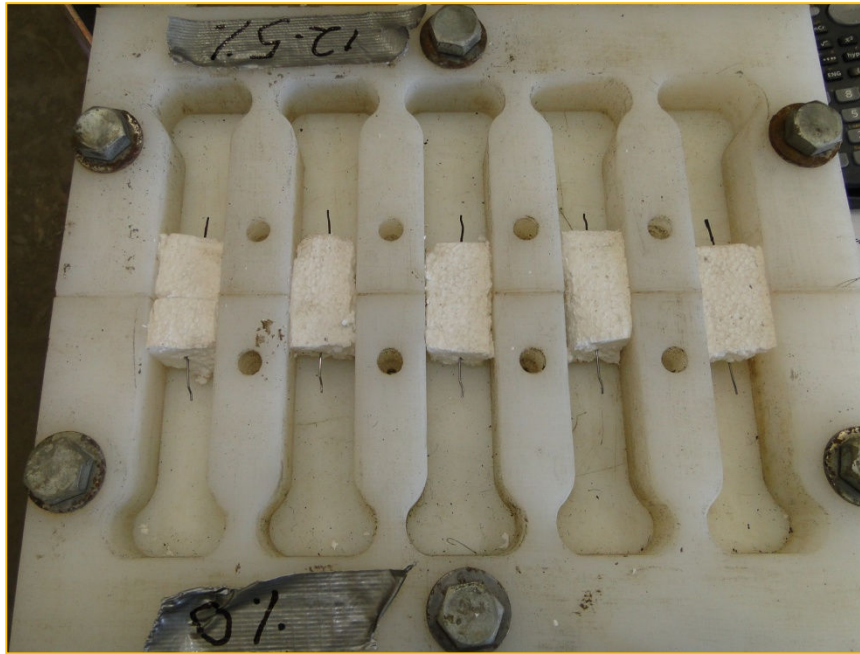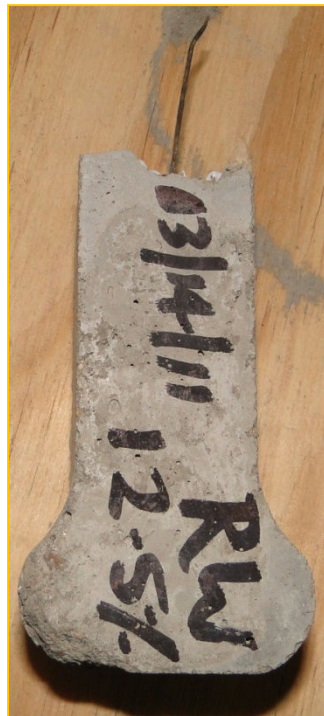
Figure 3.11 Fiber pullout specimen preparation



Figure 3.12 Pullout specimen

**Curing of beam specimens.** After casting, all beam specimens were covered with plastic sheets to allow curing. Beams were demoulded after one day and stored in the laboratory until tested.

3.1.5 Beam Test and Setup

**Instrumentation**

To be able to analyze the performance of the beams under loading more precisely, a number of instrumentation was needed. This consisted of strain gauges and linear variable transducers (LVDT) which were connected to a data acquisition system connected to a computer for storage.

*LVDT*

Two transducers were installed at the supports positioned at the midpoint of the top plate to monitor the deformations. One transducer was installed at the bottom of the beam directly above the loading point to measure the deflection of the beam. These were then connected to the data acquisition system for recording of data. The Figure 3.13 below shows the installation of the LVDTs.

(a)                                          (b)

Figure 3.13 Typical installation of LVDT at (a) the support and (b) the bottom of beam directly below the load point

*Grid*

Grids measuring 3x3 in. were drawn on the beam throughout the entire shear span and labeled. These were useful to ensure that the cracks drawn on paper were at the exact position as those on the beam. Figure 3.14 below shows the grids as well as position of the strain gauges drawn on the beam.
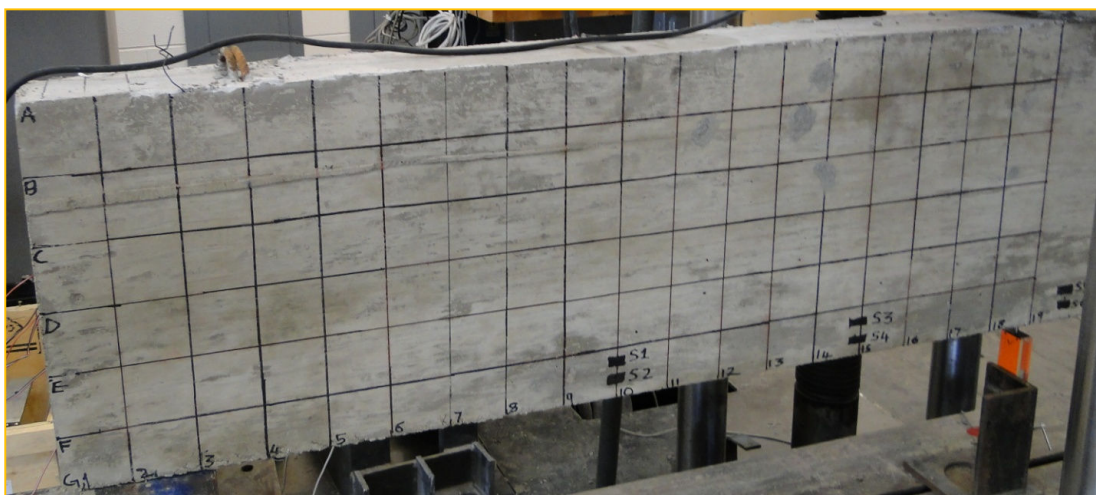


Figure 3.14 Grid lines and strain gauges positions

**Load setup and loading devices**

The beams were tested using a 400 kips universal testing machine under monotonic loading. The force from the machine was measured by an external 500-kip load cell placed between the beam and the actuator which was also attached to the data acquisition system. As mentioned earlier a non-shrink grout was applied between the beam and the plate and then the load cell was placed after the grout had hardened. The beam was supported on both sides at 4 inches from the end of the beam. Plates measuring 18 x 6 x 1 in. were used at the support whereas at the load point, a plate measuring 6 x 6x 1 in. was used (Figure 3.15). These plates were used at the supports and the loading point to distribute the loads such that bearing stresses remained below acceptable limits. The test specimens were placed on top of steel spreader beams.
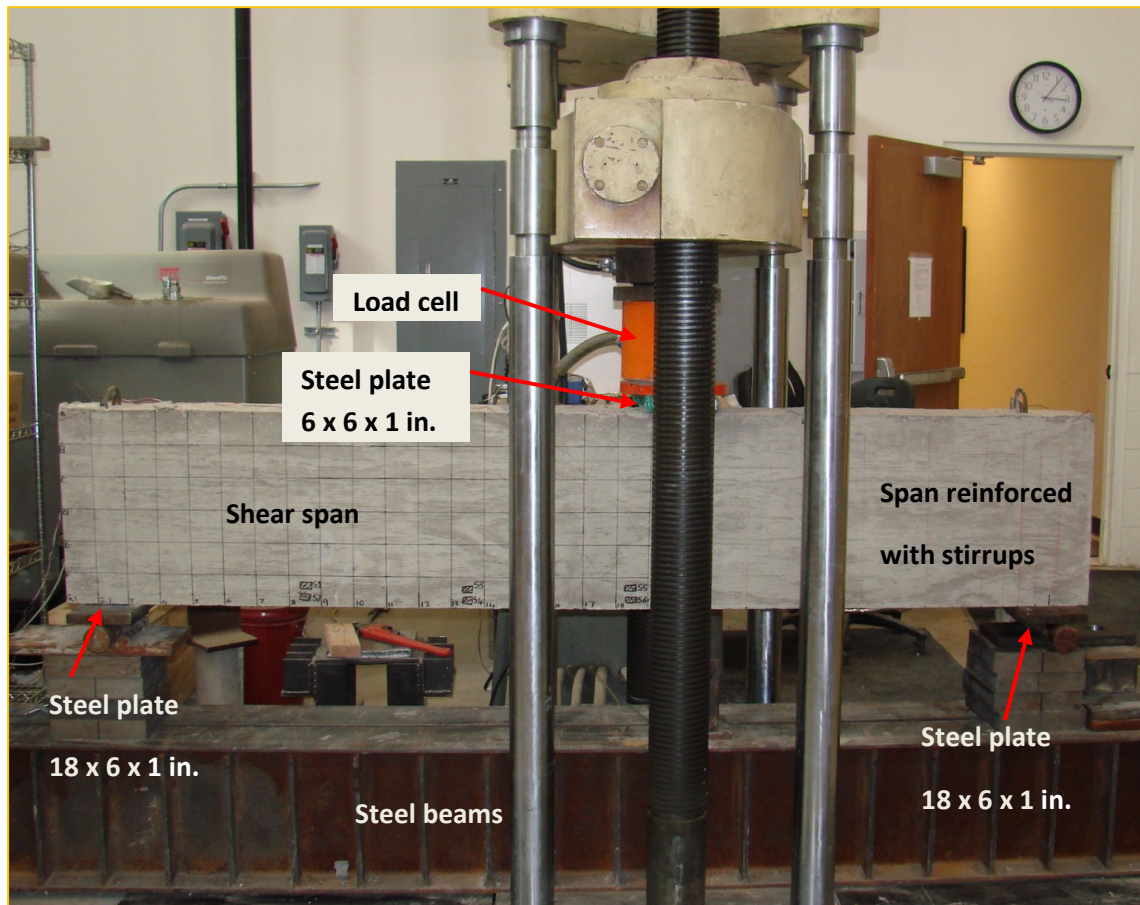
Figure 3.15 Beam test setup

3.1.6 Material Testing

*3.1.6.1 Compressive Strength*

The cylinders whose preparation and casting was explained above are now ready to be

tested. The ends of the cylinders were capped in accordance to ASTM C617/C617M with

a sulphur compound to ensure uniform axial loading. The cylinders were tested using the

500 kip compression machine and in accordance to ASTM C39 (Figure 3.16). The load

determined by the beam is them divided by the area of the loaded surface ($\pi$ x diameter of

cylinder) to get the compressive strength. The average was then determined for all

cylinders tested from one beam. The compressive strength of all the cylinders tested is given in appendix III.



Figure 3.16 Flexural strength test setup

*3.1.6.2 SFRC Flexural Strength Test*

**Test setup**

The beam specimens were tested at the age of 28 day in accordance to ASTM C 1609. The three point loading test is as shown in Figure 3.17 below. The specimen setup is the same to that of ASTM C78 but it incorporates a closed-loop servo-controlled testing system and roller supports that are free to rotate on their axis. The specimen was setup in such a way that it is loaded at the third points. The span length was 18 inches. The beams

were loaded at a rate of 0.005 inches per second. Two linear variable differential transducers (LVDT) were attached on each side of the beam to measure the net deflection of the beam. The test was terminated at a net deflection of 0.12 in. which is equivalent to 1/150 of the span length.
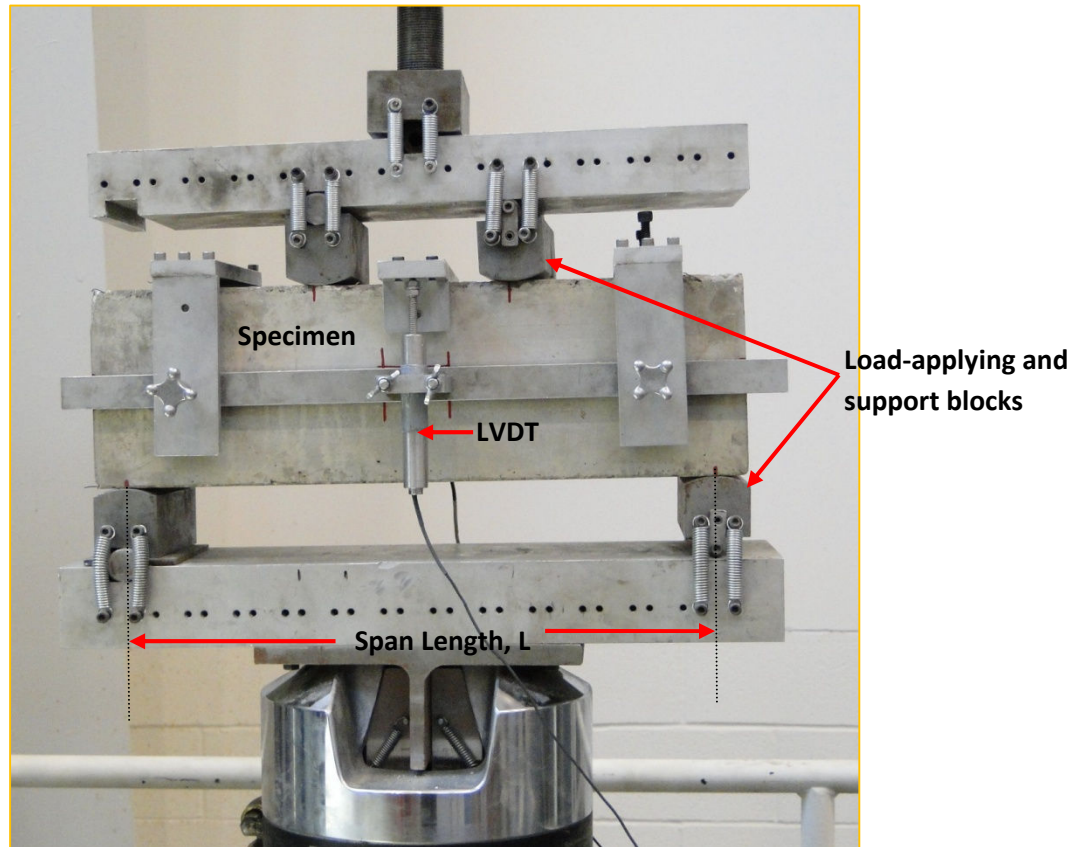


Figure 3.17 ASTM Beam Setup

**Data processing**

After the test, measurement were taken of the depth of compression region (c), crack width at the bottom face (w), and the largest distance from crack to support (a). Results should not be used if fracture occurs outside the middle third of the specimen.

A net deflection was then determined from the deflections recorded from the two LVDTs by taking their average. A load versus deflection curve was then plotted as will be seen in chapter four.

### 3.1.6.3 Single Fiber Pullout Test

**Pullout test setup**

The top of the specimen was gripped by a specially designed clamp which was attached to the load cell of the testing machine. The body of the specimen was restrained by a grip used to test ASTM tensile mortar specimens. The free length of the specimen should be minimized in order to simulate a fiber pulled in a typical cracked tensile specimen and minimize the effects of free elongation of the fiber. One LVDT was placed to the side of the specimen to measure the differential movement between the fiber end and the fixed matrix specimen (slip). Figure 3.18 below show the test setup as described above.
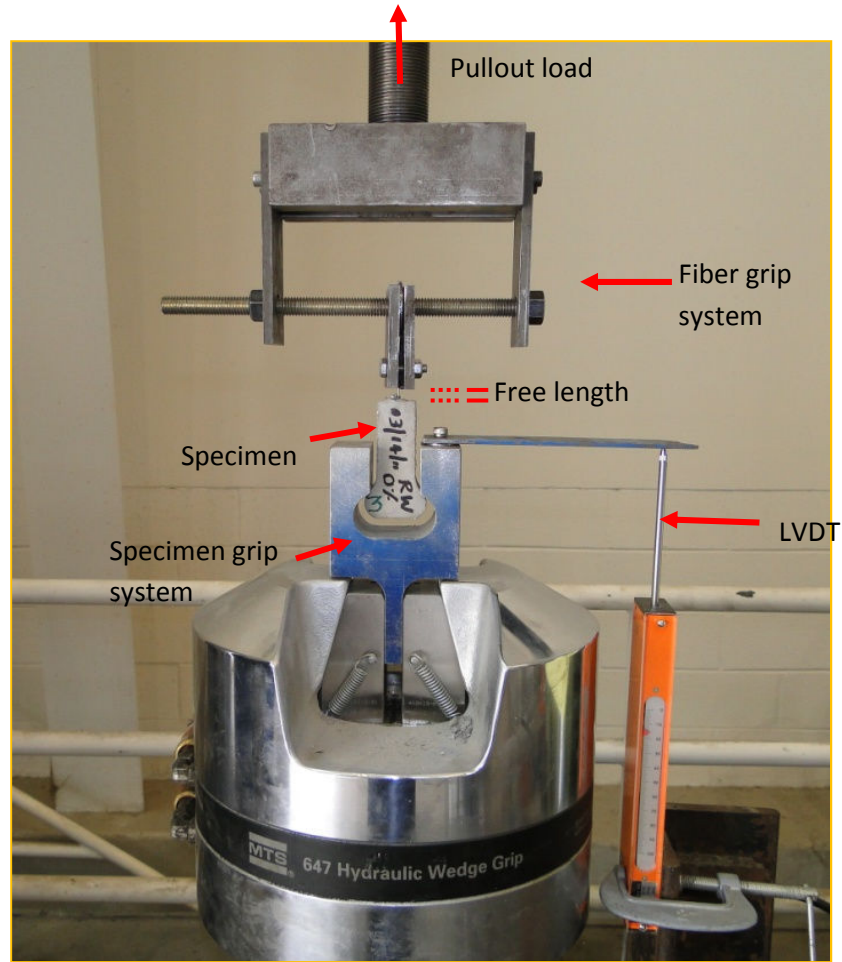
Figure 3.18 Fiber pullout test setup

**Data processing**

The values of the pullout load and corresponding slip were recorded using a data acquisition system and stored. A graph of pullout load versus slip was then plotted using the stored data.

## 3.2 Experimental Program on Alkali-Silica Reaction in SFRC

3.2.1 Introduction

Relevant data is needed in order to predict the influence of fibers in arresting cracks and expansion due to ASR. The ASTM standard methods for the identification of ASR

expansion were used mainly the C1260 and C1293.In this chapter the test methods used are described in general.

Deterioration of concrete due to ASR is largely known to develop faster under conditions of high relatively humidity of concrete. Therefore the test methods used utilize high relative humidity to accelerate expansion due to ASR.

The experimental program attempts to answer the following questions:

1. What are the effect of fibers on the expansion due to ASR as well as the effect on arresting cracks due to ASR?

2. How do these results change if the fiber content is varied and different fiber types used?

Premature concrete deterioration associated with ASR and DEF progresses faster under conditions of high internal relative humidity of concrete (Boenig, 2000). It should therefore be possible to evaluate the relative effectiveness of proposed mitigation treatments indirectly, by comparing the extent to which they limit the internal relative humidity of concrete subjected to cycles of wetting and drying. During the wetting stage of a cycle, an ideal mitigation treatment would keep the internal relative humidity of a concrete specimen lower than that of an untreated control specimen. During the drying stage, an ideal mitigation treatment would permit a treated specimen to lose internal moisture at the same rate as an untreated control specimen. Under repeated cycles of wetting and drying, a specimen with an ideal mitigation treatment would stay consistently drier inside, than an untreated control specimen.

Below are discussions on the key components of the experiment and how they were obtained. Also how the key components relate and their specific importance in impacting ASR are discussed. These are important according to TXDOT the data is recorded for the Premature Concrete Deterioration Database (PCDD).

3.2.2 Material Information

In this chapter the materials that have been used throughout this research project are discussed. All different types of aggregates, cement, fibers and admixtures used in this research are included.

All material properties discussed therein are based on mill certificates, manufacturer's data sheets, or analytical testing.

*3.2.2.1 Portland Cement*

The chemical and physical properties of portland cement play important roles in ASR. The parameters and properties considered are:

- **Type:** The type of portland cement according to ASTM C 150 and ASTM C 1157 was collected, along with its designation (e.g., Type I, Type II, etc.). This information is important because the type of cement will reflect the chemical and physical nature of the cement. Portland cement was used (ASTM) type II for this research. The cement used in this research was collected from Hanson Precast Company.

The following Table 3.7 below shows the critical information needed to give an idea of the chemical composition of the cement used. This information is obtained from the mill sheet obtained from the cement plant.

Table 3.7 Chemical Properties of Portland Cement

| Chemical Properties | % |
|---|---|
| Silicon Dioxide ($SiO_2$) | 19.80 |
| Aluminium Oxide ($Al_2O_3$) | 5.50 |
| Iron Oxide ($Fe_2O_3$) | 2.00 |
| Calcium Oxide (CaO) | 61.60 |
| Magnesium Oxide (MgO) | 2.30 |
| Sulfur Trioxide ($SO_3$) | 4.20 |
| Total Alkali ($Na_2Oeq$) | 0.95 |
| Tricalcium Silicate ($C_3S$) | 45.50 |
| Tricalcium Aluminate ($C_3A$) | 11.10 |

- *Alkali Content* – the alkali content of portland cement, expressed as Na2Oe or equivalent alkali content, has a major impact on both ASR. High alkali contents increase the possibility of ASR occurring by increasing the pH of the pore solution and the solubility of reactive silica. One should keep in mind that the Na2Oe of a given portland cement is not in itself, an accurate indicator of ASR potential, but rather it is the total alkali loading of the concrete mixture that determines ASR potential.

- **Physical Properties:** In addition to the chemical characteristics described above, the physical characteristics of portland cement namely fineness and compressive strength can play an important role, primarily in DEF which this research is not covering.

## 3.2.2.2 Fine Aggregates

A large proportion of the concrete aggregates in Texas are potentially reactive with regard to ASR. Three types of fine aggregates were used in this research of which one was nonreactive.

The sizes of the fine aggregates were graded according to ASTM C1260 and C1293. Natural fine aggregates were used. Reactive fine aggregates used for the mortar bar test were fine Bristol aggregates, producer code number 790 mixed with reactive sand from Whitney, producer number 706. The mortar bar test was performed in Hanson to test the reactivity of the fine aggregates used in this research. Only reactive aggregates were used that is those with an expansion greater than 0.10 percent.

## 3.2.2.3 Coarse Aggregates

Four types of coarse aggregates were used in this research of which one was nonreactive. The sizes were graded according to ASTM C1260 and C1293.All the aggregates used were already crushed to required sizes at Hanson Precast Company. Both crushed stone and gravel were used for the reactive coarse aggregates while crushed stone was used for the nonreactive coarse aggregates. The reactive coarse aggregates are all from Texas quarries. The reactive coarse aggregates used in the mortar bar test were crushed aggregates from Bristol, producer number 790 and crushed aggregates from Davis quarry. The reactive coarse aggregates used for the prism test were pea gravel from Whitney, producer number 706 as well as nonreactive crushed stone from Davis. These aggregates were chosen due to their known reactivity from the mortar bar test performed at Hanson Precast Company.

*3.2.2.4 Water*

The water used in this research was the normal tap water but reference was made to specification D1193 to ensure that it conformed to Type IV water.

*3.2.2.5 Fibers*

Twist fibers were used in this research to mitigate the effects of ASR. These fibers were chosen due to their small diameter and hence their ability to arrest cracks and prevent them from widening. It was also our intention that the fibers will reduce the expansion of the ASR gel and hence reduce expansion of the concrete due to ASR.

Also microfibers were used in the mortar bar test as it made it possible to use the standard molds for this test. These fibers were provided by the Maccaferri Company. The Table 3.8 below shows the mechanical and geometrical properties of the fibers used.

Table 3.8 Fiber Properties
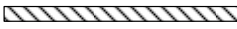
| Fiber | Geometrical Configuration | Diameter mm (in) | Length mm (in) | Aspect Ratio |
|-------|--------------------------|------------------|----------------|--------------|
| Twist Fiber | | 0.2 (0.008) | 25.4 (1.0) | 125 |
| Microfiber | | 0.03 (0.001) | 1.27 (0.5) | 500 |



Figure 3.19 Twist fiber

Figure 3.20 Microfibers

*3.2.2.6 Sodium Hydroxide Solution (NaOH)*

The NaOH solution used in this research was as specified in ASTM C1260 and C1293.That is NaOH USP or technical grade provided that Na+ and OH- are shown by chemical analysis to lie between 0.99N and 1.01N. The NaOH solution used in this research was donated by Hanson Pipe & Precast Company.

3.2.3 Material Preparation

The preparation of the materials required was determined by the test method used. Both ASTM C1260 and C1293 require unique guidelines as given in the standard which should be followed to achieve satisfactory results. The subsequent sections which include material processing mix proportioning, casting of specimens and conditioning will be dealt with as per the method in use.

*3.2.3.1 Accelerated Mortar-Bar Test (ASTM C1260)*

 The Accelerated mortar-bar expansion test is based on the National Building Research Institute (NBRI) or South African mortar-bar test (Oberholster and Davies, 1986) and is a modification of ASTM C 227.  Although aggregate and test specimen preparation are the same, the mortar bars are stored in a 1 Normal NaOH solution so as to provide an immediate source of sodium and hydroxyl ions to the bars and maintained at a temperature of 80 °C to accelerate the alkali-silica reaction. Comparator readings are taken over a period of 14 days. The test conditions are thus conditioned to be more severe than most field environments. If the average expansion is less than 0.10 % on the 16th day after casting, then the cement-aggregate combination is considered non-reactive. If the average expansion is between 0.10% and 0.20 %, the aggregate may be considered slowly reactive and additional confirmatory tests should be performed. If average expansion is greater than 0.20 %, the aggregate is considered deleteriously reactive.

Investigators have found that the method can identify slowly reactive rock types that previously could not be detected by other reactivity tests (Stark et al., 1993; Davies and Oberholster, 1986, 1987; Hooton and Rogers, 1989, 1992; Hooton, 1990). Work done on known reactive and non-reactive rock types by Stark et al. (1993) suggests modification of the test interpretation criteria for some slowly reactive aggregate types: to eliminate the gray area between 0.10 and 0.20 % expansion, it has been suggested that expansions greater than 0.08 percent be interpreted as potentially deleterious and expansions of 0.08 percent or less as non-deleterious. These criteria are based on using a 1N NaOH immersion test solution. Stark et al. (1993) also investigated a linear regression equation

that relates the concentration of the NaOH solution to cement alkali level for a given water-cement ratio.

**Material processing**

*Aggregate preparation*

Aggregate processing was done according to the guidelines given in ASTM C1260 as outlined below:

- The aggregates were dried in an oven for 24 hours in order to remove any existing moisture.

- Coarse aggregates are crushed to achieve a particle size distribution identical to that of fine aggregates.

- Both fine and crushed coarse aggregates are sieved using a sieving machine. All aggregates were graded according to table 1 of the standard shown here as Table 3.9.

Table 3.9 Grading Requirements

| Sieve size | | Mass% |
|---|---|---|
| **Passing** | **Retained on** | **Mass%** |
| 4.75mm (No. 4) | 2.36 mm (No. 8) | 10 |
| 2.36mm (No. 8) | 1.18 mm (No. 16) | 25 |
| 1.18mm (No. 16) | 600 μm (No. 30) | 25 |
| 600 μm (No. 30) | 300 μm (No. 50) | 25 |
| 300 μm (No. 50) | 150 μm (No. 100) | 15 |

- The aggregates retained on each of these five sieve sizes were then washed in order to remove any smaller particles present on their surfaces.

- After this, the washed aggregates were placed again in the oven to dry completely.

- The portions of aggregates were stored individually in clean containers having tight-fitting covers.

*Cement preparation*

A Portland cement meeting the specifications C 150 were used for the test. The cement was passed through an 850-µm (No. 20) sieve to remove any lumps before use.

**Mixture Proportions**

The mix proportion was done according to the standard for the control specimens whereas for the specimen containing fibers, 1% by volume of fiber was added in the mix. The dry materials for the mortar were proportioned using one part of cement to 2.25 parts of graded aggregate by mass. The quantity of aggregates is made up by recombining the portions retained on the various sieves as discussed above. A water-cement ratio equal to 0.47 by mass was used in the mix. The mix proportion is as shown in Table 3.10.

Table 3.10 Mix Proportion for Accelerated Mortar Bar Test

| Specimen | Cement | Aggregates | Fiber | Water | Total Weight |
|----------|--------|------------|-------|-------|--------------|
| PC | 19.47 | 43.82 | 0 | 9.15 | 72.45 |
| SFRC | 19.26 | 43.35 | 0.77 | 9.06 | 72.45 |

Note: All weights are in pounds

**Casting of the mortar bars**

The mortar bar specimens used for this research were not the standard size as specified in the C1260 standards. This is mainly due to the size of fibers used which requires that a large size of specimen is used to prevent the fibers from aligning. If microfibers were used in the specimens then the standard size of bars would have been used. In the first preliminary tests, reactive coarse aggregates were used. The aggregates were obtained from Hanson Precast Company whereby the reactivity of the aggregates was tested by the mortar bar test. The standard ASTM beam measuring 6 x 6 x 20 inches was used for the first batch of test. The mixing of the mortar was performed in accordance to requirements in C305.The mould was not oiled so as to prevent the oil inhibiting water penetration into the specimen as this is needed for ASR to take place.

 The test specimens were molded in not more than 2 mins and 15 seconds after mixing. The molds were filled and vibrated by the table-top vibrator. The molded specimens were then immediately placed in the curing room for 24 hours.

**Specimen Conditioning**

After 24 hours, the specimens were removed from the molds and marked for identification. Initial comparator readings were taken and recorded after which the specimens were immersed in a water bath at $80^{\circ}$C for 24 hours. The mortar bars were removed from the water bath one at a time and their surfaces dried. The expansion of the specimen was marked and recorded. The specimens were then placed in a container with sufficient 1N NaOH at $80^{\circ}$C for samples to be totally immersed. The container was sealed and returned in the oven. Although the container was tightly sealed, some evaporation of the NaOH occurred sometimes and the solution was returned to previous level using distilled water. Subsequent comparator readings were taken periodically for 14 days after the first reading.

The preliminary results from the expansion measurements are as shown in Table 3.11 below.

Table 3.11 16-Day Prism Expansion

| Specimen | Expansion (in.) |
|---|---|
| Plain Concrete | 0.141 |
| SFRC (1% volume fraction) | 0.090 |

The results clearly show a reduction in the expansion between the control specimen and the fiber reinforced specimen after 14 days of curing. The specimens were then placed outside the laboratory and measurements taken on expansion. Visual observation was

also done to check for cracks in the specimens and compare the crack formation in both the control and the fiber reinforced concrete.



Figure 3.21 Specimens immersed in 1N NaOH solution.

*3.2.3.2 Accelerated Concrete Prism Test (ASTM C1293)*

The concrete prism test (CPT) takes a full year to complete when assessing aggregate reactivity and 2 years when evaluating the efficacy of supplementary cementing materials (SCMs).This length of time is often seen to be excessive when an aggregate must be tested for specification requirements or job acceptance. Therefore in this research the accelerated prism test was used whereby the testing temperature was 140°F (60°C) instead of 100°F (38°C) while still retaining a strong correlation with field performance. ASTM C 1293 is generally accepted to be the best predictor of field performance and hence we decide to use it in this research.

In ASTM C 1293, concrete prisms are cast with square cross sections of 3.00 ± (75 ± 0.7mm) and are 11.25 in (285 mm) in length. Using ASTM C150 Type I Cement with a 0.9 ± 0.1 Na2Oeq (equivalent alkali), a cement content of 708 lb/ft$^3$ (420 kg/m$^3$) is specified for this test method. A certain amount of NaOH is added to the mixing water to obtain a total alkali content of 1.25 percent Na2Oeq (by mass of cement), which equates to a total alkali content in the concrete mixture of 4 lb/ft$^3$ (5.25 kg/m$^3$).

**Material processing**

Aggregate processing was done according to the guidelines given in ASTM C1293 as outlined below:

- The aggregates were dried in an oven for 24 hours in order to remove any existing moisture.

- Although the standard specifies that a reactive coarse aggregate should be used with a nonreactive fine aggregate and vice versa, this research used both reactive fine and coarse aggregates so as to get maximum expansion. This was done with the hope of getting faster reaction leading to cracking of concrete thus evaluate the effect of fibers in arresting cracks.

- The fine aggregate were tested using the grading as delivered to the laboratory.

- The coarse aggregates were sieved using a sieving machine and combined in accordance with the requirements in Table 1 of the standard shown here as Table 3.12.

Table 3.12 Grading Requirements

| Sieve Size | | Mass Fraction | |
|---|---|---|---|
| Passing | Retained | Coarse | Intermediate |
| 19.0-mm | 12.5-mm | 1/3 | - |
| 12.5-mm | 9.5-mm | 1/3 | 1/2 |
| 9.5-mm | 4.75-mm | 1/3 | 1/2 |

## Mixture Proportions

The mix proportion was done according to the standard for the control specimens whereas for the specimen containing fibers, 1% by volume of fiber was added in the mix. A dry mass of coarse aggregate per unit volume of concrete equal to $0.70 \pm 0.02$ of its dry-rodded bulk density as determined by Test Method C 29/C 29M was used. A water-cement ratio equal to 0.46 by volume was used in the mix. The mix proportions are as shown in table 3.13 the fiber volume fraction is to be varied at 0%, 0.5%, 0.75%, 1% and 1.5%. The preliminary test done using the prism test did not contain any fibers. This was to test if the accelerated prism test would actually result in faster expansion .

Table 3.13 Mix Proportion for the Accelerated Prism Test

| Fiber volume | Cement | Sand | Coarse aggregate | Water | Fiber |
|---|---|---|---|---|---|
| 0% | 14.73 | 17.97 | 41.68 | 6.77 | 0 |
| 0.50% | 14.49 | 17.67 | 41.00 | 6.66 | 1.33 |
| 0.75% | 14.37 | 17.53 | 40.65 | 6.61 | 2.00 |
| 1% | 14.25 | 17.38 | 40.32 | 6.55 | 2.65 |
| 1.50% | 14.01 | 17.09 | 39.64 | 6.44 | 3.98 |

- NaOH was dissolved in the mixing water and added as required to bring the alkali content of the concrete mixture, expressed as $Na_2Oe = \% Na_2O + 0.6583 \% K_2O$, up to 1.25 % by mass of cement. The calculations performed as shown in appendix IV.

**Casting of the mortar bars**

The mortar bar specimens used for this research were not the standard size as specified in the C1293 standards as was explained above. The standard ASTM beam was used for the first batch of test but in this case it was partitioned to two as shown below to give two beams of 6 x 6 x 10 inches each. The mixing of the mortar was performed in accordance to requirements in C305.The mould was not oiled so as to prevent the oil inhibiting water penetration into the specimen as this is needed for ASR to take place.

Figure 3.22 Partitioning of the ASTM beam into two equal sections.

The test specimens were prepared according to the requirements in test method C 157/ C157M. The molds were filled and vibrated by the table-top vibrator as shown in Figure 3.24 below. The molded specimens were then immediately placed in the curing room for 24 hours.
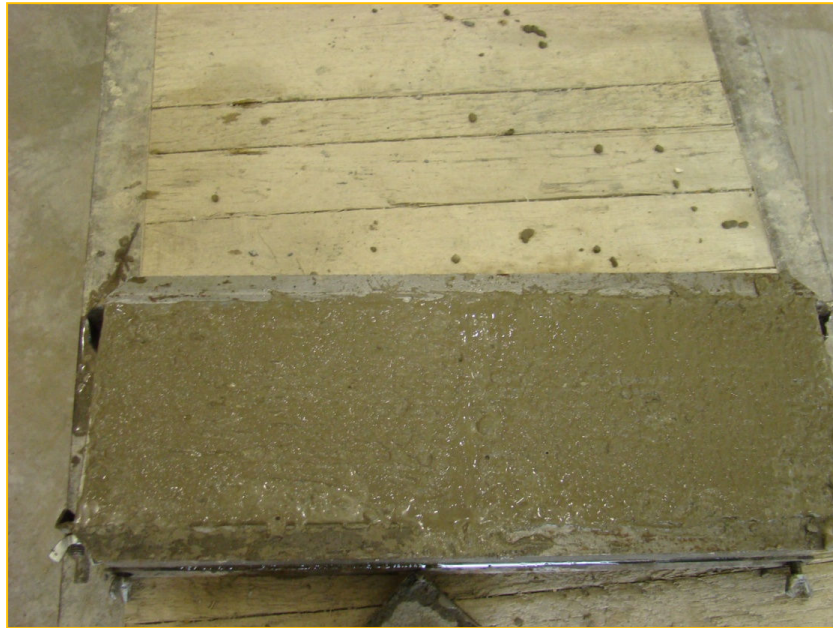
Figure 3.23 Cast specimen

**Specimen Conditioning**

After 24 hours, the specimens were removed from the molds and marked for identification. Initial comparator readings were taken and recorded after which the specimens were put in storage containers with water at $60^{\circ}$C. The specimens were not to touch the water as the water was only to ensure 100% humidity. The Figure 3.25 below shows the setup of the specimens.

Figure 3.24 Specimen conditioning setup

Subsequent comparator readings were taken periodically for 13 weeks. After 13 weeks of measurement, no difference in the expansion was observed. It is believed that this test would require more time for expansion to be realized. The specimens were therefore placed outside the laboratory and measured every few weeks.

### 3.2.3.3 Accelerated Mortar Bar Test using Microfibers

The next round of tests was performed using microfibers from the Maccaferri Company. Since the fibers are small enough, the standard test molds were used measuring 1 x 1 x 11 inches having a 10-in gauge length. Specimens containing 0% and 1% volume fraction of fibers were cast to determine the influence of fibers on the expansion due to ASR. Two mortar bars were cast for each volume fraction of fibers. The material preparation and casting then followed the procedure as explained in section 3.1.3.1. This test was

conducted in the Hanson Pipe and Precast Company laboratory. The curing and conditioning was also done in the laboratory.



Figure 3.25 Compaction of the mortar in the mold

The specimens were immersed in NaOH solution and placed in the oven at a temperature of 80°C for a period of 14 days (Figure 3.27). The measurement of expansion was made using a suitable apparatus for the measurement of length changes (Figure 3.28).



Figure 3.26 Specimen conditioning in NaOH solution
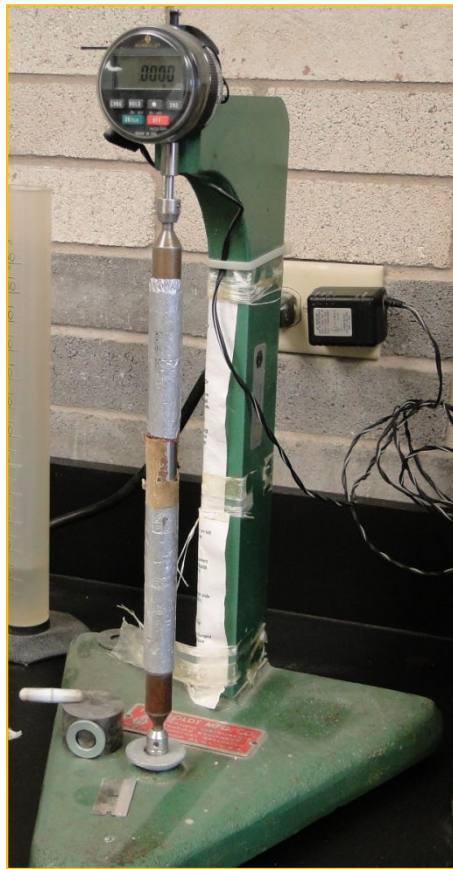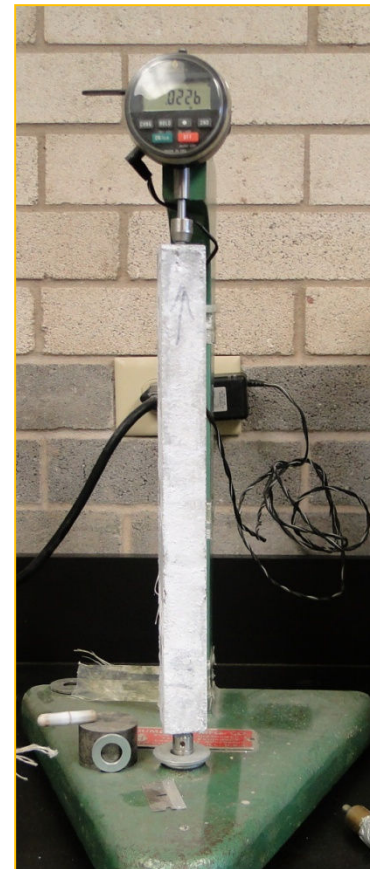
(a)                                              (b)

Figure 3.27 (a) Checking the dial gauge reading using reference bar and (b) measuring the change in length of the specimen

The results from the expansion test (Table 3.14) show that there is a decrease in the expansion due to ASR when steel microfibers are added to the concrete. This results support the findings made earlier when using conventional steel fibers.

Table 3.14 16-Day Mortar Bar Expansion

| Specimen | Expansion (in.) |
|----------|-----------------|
| Plain Concrete | 0.067 |
| SFRC (1% volume fraction) | 0.0195 |

These specimens were also stored to check the effect of fibers on cracking due to ASR after a long exposure time to the elements.

3.2.4 Proposed Research Plan

This research is a long term investigation on the effect of adding steel fibers to the expansion of concrete due to ASR. The test will take a span of four years to be completed. More specimens will be cast with different fiber content and laid outside to be exposed to the natural elements of the weather. These specimens will be periodically examined for cracks and for any expansion and the results recorded. Some petrographic analysis is also been considered whereby the concrete specimen will be subjected to microscopic analysis to determine the main mechanical and microstructural characteristics of SFRC subjected to ASR. A conclusion will then be made from the acquired results on the influence of fiber in minimizing expansion and crack widening.

CHAPTER 4

DATA ANALYSIS AND RESULTS

**4.1 Introduction**

This chapter contains a detailed analysis and discussion on the results of the beam test and on the mechanical properties tests. Each beam will be analyzed separately to fully understand its behavior, including its load versus deflection relationship and crack pattern. A comparison will then be made between the different beams tested. A comparison will also be made between the different specimens for each of the small specimen tests.

**4.2 Beam Results and Analysis**

The beams were setup as was explained in the previous chapter and monotonically loaded to failure. Load was applied to the beam at 5-10 kip intervals and the beam visually observed for cracks. A permanent marker was used to trace the cracks on the beam and this was at the same time transferred to a printed paper replica of the beam for records. Below is a summary for each of the beams that were tested.

4.2.1 RC

Load was applied in increment of 5 kips and visually observed for cracks. The first visible crack occurred at a load of 15 kips and was due to flexure. Subsequent flexural cracks developed at the bottom fiber at a load of 20 kip (Figure 4.1).
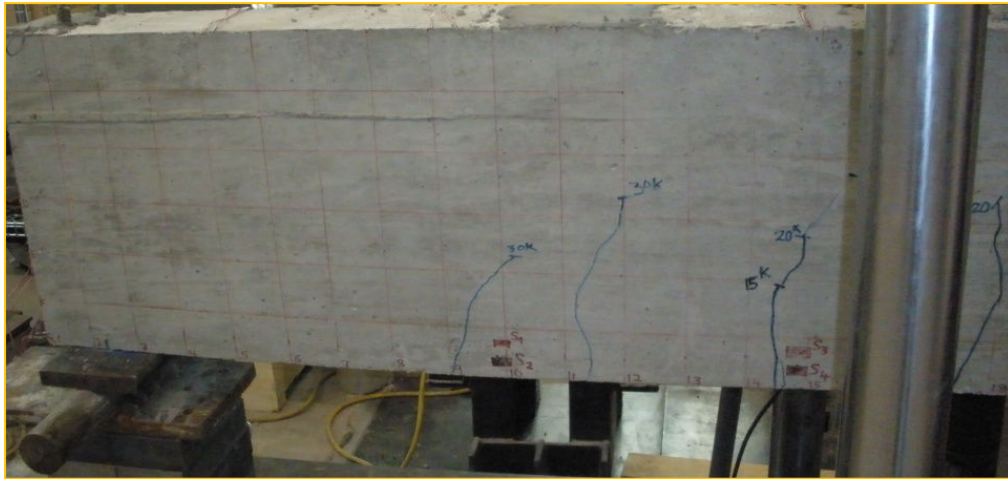
Figure 4.1 Formation of flexural cracks

At loads of 30 and 40 kips, some flexural cracks showed the change of propagation angles from 90 degree to close to 45 degree with respect to beam axis. These cracks propagated towards the loading point as the applied load increased. Also some web shear cracks developed at a load of 40 kip.

At the ultimate load of 42 kips, a sudden brittle shear failure occurred with the web shear crack opening up (Figure 4.2). The web shear cracks begun to propagate to the bottom and to the loading point before failure. The summary of the test is also tabulated on Table 4.1

Figure 4.2 Shear failure at 42 kips

Table 4.1 RC Summary of Test Results

| Description | Corresponding Applied Load (kips) | Corresponding Shear Force* (kips) | Corresponding Deflection (in.) | Normalized Shear Strength** |
|---|---|---|---|---|
| The first visible crack (flexure under loading point) | 15 | - | 0.0989 | - |
| The first visible shear crack(formation of flexural-shear) | 30 | 12 | 0.1537 | 1.80 |
| The first visible web shear crack | 40 | 16 | 0.2076 | 2.41 |
| The ultimate stage | 42 | 16.8 | 0.2159 | 2.51 |

*: shear force = applied load x 0.4

**: Normalized shear strength = shear force/$\sqrt{f_c'}*b_w*d$ ($f_c'$=4800 psi, $b_w$=6 in., d = 16 in.)

Data was retrieved from the computer and the load versus deflection curve plotted for the

beam (Figure 4.3).

134
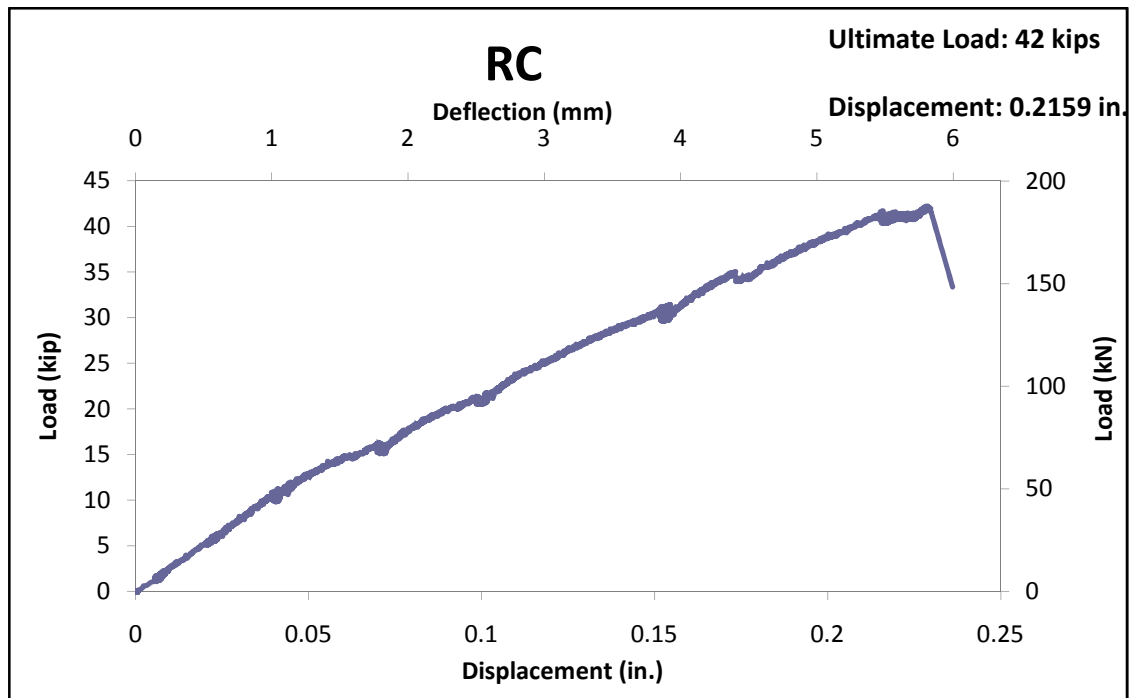
Figure 4.3 Load deflection curve

**Discussion of results**

The beam failed suddenly as is expected of reinforced concrete as there was no kind of reinforcement to allow for gradual failure. The normalized shear crack was found to be 2.51 which is much larger than 2 which was used in the calculations. This value would have been much closer to 2 had the concrete reach its targeted compressive strength.

4.2.2 SFRC1

Load was applied in increment of 10 kips and visually observed for cracks. The first visible crack occurred at a load of 20 kips and was due to flexure. Additional flexural developed at the bottom fiber at loads of 30 kip (Figure 4.4)
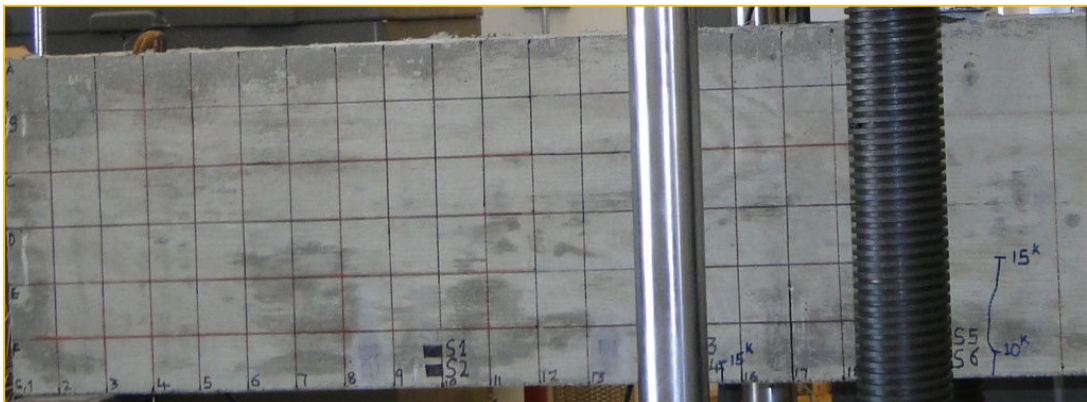
135

Figure 4.4 Formation of flexural cracks

Also at a load of 30 and 40 kips; some flexural cracks showed the change of propagation angles from 90 degree to close to 45 degree with respect to beam axis. These cracks propagated towards the loading point as the applied load increased. With subsequent loading, new shear cracks appeared and propagated towards the loading point. At a load of 70 kips, the first web shear cracks appeared and begun to propagate to the bottom of the beam and to the loading point. At the ultimate load of 90 kips, web shear failure occurred (Figure 4.5) followed by the crushing of concrete at the loading point. Fiber pull-out could also be observed at the crack point (Figure 4.6).

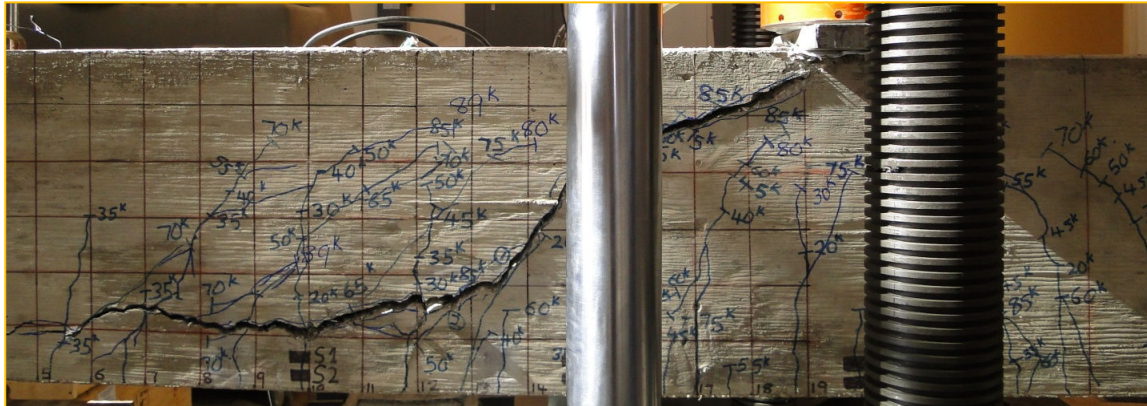Figure 4.5 Shear failure at 90 kips
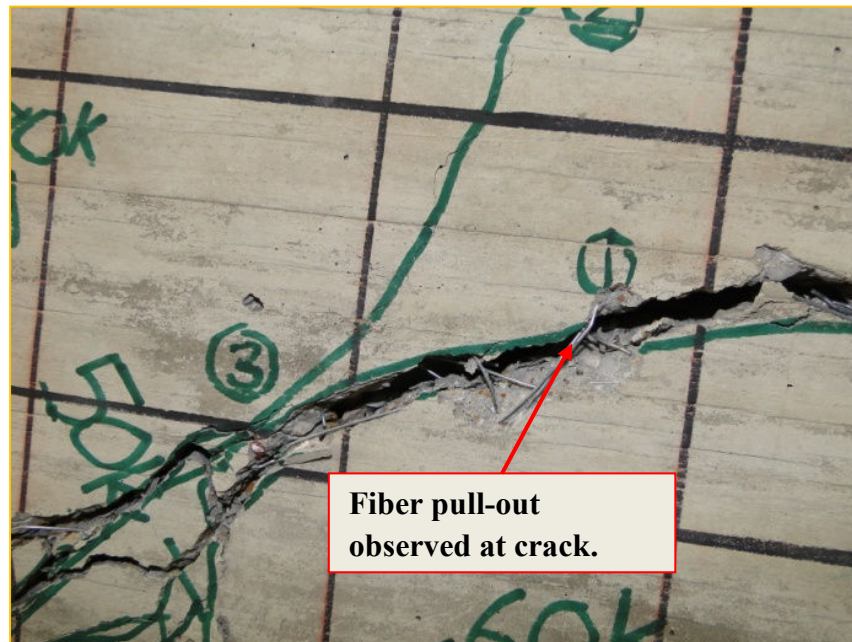


Figure 4.6 Fiber pullout in SFRC1 beam specimen

Table 4.2 shows the summary of test results whereas figure 4.7 shows the graph of load versus deflection.

Table 4.2 SFRC1 Summary of Test Results

| Description | Corresponding applied load (kips) | Corresponding shear force* (kips) | Corresponding deflection (in.) | Normalized shear strength** |
|---|---|---|---|---|
| The first visible crack (flexure under loading point) | 20 | - | 0.0890 | - |
| The first visible shear crack(formation of flexural-shear) | 30 | 12 | 0.1336 | 1.59 |
| The first visible web shear crack | 70 | 28 | 0.3247 | 3.70 |
| The ultimate stage | 90 | 36 | 0.4661 | 4.76 |

*: shear force = applied load x 0.4

**: Normalized shear strength = shear force/$\sqrt{f_c'}$*$b_w$*d ($f_c'$=6206 psi, $b_w$=6 in., d = 16 in.)
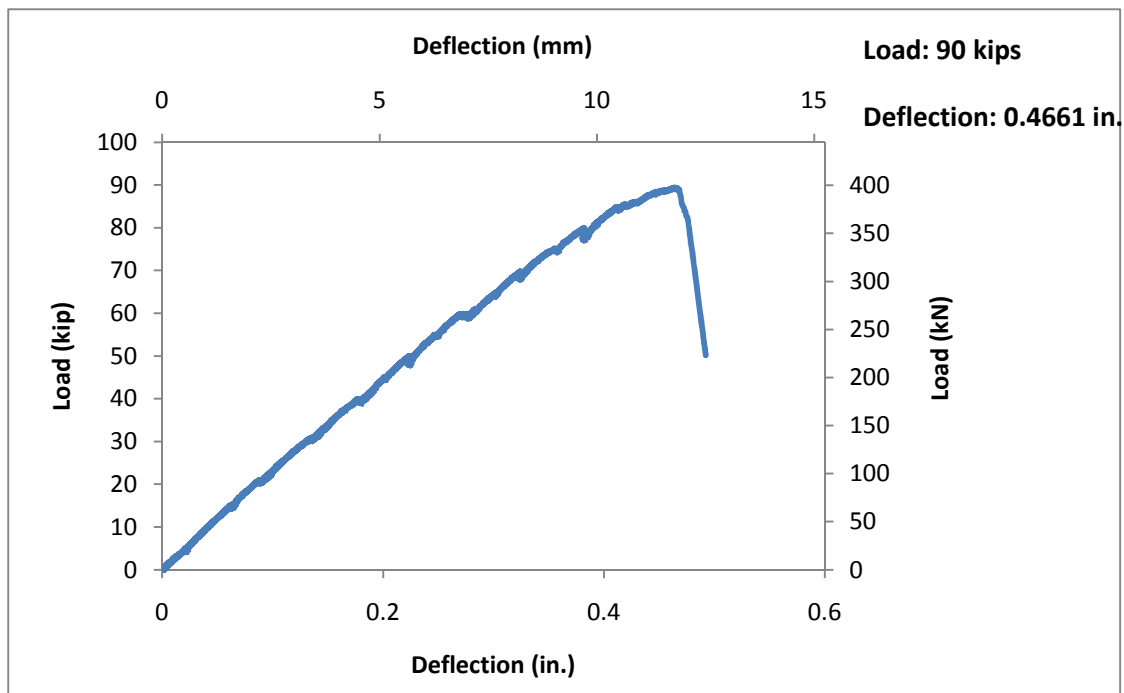


Figure 4.7 SFRC1 Load-deflection curve

**Discussion of results**

There was gradual failure as opposed to the sudden failure in RC. This is due to the property of the fibers to bridge cracks and redistribute tensile stresses hence also a higher failure load. The normalized shear strength of the beam was higher than the 3.5 value used in the design calculations.

4.2.3 SFRC2

Load was applied in increment of 5 kips and visually observed for cracks. The first visible crack occurred at a load of 10 kips and was due to flexure. Additional flexural cracks developed at the bottom of the beam at a load of 15 kip (Figure 4.8).
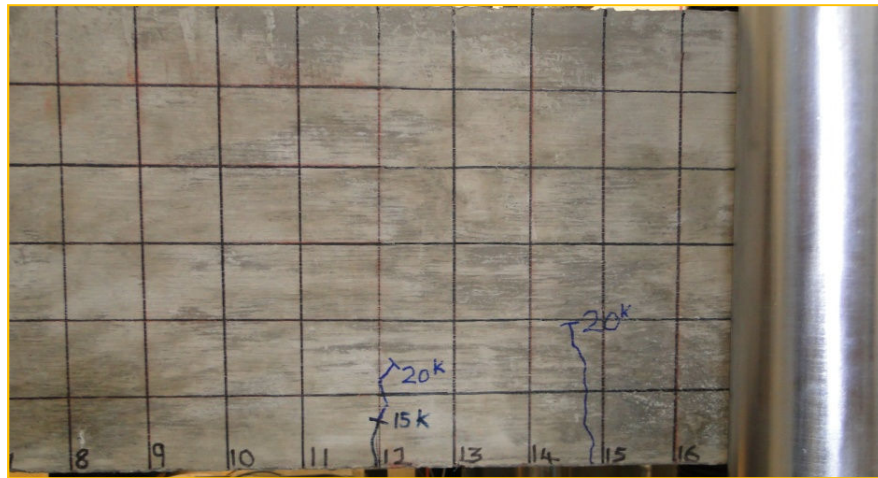


Figure 4.8 Formation of flexural cracks on SFRC2

At a load of 20 kips, some flexural cracks showed the change in the angle of propagation from 90 degree to close to 45 degree with respect to beam axis. These cracks propagated towards the loading point as the applied load increased. With subsequent loading, new shear cracks appeared and propagated towards the loading point. At a load of 50 kips, the first web shear cracks appeared and begun to propagate to the bottom and to the loading point. At the ultimate load of 89 kips, web shear failure (Figure 4.9) occurred preceded

by the crushing of concrete at the loading point. Fiber pull-out could be observed at the crack point (Figure 4.10).



Figure 4.9 SFRC2 shear failure at 89 kips
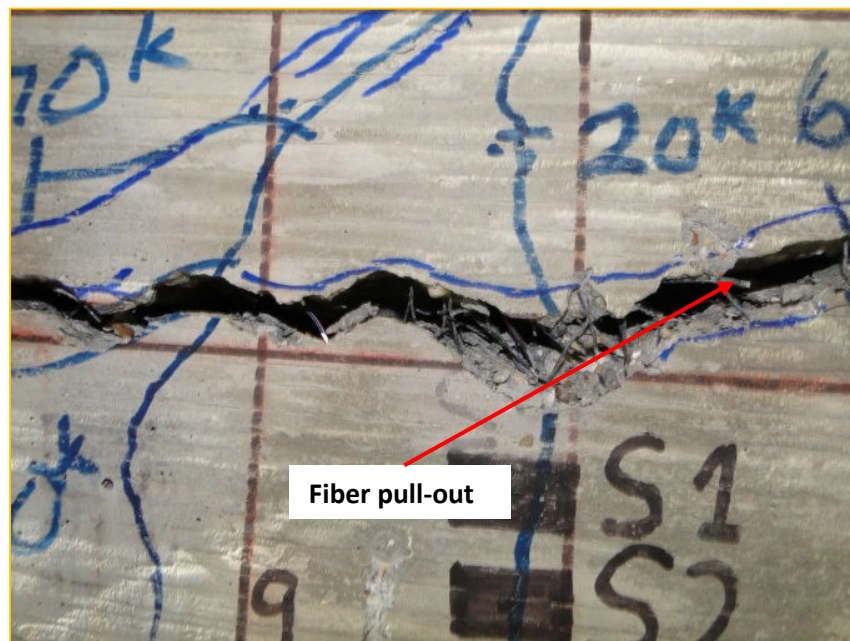


Figure 4.10 Fiber pullout in SFRC2 beam specimen

A summary of the test data and the load deflection curve is displayed in Table 4.3 below.

Table 4.3 SFRC2 Summary of Test Results

| Description | Corresponding applied load (kips) | Corresponding shear force* (kips) | Corresponding deflection (in.) | Normalized shear strength** |
|---|---|---|---|---|
| The first visible crack (flexure under loading point) | 10 | - | 0.0890 | - |
| The first visible shear crack(formation of flexural-shear) | 20 | 8.0 | 0.0733 | 1.02 |
| The first visible web shear crack | 50 | 20.0 | 0.1950 | 2.55 |
| The ultimate stage | 89 | 35.6 | 0.3802 | 4.53 |

*: shear force = applied load x 0.4

**: Normalized shear strength = shear force/$\sqrt{f_c'}$*$b_w$*d ($f_c'$=6673 psi, $b_w$=6 in., d = 16 in.)
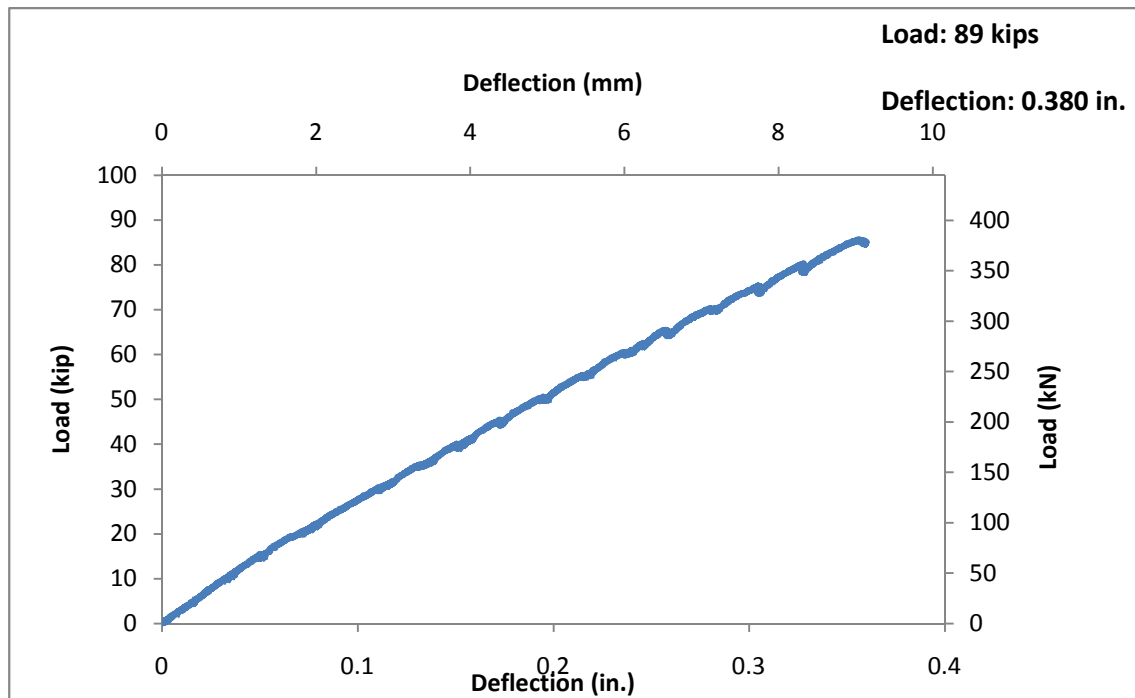
Figure 4.11 SFRC2 load-deflection curve

**Discussion of results**

It is clear from the results that there is not much difference in the ultimate load between SFRC1 and SFRC2. The normalized shear is also seen to be higher than the 3.5 value used in the design calculations. The mode of failure is seen to be through fiber pullout as could be seen at the crack area.

4.2.4 SFRC3

Load was applied in increment of 5 kips and visually observed for cracks. The first visible crack occurred at a load of 10 kips and was due to flexure. Additional flexural cracks developed at the bottom fiber at loads of 15 and 20 kip.

Figure 4.12 Formation of flexural cracks in SFRC3

At a load of 20 kips, some flexural cracks showed the change of propagation angles from 90 degree to close to 45 degree with respect to beam axis. These cracks propagated towards the loading point as the applied load increased. Crack propagation and formation was delayed at 25 to 30 kip load as could be seen by the lack of visible cracks at that stage.

With subsequent loading, new shear cracks appeared and propagated towards the loading point. At a load of 55 kips, the first web shear cracks appeared and begun to propagate to the bottom and to the loading point. At the ultimate load of 68 kips, web shear failure occurred preceded by the crushing of concrete at the loading point (Figure 4.13). Tensile cracks were also observed at the top of the beam. Some fibers appeared to be broken or deformed at the crack point (Figure 4.14). Fiber pull-out could also be observed at the crack point.
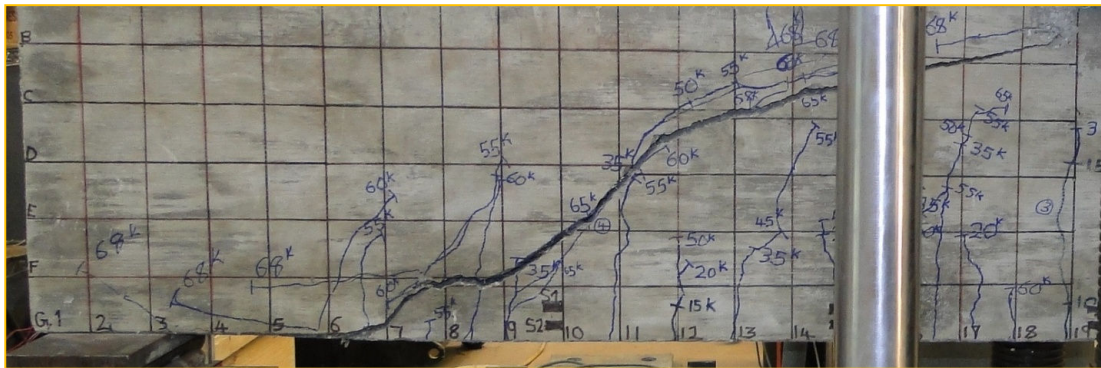
Figure 4.13 SFRC3 shear failure at 68 kips
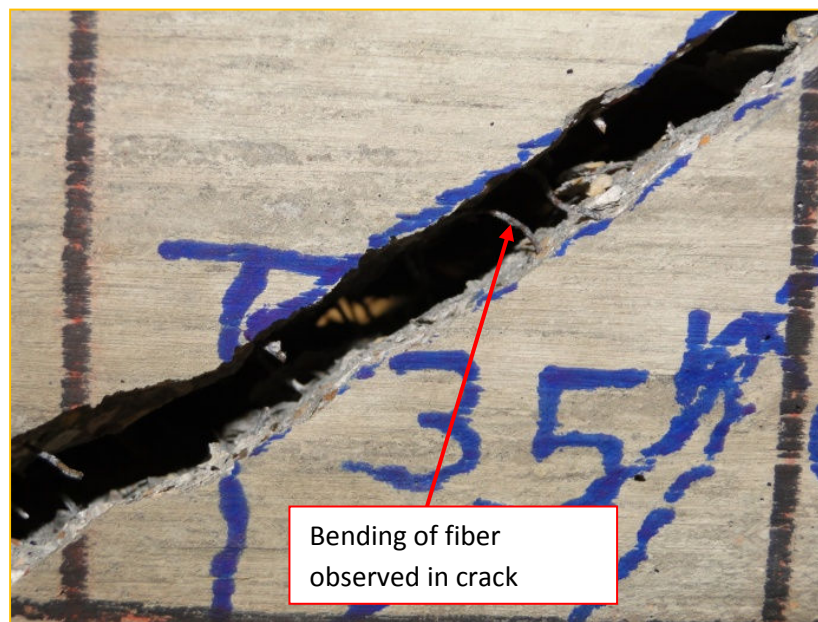


Figure 4.14 Fiber pullout and bending in SFRC3

The load-deflection curve was plotted as shown as well as tabulation of test data.

Table 4.4 SFRC3 Summary of Test Results

| Description | Corresponding applied load (kips) | Corresponding shear force* (kips) | Corresponding deflection (in.) | Normalized shear strength** |
|---|---|---|---|---|
| First visible crack (flexure under loading point) | 10 | - | 0.0335 | - |
| First visible shear crack (formation of flexural-shear) | 20 | 8 | 0.0753 | 1.01 |
| First visible web shear crack | 55 | 22 | 0.2187 | 2.76 |
| At ultimate stage | 68 | 27 | 0.2660 | 3.39 |

*: shear force = applied load x 0.4

**: Normalized shear strength = shear force/$\sqrt{f_c'}*b_w*d$ ($f_c'$=6873 psi, $b_w$=6 in., d = 16 in.)
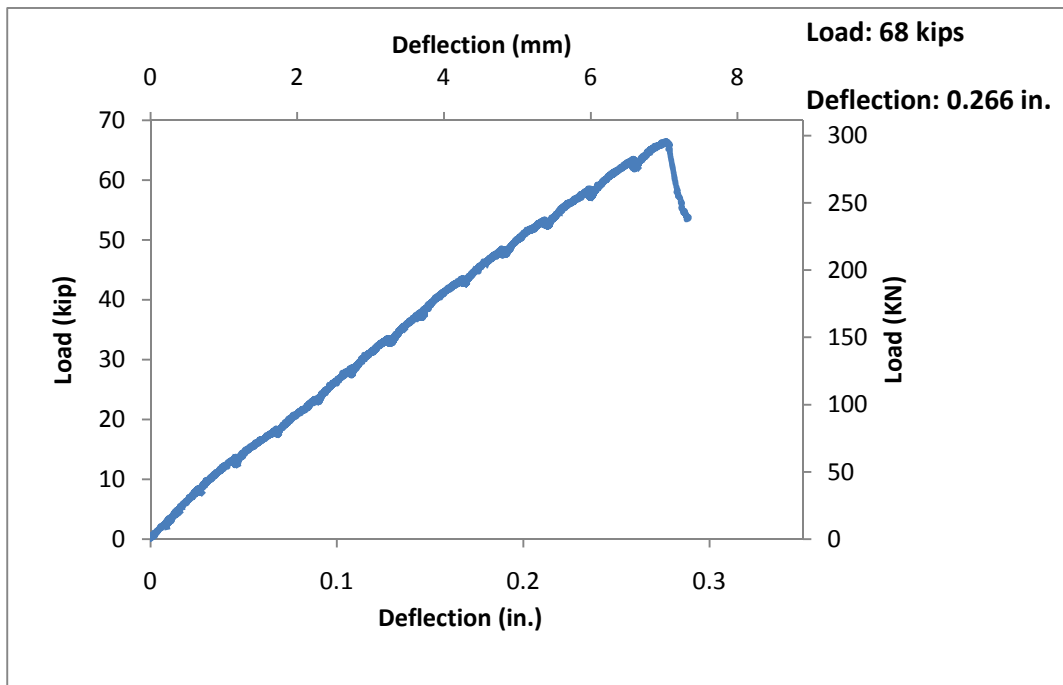


Figure 4.15 SFRC3 load-deflection curve

**Discussion of results**

The normalized shear strength of SFRC3 is seen to have reduced substantially. This can be explained by the observation that some of the fibers failed by fiber fracture instead of pullout. This reduced the ability of the fibers to redistribute the strains hence failure at a lower ultimate load.

**Comparison and discussion of beam results**

The Table 4.5 below tabulates the summary of the results on the beam tests.

Table 4.5 Comparison of Beam Test Results

| Beam | Degree of Corrosion (%) | Targeted f'$_c$ (psi) | Measured f'$_c$ (psi) | Peak Load (kip) | Deflection at ultimate (in.) | Normalized Shear Strength |
|------|------|------|------|------|------|------|
| RC | 0 | 6000 | 4800 | 42 | 0.2159 | 2.51 |
| SFRC1 | 0 | 6000 | 6206 | 90 | 0.4661 | 4.76 |
| SFRC2 | 12.5 | 6000 | 6673 | 89 | 0.3802 | 4.53 |
| SFRC3 | 50 | 6000 | 6873 | 68 | 0.2660 | 3.39 |

It is clear from the all the above results that:

- Fiber reinforced concrete has a higher peak load compared to that of RC. It is also allows for a higher normalized shear. There is more than 100% increase in the shear capacity.

- There is almost no change in the shear capacity between SFRC beams having no corrosion and those having 12.5% reduction in minimum diameter. Observation of fibers at the crack point showed fiber pullout in both the SFRC1 and SFRC2.

- There is a 24% decrease in the peak load between SFRC beam without corrosion and that with 50% reduction in minimum fiber diameter. This also led to a reduction in the normalized shear stress. When the crack at failure was observed, some fibers were seen to be broken while others were bent. However some of the fibers had pulled out from the matrix. Also during the SFRC3 beam test, there was a lack of propagation or formation of cracks between load increments of 25 kips and 30 kips. This has been explained by different researchers as been due to change in the once smooth surface of the fiber that resists pullout and delays crack propagation.

### 4.3 Fiber Pullout Test Results and Analysis

The test was conducted as was explained in section 3.1.6.3 above and the results are as shown below.

4.3.1 SFRC1

The graph of pullout load versus slip is shown below. All specimens tested pulled out from the matrix and no fiber fracture was observed.
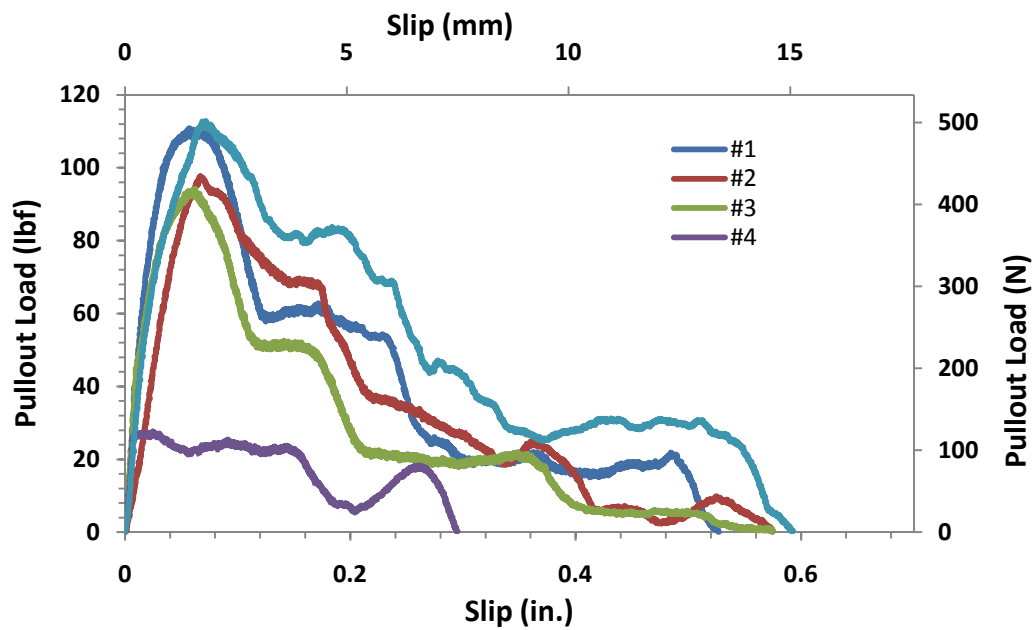
Figure 4.16 SFRC1 load versus slip



Figure 4.17 Fiber after pullout

4.3.2 SFRC2

For the SFRC beams tested, 60% of the specimens tested experienced fiber pullout while the rest showed fiber fracture before pullout (figure 4.18).
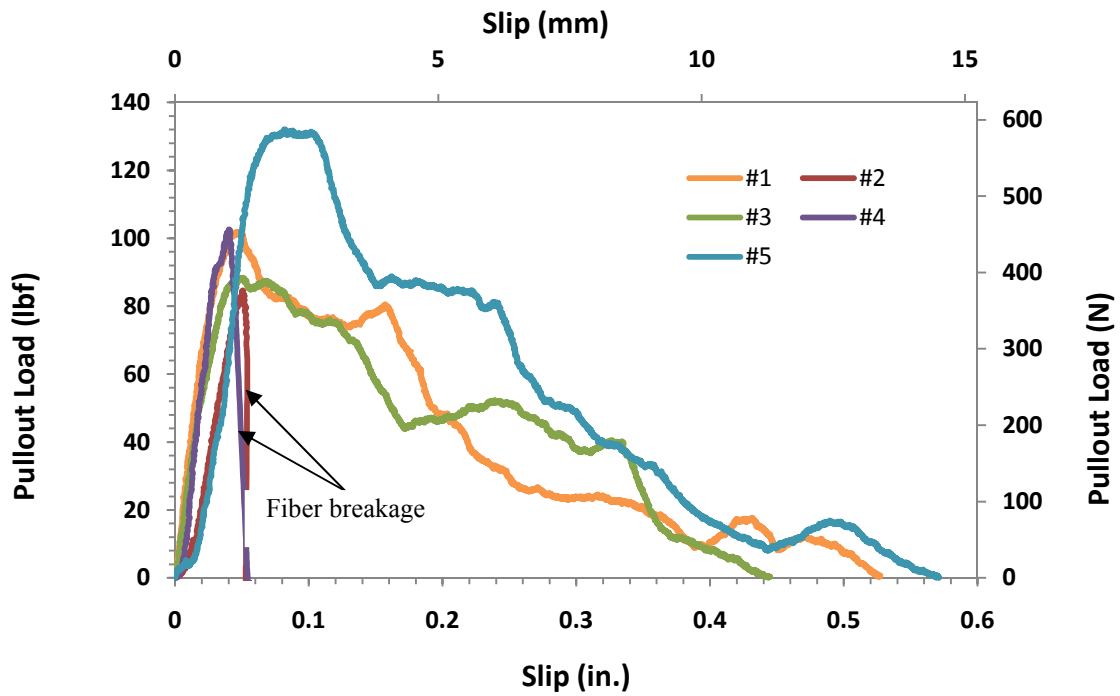
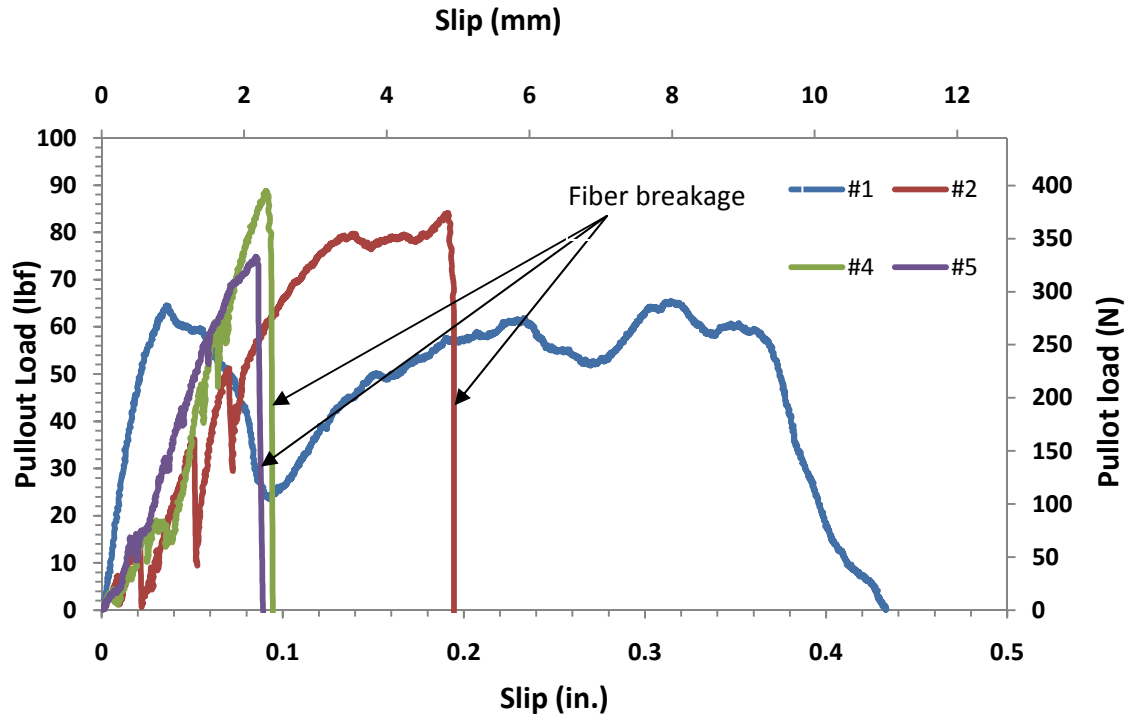Figure 4.18 SFRC2 pullout load versus slip



(a)                                                 (b)
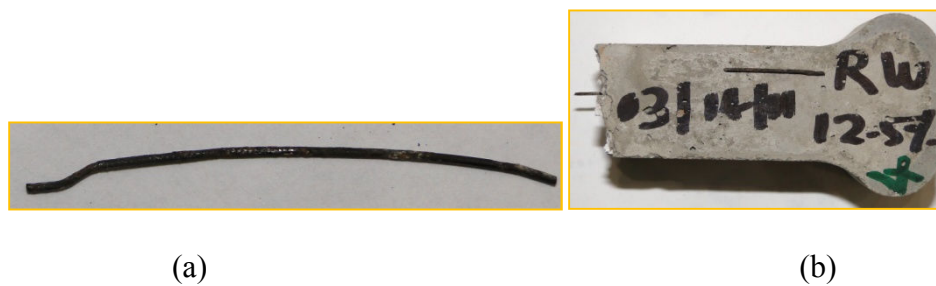
Figure 4.19 SFRC2 (a) Fiber pullout and (b) breaking of fiber before pullout

### 4.3.3 SFRC3

80% of the specimens in this test showed fiber fracture while the rest showed fiber pullout (figure 4.20).

Note: Specimen #3 broke before testing

Figure 4.20 SFRC3 pullout load versus slip



(a)                                      (b)
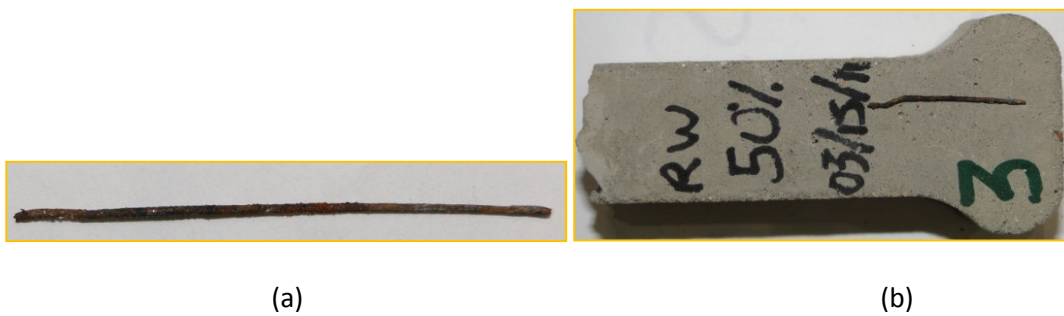
Figure 4.21 SFRC3 (a) Fiber pullout and (b) fiber breaking before pullout

**Discussion of results**

The typical pullout response of hooked fibers can be seen in the above graphs. This can

be explained as follows:

- The ascending part of the graph which is due to the bond between the fiber and the matrix.

- Due to full debonding, there is a sudden drop but the load recovers and keeps increasing to the first peak due to the mechanical anchorage of the hooks at the embedded end of the fiber.

- During pullout of the fiber, the hooks at the embedded end tend to straighten up due to plastic deformation along the matrix tunnel. Due to the two hooks at the embedded end, there are two peaks. One peak is when the first hook is straightened when pulling out and the second peak when the second hook undergoes the same pulling out of the matrix.

From past research on hooked fibers, it is expected that an increase in diameter of the fiber increases the peak pullout load due to an increase in the mechanical anchorage to straighten the fiber. The results however show that the SFRC2 had a slightly higher peak than SFRC1. This may be explained as increase in friction between the fiber and matrix due to the formation of corrosion products on the surface on the fiber.

SFRC3 is shown to fail in fiber fracture than fiber failure which may explain the decrease in the shear strength. It also has a lower peak strength compared to SFRC1 and SFRC2 and this is due to the decrease in the fiber diameter which affects the peak load much more than the increase in friction does.

## 4.4 Flexural Load Test Results and Analysis

The test was conducted as was explained in section 3.1.6.2 above and the results recorded. The results are as displayed below.

4.4.1 SFRC1

The specimens having no corrosion were setup and tested according to ASTM C1609 -10 Test Method for Flexural Performance of Fiber-Reinforced Concrete Using Beam with Third-Point Loading. The deflection as received from the two transducers was then recorded in the data acquisition system. The first peak load was used as the beam's peak load. A crack was seen to originate at the bottom of the beam followed by smaller cracks originating from the first crack formed as the load increased. With increase in the deflection after peak load, the load decreased and cracking noises could be heard which are indicative of fiber pullout. The average compression region depth was 0.75 inches. The average crack width at the bottom face of the beam was 0.19 inches. All the specimens cracked within the range required.

The graph below shows the load versus deflection curve of the specimens.
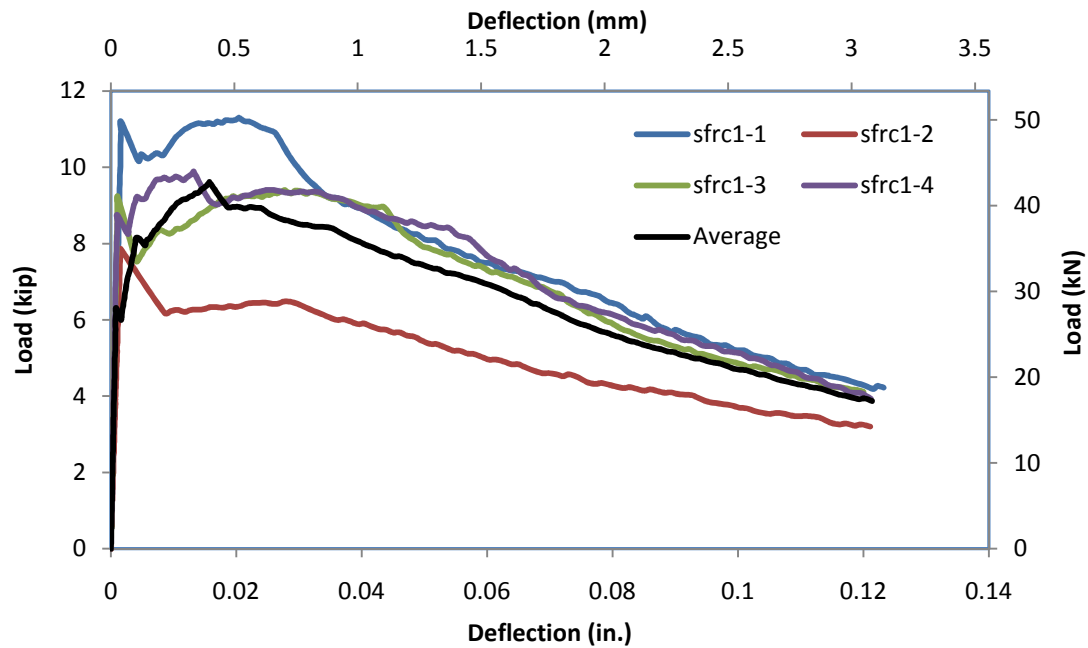
Figure 4.22 SFRC1 Load-Deflection Curves

The curves for the different specimens were pretty consistent except for some differences in the peak load. This can be attributed to the uncertainty in the fiber distribution from one specimen to the other.

4.4.2 SFRC2

SFRC2 showed cracks to initiate at the bottom and propagate to the top part of the beam with increase in load. The beam was seen to be still able to take more load even after a deflection of 0.12 inches. Cracking sounds were heard as the crack opened which was indicative of fiber pullout. The average compression region depth was measured to be between 0-0.1 inches. Also the average crack width at the bottom face of the beam was measured to be 0.2 inches. All specimens cracked within the required range.

From the study of the fibers at the crack, it showed that most fibers actually pulled out as opposed to fracturing. Despite this some fiber fracture was also observed which can explain the decrease in ductility between SFRC1 and SFRC2.
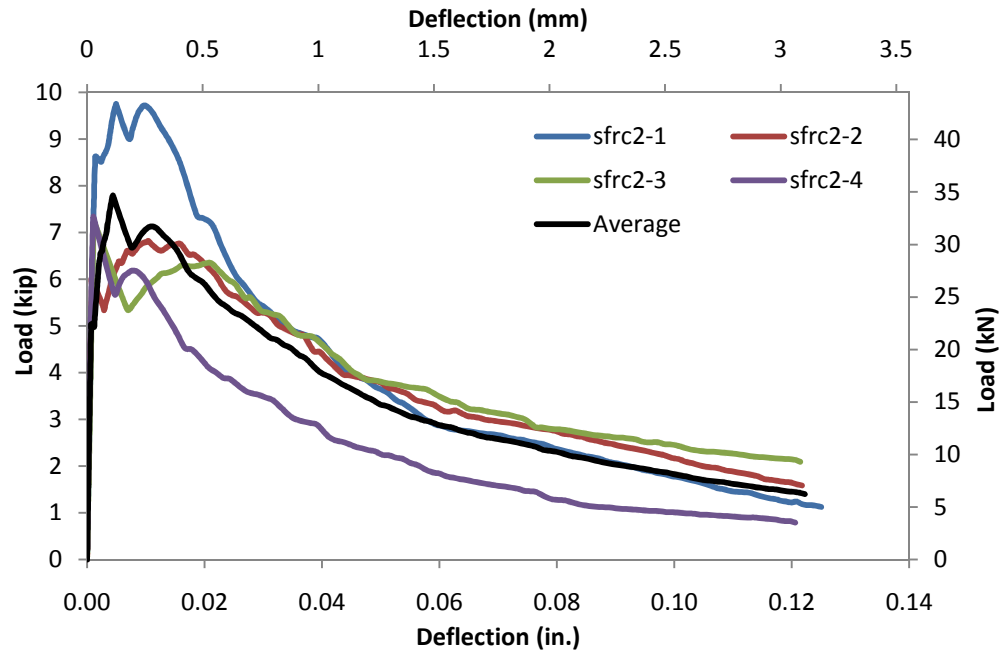

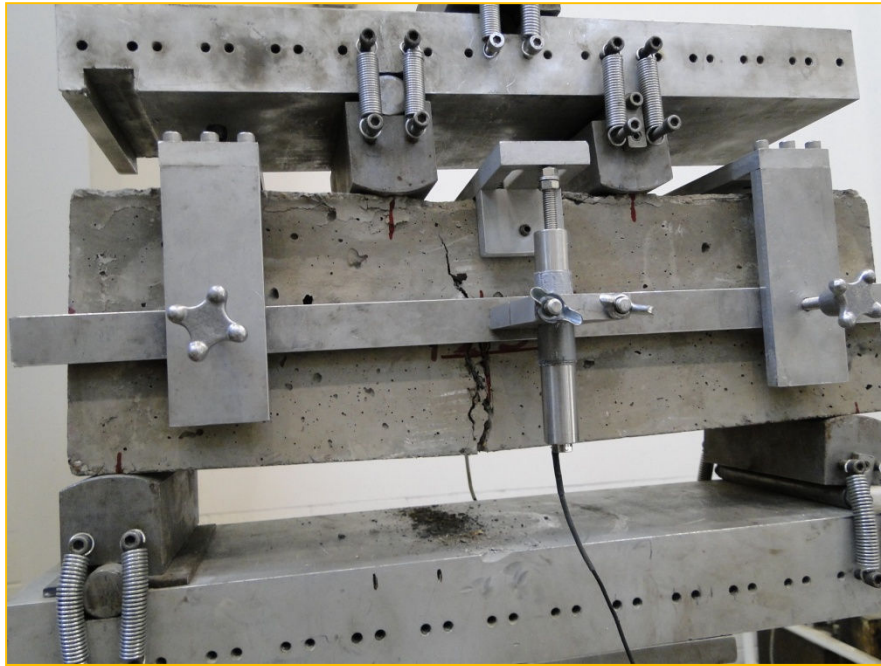
Figure 4.23 SFRC2 Load-Deflection Curves

Figure 4.24 SFRC2 Specimen at Failure

### 4.4.3 SFRC3

The average compression region depth for the SFRC3 specimens was found to be zero inches. The average crack width was found to be 0.28 inch although one should keep in mind that this is subject to errors due to concrete spalling at the edge of the crack. The crack in all the specimens was found to fall within the require range of 6-12 inches.

There is a good consistency in the results although some difference in the peak load is observed. For specimen two in this batch, a loud cracking noise was observed followed by a drastic decrease in the load. This is suspected to be due to fiber fracture. The ductility of the particular specimen is seen to have been reduced significantly.

The rest of the specimens showed some ductility although most of them could not carry any load past a deflection of 0.12 inches. The crack width was found to be quite large

compared to SFRC1 and SFRC2. From the observation of fibers at the crack point, both fiber pullout and fiber fracture was observed to have occurred.
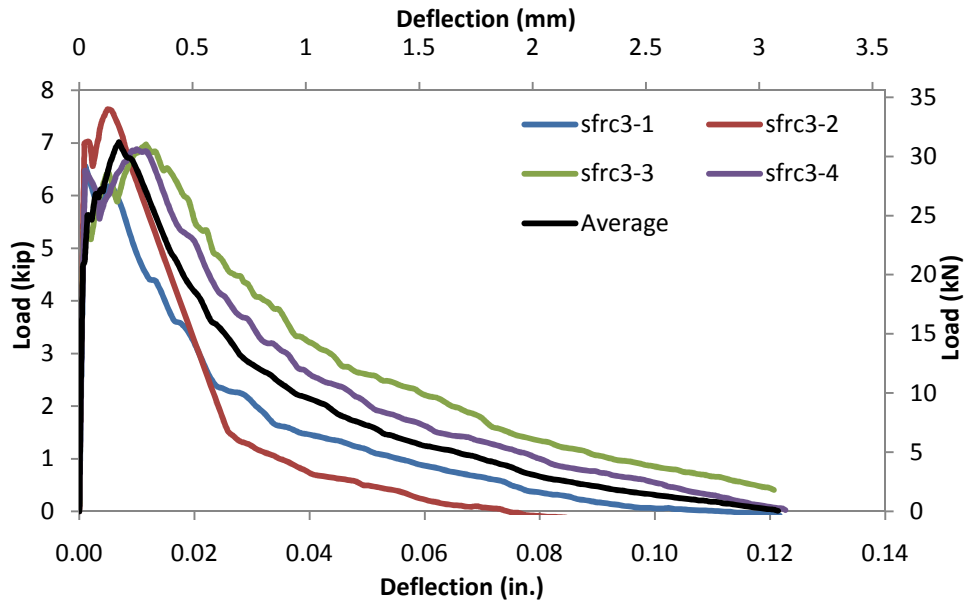


Figure 4.25 SFRC3 Load-Deflection Curves

**Discussion of results**

A graph showing the comparison between the three different SFRC beams is shown below. The graph was constructed from the average curves from the three types of SFRC specimens.
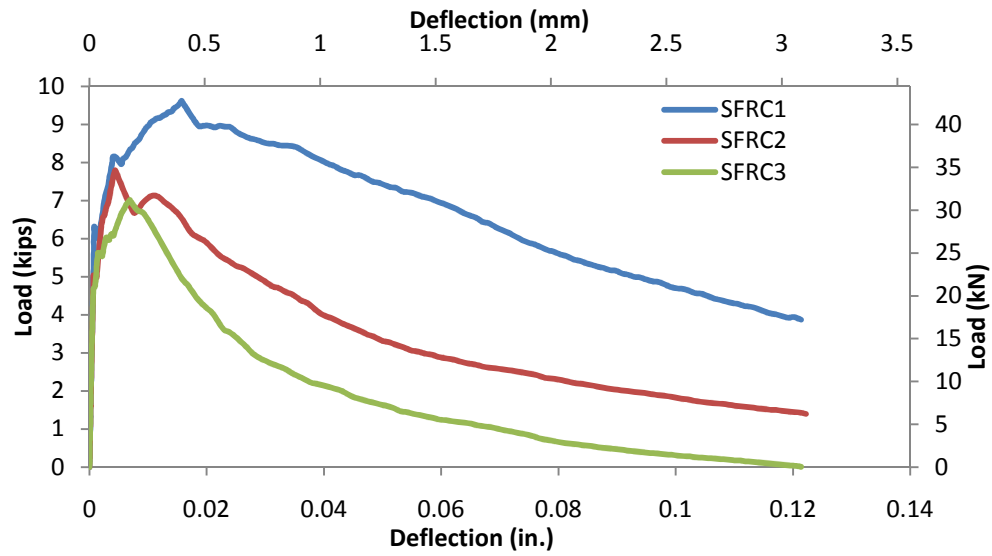
Figure 4.26 Comparator Load-Deflection Curves

From the graph above it is clear that the ductility of the SFRC2 and SFRC3 has decreased exponentially due to corrosion. However SFRC2 still retains some ductility as compared to SFRC3 which can be seen not to be able to carry more load past a 0.12 inch deflection.

CHAPTER 5

CONCLUSIONS AND RECOMMENDATIONS

The work carried out in this research aimed to show the performance of steel fiber reinforced concrete in corrosive environments. It precisely focused on investigating the effect of corrosion of fibers on the shear capacity of SFRC. The initial investigation of alkali-silica reaction in SFRC has also been discussed and conclusions are made based on the preliminary results already acquired.

**5.1 Conclusions**

The following conclusions were made based on the results.

1. It is clear from the large-scale tests done in this research and from various researchers that addition of steel fibers increase the shear capacity of the concrete member.

2. Experimental results have shown that a fiber corrosion of less than 12.5% of the minimum fiber diameter has no effect on the shear capacity of the SFRC beam. Considering that this research focused on the worst case scenario, it is therefore evident that SFRC specimens with corrosion on the surface or near the crack of 12.5% will have similar performance to SFRC specimens without any corrosion.

3. A decrease in the minimum fiber diameter of 50% led to a decrease in the shear strength of the beam by 24%. It is therefore expected that for real

conditions where corrosion will only occur near the surface and on the fibers near the crack then the reduction in shear strength will be much less than for this extreme case.

4. The fiber pullout results showed an increase in the pullout strength for SFRC2. This suggests that there is an increased bond and friction between the fiber and the matrix due to the formation of corrosion products on the surface of the fibers. However for higher corrosion extent as seen for the 50%, there is fracture of the fiber due to localized areas having higher corrosion (pitting) which can also explain the reduction in the shear strength and ductility in the experimental tests. Fiber fracture occurred at severely corroded locations therefore limiting strength and ductility.

5. The results from the flexural-load tests showed that there is a more dramatic reduction in ductility between the different degrees of corrosion compared to the shear strength from the beam test. We can therefore conclude that corrosion affects toughness and ductility of steel fiber reinforced concrete to a much higher extent than it does the shear strength.

6. It is clear from this study that although fibers in SFRC have essentially no cover, corrosion which will occur on fibers near the surface and near cracks, will lead to no change in shear capacity for a corrosion extent of below 12.5% whereas for 50% corrosion, there is expected to be little effect on the capacity. Hence the SFRC can perform well in environments having high chloride contents for example in marine applications. The findings from this research

can therefore provide data that the ACI 318-08 Section R11.4.6.1 (f) needs on the performance of fibers as shear reinforcement in concrete members exposed to chlorides.

Based on the initial investigation on Alkali-Silica Reaction in Steel Fiber Reinforced Concrete some conclusions can be made.

1. From the preliminary results on expansion, it is believed that fibers reduce the expansion in Concrete due to ASR.

2. Although more investigations still need to be done, these initial results seem to suggest that conventional fiber can be as effective as microfibers in controlling ASR.

## 5.2 Recommendations

Based on the results of the present study the following recommendations are made:

1. More research is needed to evaluate the shear capacity of the beam when the corrosion extent is between 12.5% and 50% so as to have a clear understanding on the corrosion threshold.

2. Research should be done on the beams exposed to corrosive field conditions so as to get the exact effect on the fibers and consequently on the shear capacity of the SFRC beams.
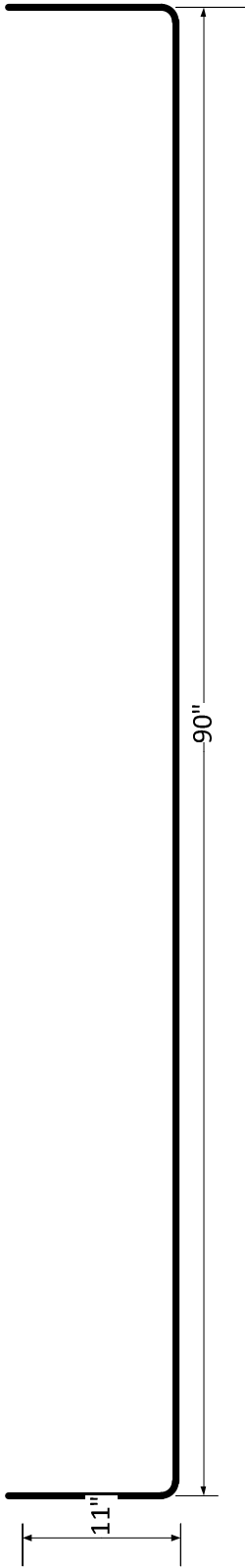
APPENDIX I
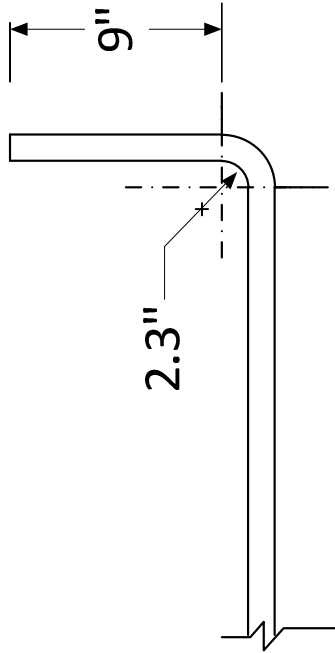

REINFORCEMENT SPECIFICATION
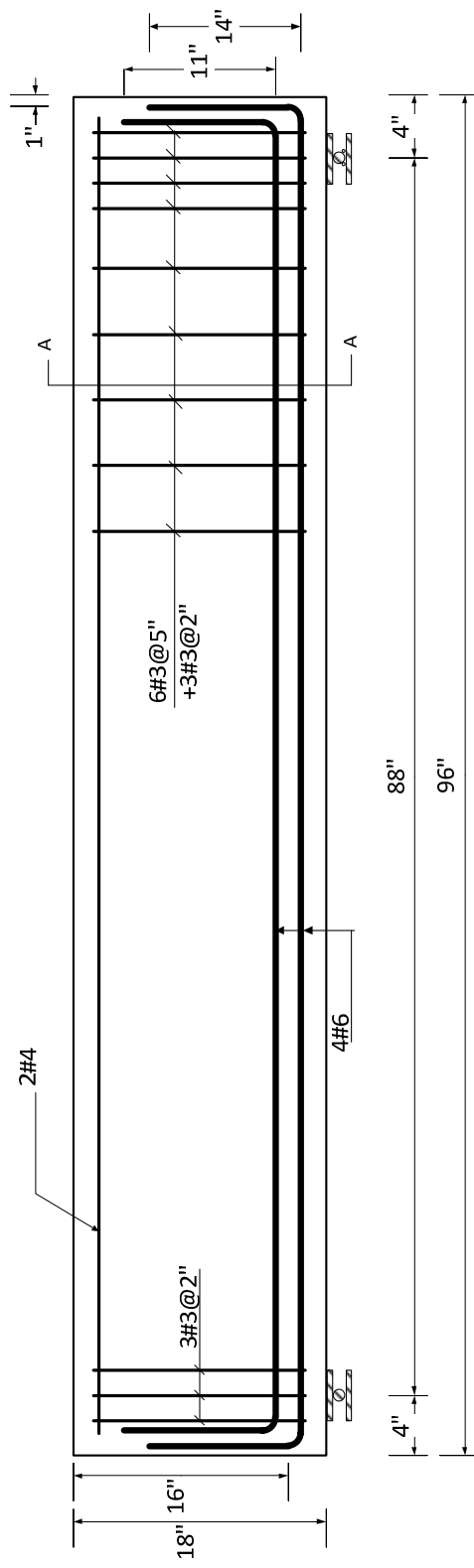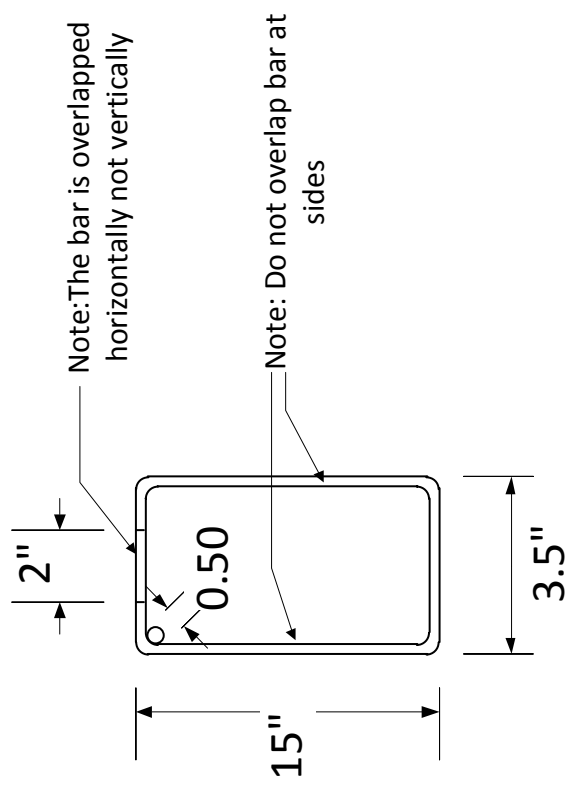
*Longitudinal Reinforcement Detail*

162

90"

11"

9"

2.3"
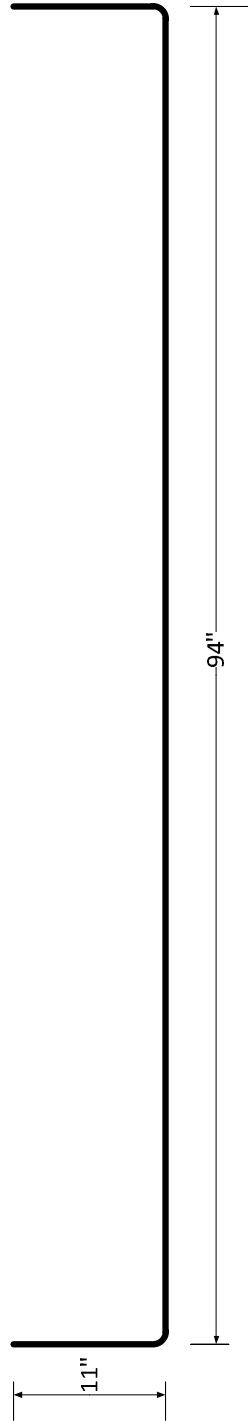
*Hook Details*

*Stirrup Details*

Note:The bar is overlapped horizontally not vertically

Note: Do not overlap bar at sides

2"

0.50

3.5"

15"

APPENDIX II

CALCULATION OF SHEAR AND FLEXURAL STRENGTH

$f_c := 6000\,psi$     $a := 52.5\cdot in$     $a' := 35.5\cdot in$     $f_y := 60000\,psi$     $A_s := 1.76\,in^2$

$d := 16\cdot in$     $b := 6\cdot in$

$\dfrac{a}{d} = 3.281$

$\rho := \dfrac{A_s}{b\cdot d} \rightarrow 0.0183333333333333333333$

$V_c := 2\cdot\sqrt{f_c}\cdot b\cdot d\cdot\sqrt{psi} = 14.872\,kip$

$P_s := \dfrac{a + a'}{a'}\cdot V_c = 36.866\,kip$

$a_c := \dfrac{A_s\cdot f_y}{0.85\cdot f_c\cdot b} = 3.451\cdot in$

$M_n := A_s\cdot f_y\cdot\left(d - \dfrac{a_c}{2}\right) = 1.507\times 10^3\cdot kip\cdot in$

$P_b := \left(\dfrac{a + a'}{a'}\right)\cdot\dfrac{M_n}{a} = 71.174\,kip$

For 0.75% fiber

$V_s := 3.5\cdot\sqrt{f_c}\cdot b\cdot d\cdot\sqrt{psi} = 26.026\,kip$

$P_{sv} := \dfrac{a + a'}{a'}\cdot V_c = 36.866\,kip$

## Design of stirrups

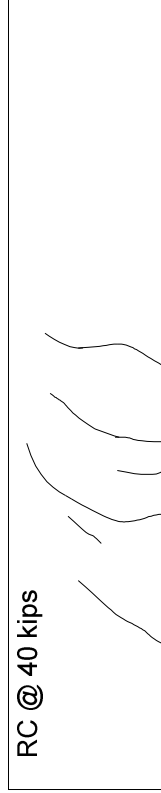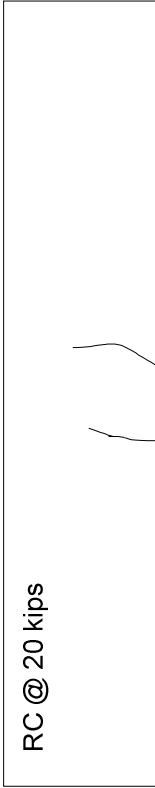$V_n := V_c + V_s = 40.899\,kip$

The corresponding load is

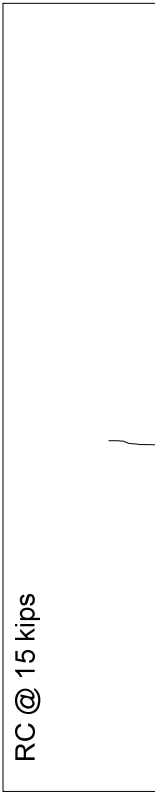$P := \dfrac{(a + a')}{a}\cdot V_n = 68.554\,kip$

166

APPENDIX III

CYLINDER COMPRESSIVE STRENGTH
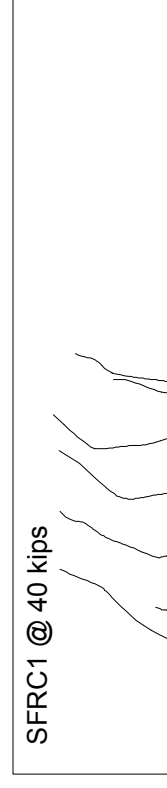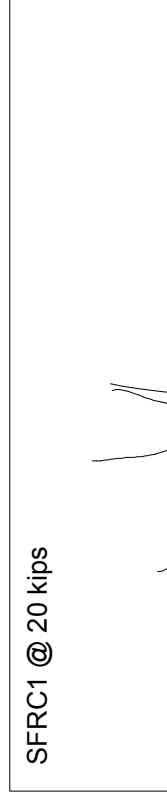
| Specimen | #1 | #2 | #3 | #4 | #5 | #6 | Average Strength | Standard deviation | Coefficient of variation |
|----------|------|-------|-------|--------|-------|-------|---------|---------|---------|
| RC | 62.5 | 55.08 | 67.27 | 60.19 | 60.23 | 63.04 | 4.88 | 0.32 | 0.06 |
| SFRC1 | 58.09 | 86.64 | 72.53 | 76.71 | 88.98 | 85.07 | 6.20 | 0.92 | 0.14 |
| SFRC2 | 78.62 | 61.85 | 85.95 | 100.68 | 89.2 | 86.78 | 6.67 | 1.02 | 0.15 |
| SFRC3 | 90.72 | 89.02 | 87.64 | 88.45 | 96.63 | 71.77 | 6.87 | 0.81 | 0.09 |

APPENDIX IV

CRACK PATTERN IN BEAM SPECIMENS

1. **RC**

RC @ 15 kips

RC @ 20 kips

RC @ 40 kips

RC @ Failure

2. **SFRC1**

SFRC1 @ 20 kips

SFRC1 @ 40 kips

SFRC1 @ 60 kips

SFRC1 @ Failure

**3. SFRC2**

SFRC2 @ 20 kips

SFRC2 @ 40 kips

SFRC2 @ 60 kips

SFRC2 @ Failure
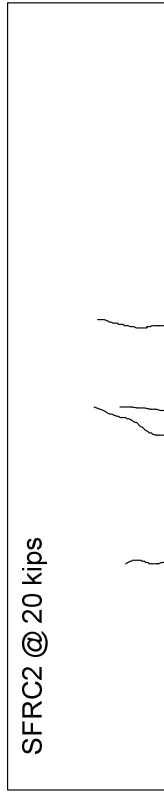
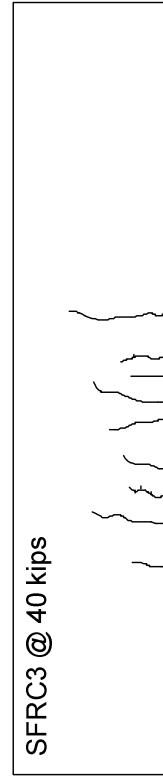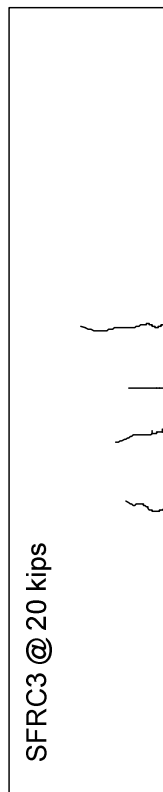**4. SFRC3**

SFRC3 @ 20 kips

SFRC3 @ 40 kips

SFRC3 @ 60 kips

SFRC3 Failure
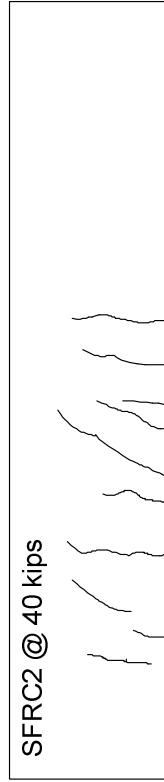
APPENDIX V

CALCULATION OF NAOH REQUIRED FOR THE PRISM TEST

Cementitious materials content of $1m^3$ concrete = 13.15 lb
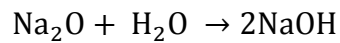
Cement content of concrete = 13.15 lb

Amount of alkali in the concrete = $13.15 \times 0.90\%$ = 0.12 lb

Specified amount of alkali in concrete = $13.15 \times 1.25\%$ = 0.17 lb

Amount of alkali to be added to the concrete = $0.17 - 0.12$ = 0.05 lb

The difference is the amount of alkali expressed as Na2O equivalent to be added to the mix water. The conversion factor to convert Na2O to NaOH is:

Since

$$Na_2O + H_2O \rightarrow 2NaOH$$

| Compound | Molecular Weight |
|----------|------------------|
| Na₂O | 61.98 |
| NaOH | 39.997 |

Then the conversion factor is:

$$2 \times \frac{39.997}{61.98} = 1.291$$

Amount of NaOH required for the mix containing 1% fiber is therefore:

$$0.05 \times 1.291 = 1.898 \text{ lb/m}^3$$

# REFERENCES

ACI Committee 318. (2008), Building Code Requirements for Structural Concrete (ACI 318-08) and Commentary (318R-08), American Concrete Institute, Farmington Hills, MI.

ACI Committee 544. (1996), Report on Fiber Reinforced Concrete (ACI 544.1 R-96), American Concrete Institute, Farmington Hills, MI

ASTM  C 1609/C 1609M  – 05, Standard Test Method for Flexural Performance of Fiber-Reinforced Concrete (Using Beam With Third-Point Loading),  ASTM International, PA, United States.

ASTM C 39/C 39M – 05, Standard Test Method for Compressive Strength Cylindrical Concrete Specimens, ASTM International, West Conshohocken, PA, pp. 22-28.

ASTM C 1260-08, Standard test method for potential alkali reactivity of aggregates (mortar-bar method), Annual Book of ASTM Standards v. 04.02, Concrete and Aggregates, American Society for Testing and Materials, Philadelphia, 2007, pp. 681– 685.

Morse, D.C. and Williamson, G.R., 1977, "Corrosion behavior of steel fibrous concrete," Technical report, M-217, US Army Corps of Engineers, Construction Engineering Research Laboratory, Chaimpaign, IL.

Mangat, P.S. and Gurusmany, K., 1985, "Steel fibre reinforced concrete for marine applications," Proceedings 4th International Conference on Behaviour of Offshore Structures, Delft, The Netherlands, Elsevier, Amsterdam, pp. 867– 879.

Mangat, P.S and Gurusmany, K., 1987, "Permissible crack width in steel fibre reinforced marine concrete," Mat. Struct., 20, pp. 334– 338.

Mangat, P. S. and Gurusamy, K., 1987, "Chloride diffusion in steel fibre reinforced marine concrete", Cement Concrete Res., pp. 385-396.

Mangat, P. S. and Gurusamy, K., 1985, "Steel fibre reinforced concrete for structural repair", Proceedings of the 2nd International Conference on Structural Faults and Repair, ICE, London, pp. 97-106.

Swamy, R.N., 1980, "Prospects of fibre reinforcement in structural applications", Materials Research Society Symposium on Advances in Cement-Matrix Composites.

Hannant, D. M. and Edgington, J., 1975, "Rilem Symposium on fibre reinforced cement and Concrete", Construction Press, Lancaster, Vol. 1, pp. 159-169.

Hannant, D. J., 1975, "Additional data on fibre corrosion in cracked beams and theoretical treatment of the effect of fibre corrosion on beam load capacity", Rilem Symposium on Fibre Reinforced Cement and Concrete, Vol. II, pp. 533-538.

Edgington, J., Hannant, D. J. and Williams, R. I. T., 1978, "Steel fibre reinforced concrete", Practical Studies from the BRE on Concrete, CP69/74, The Construction Press, Lancaster, Vol. 1, pp. 154-170.

Naaman, A. E., 1985, "Fiber Reinforcement for Concrete," Concrete International: Design and Construction, Vol. 7, No. 3, pp. 21-25.

Tuutti, K., 1982, "Corrosion of steel in concrete," Swedish Cement and Concrete Research Institute, Stockholm, Sweden. CBI Research Report no. 4.82.

Weydert, R., Schiessl, P., 1998, "Corrosion of steel fibres in cracked and uncracked steel fibre reinforced concrete," In: Research report no. 516, University of Aachen (ibac), Germany.

Jäggi, S., Böhni, H. and Elsener, B., 2001, "Macrocell Corrosion of Steel in Concrete-Experiment and Numerical Modelling," Riva di Gardia Associazione Italia Mettalurgia, Milan.

Shroff, J.k., 1966, "The Effect of a Corrosive Environment on the Properties of Steel Fiber Reinforced Portland Cement," Master's thesis, Clarkson College of Technology, Potsdam, New York.

Dinh, H.H., 2009, "Shear Behavior of Steel Fiber Reinforced Concrete Beams without Stirrup Reinforcement," PhD Dissertation, The University of Michigan, Ann Arbor, MI.

Naaman, A.E., and Kosa, K., 1990, "Corrosion of Steel Fiber Reinforced Concrete," ACI Structural Journal, Vol. 87, No. 1, pp. 27-37.

Chao S.-H., Naaman, A.E., and Parra-Montesinos, G.J., 2009, "Bond Behavior of Reinforcing Bars in Tensile Strain-Hardening Fiber-Reinforced Cement Composites," ACI Structural Journal, Vol. 106, No. 6, pp. 879-906.

Naaman, A. E., and Shah, S. P., 1975, "Bond Studies of Oriented and Aligned Fibers," Proceedings, RILEM Symposium on Fiber Reinforced Concrete, London, pp. 171-178.

Naaman, A. E., and Shah, S. P., 1976, "Pullout Mechanism in Steel Fiber Reinforced Concrete," ASCE Journal, Structural Division, Vol. 102, No. ST8, pp. 1537-1548.

Bentur, A., 1998, "Durability of fiber reinforced cementitious composites," in J.P. Skalny and S. Mindess (eds), Materials Science of Concrete-V, The American Ceramic Society, Westerville, OH, pp. 513–536.

Granju, J.-L. and Baluch, S.U., 2005, "Corrosion of steel fibre reinforced concrete from the cracks," Cem. Concr. Res. 35, pp. 572–577.

Morrison, J., Shah, S. P. and Jeng, Y. S., 1988, "Analysis of the Debonding and Pullout Process in Fiber Composites," Engineering Mechanics Journal, ASCE, Vol. 114, No. 2, pp. 277-294.

Sandberg, P., 1995, "Critical evaluation of factors affecting chloride initiated reinforcement corrosion in concrete," Report TV BM-7088, Division of Building Materials, Lund Inst. of technology, Sweden.

Farny, J. A., and Kosmatka, S. H., 1997, "Diagnosis and Control of Alkali-Aggregate Reactions in Concrete." Portland Cement Association.

Williamson, G. R., 1978, "Steel Fibers as Web Reinforcement in Reinforced Concrete," Proceedings US Army Science Conference, West Point, Vol. 3, pp. 363-377.

Schupack, M., 1986, "Durability of SFRC Exposed to Severe Environments," Steel Fiber Concrete, Elsevier Applied Science Publishers, Ltd., pp. 479-496.

Higgins, C. and Farrow III, W.C., 2006, "Tests of reinforced concrete beams with corrosion damaged stirrups," ACI Struct. J. 103, Vol. 1, pp. 133–141.

Hoff, G., 1987, "Durability of Fiber Reinforced Concrete in a Severe Marine Environment," Fiber Reinforced Concrete Properties and Applications, SP-105, American Concrete Institute, Detroit, pp. 997- 1041.

Bektas, F., Turanli, L. and Ostertag, C. P., 2006, "New Approach in Mitigating Damage Caused by Alkali-Silica Reaction," Journal of Materials Science, V. 41, pp. 5760-5763.

Ostertag, C. P., and Yi, C. K., 2000, "Quasi-Brittle Behavior of Cementitious Matrix Composites," Materials Science Engineering, V. A278, pp. 95-98.

Yi, C. K., and Ostertag, C. P., 2005, "Mechanical Approach in Mitigating Alkali-Silica Reaction," Cement and Concrete Research, V. 35, pp. 67-75.

Helmuth, R., and Stark, D., 1989, "Alkali-Silica Reactivity Mechanisms," Material Science of Concrete III, J. Skalny and S. Mindess, eds., American Ceramic Society, Westernville, Ohio, pp. 131-208.

Folliard, K.J., Ideker, J.H., Thomas, M.D.A. and Fournier, B., 2004, "Assessing aggregate reactivity using the Accelerated Concrete Prism Test," Seventh CANMET/ACI International Conference on Recent Advances in Concrete Technology, Supplementary Papers, Las Vegas, Nevada, pp. 269–283.

Turanli, L., Shomglin, K., Ostertag, C.P. and Monteiro, P.J.M., 2001, "Reduction in alkali-silica expansion due to steel microfibers," Cem. Concr. Res. 31, pp. 827– 835.

Garci Juenger, M.C. and Ostertag, C.P., 2002, "Effect of selective positioning of steel microfibers on alkali-silica reaction," Concrete Science and Engineering 4, pp. 91–97.

Haddad, R.H. and Smadi, M.M., 2004, "Role of fibers in controlling unrestrained expansion and arresting cracking in Portland cement concrete undergoing alkali-silica reaction," Cement and Concrete Research 34, pp. 103–108.

Park, S.B. and Lee, B.C., 2004, "Studies on expansion properties in mortar containing waste glass and fibres," Cement and Concrete Research 34, pp. 1145–1152.

BIOGRAPHICAL INFORMATION

Regina Waweru was born in Nairobi, Kenya on April 24, 1983. She joined Moi University in 2003 to pursue a Bachelor of Technology degree in Civil and Structural Engineering. During her undergraduate studies, she was employed by Howard Humphreys (EA) Consulting Firm as an intern in 2007. She then defended her fifth year project ("Investigation of the influence of Super-plasticisers on the flowability and Strength of Self-Compacting Concrete (SCC) using Locally Available Materials") in 2008 and was awarded the "Best Concrete Project Award" by Bamburi Cement Company. She went on to graduate the same year with First Class Honors.

From 2008 to 2009, she was hired as a research assistant at Moi University . She worked with the lead Professor on "Mix design for Self Compacting Concrete: Pilot Tests with Crushed Stone as Coarse Aggregates" and presented the same on the 2nd International Conference on Civil Engineering and Sustainable Development held in Mombasa Kenya.

In August of 2009, she joined Graduate School at the University of Texas at Arlington. She has been working on a number or research projects related to Steel Fiber-Reinforced Concrete. Regina plans to expand her knowledge by pursuing a Doctoral Degree. Her long-term goals are to gain experience in design and become a registered engineer. She is a member of a number of professional organizations such as the American Concrete

Institute (ACI), American Society of Civil Engineers (ASCE), Precast/Prestressed Concrete Institute among others.